Statistical comparisons for the topological equivalence of proximity measures

Rafik Abdesselam[1] and Djamel Abdelkader Zighed[2]

[1] ERIC Laboratory, University of Lyon 2
Campus Porte des Alpes, 69500 Bron, France
(e-mail: rafik.abdesselam@univ-lyon2.fr)
[2] Human Sciences Institute, ISH - CNRS
69007 Lyon, France
(e-mail: Abdelkader.Zighed@ish-lyon.cnrs.fr)

Abstract. In many application domains, the choice of a proximity measure directly affects the resulting data mining methods in the clustering, comparison or structuring a set of objects. According to the notion of equivalence, like the one based on pre-ordering, some of the proximity measures are more or less equivalent, which means that they produce, more or less, the same results. In this paper, we introduce a new approach to comparing proximity measures. It is based on topological equivalence which exploits the concept of local neighbors. It defines equivalence between two proximity measures as having the same neighborhood structure on the objects. This information on equivalence might be helpful for choosing one such measure. However, the complexity $O(n^4)$ of pre-ordering approach makes it intractable when the size n of the sample exceeds a few hundred. To cope with this limitation, we propose a topological approach with less complexity $O(n^2)$. We illustrate our approach and compare empirically the two tests for thirteen proximity measures for continuous data from the literature.

Keywords: Proximity measure, dissimilarity and adjacency matrices, Spearman and Kappa tests, neighborhood graph, pre-order and topological equivalences.

1 Introduction

The proximity measures are characterized by precise mathematical properties. Are they so far, all equivalent? Can be used in practice so undifferentiated? In other words, is that, for example, the proximity measure between individuals immersed in a multidimensional space as R^p, influence or not the result of operations?

The aims of this paper is to compare the proximity measures them to detect those which are identical to those which are not. To compare two proximity measures, the approach is, so far, to compare the values of proximity matrices induced [1], [2]. To compare two proximity measures, [5] focuses on the preorders induced by the two proximity measures and assess their degree of similarity by the concordance between the induced preorders on the set of pairs of objects.

We use a statistical test for comparing matrices associated with proximity measures based on the concept of neighborhood graphs. It believes that

two proximity measures are topological equivalent if they induce the same neighborhood structure on the objects. The comparison matrix is a useful tool for measuring the degree of resemblance between two empirical proximity matrices. Like the non-parametric Spearman's or Kendall's tests on matched-pairs of continuous data used to compare two matrices of dissimilarity for measuring the degree of equivalence in pre-ordonnance, we propose the non-parametric Kappa test to compare two adjacency binary matrix for measuring the degree of equivalence in topology.

To view these proximity measures, we propose, for example, to apply an algorithm to construct a hierarchy. Proximity measures are grouped according to their degree of resemblance in pre-order and in topology.

2 Proximity measures and equivalences

In this article we limit our work to proximity measures built on R^p. Nevertheless, the approach could easily be extended to all kinds of data: quantitative or qualitative. Let us consider a sample of n individuals $x, y, \ldots$ in a space of p dimensions. Individuals are described by continuous variables: $x = (x_1, \ldots, x_p)$.

Table 1. Some proximity measures.

Measure	Short	Formula
Euclidean	Euc	$u_E(x,y) = \sqrt{\sum_{j=1}^{p}(x_j - y_j)^2}$
Mahalanobis	Mah	$u_{Mah}(x,y) = \sqrt{(x-y)^t \sum^{-1}(x-y)}$
Manhattan	Man	$u_{Man}(x,y) = \sum_{j=1}^{p} \lvert x_j - y_j \rvert$
Minkowski	Min	$u_{Min_\gamma}(x,y) = (\sum_{j=1}^{p} \lvert x_j - y_j \rvert^\gamma)^{\frac{1}{\gamma}}$
Tchebytchev	Tch	$u_{Tch}(x,y) = \max_{1 \le j \le p} \lvert x_j - y_j \rvert$
Cosine Dissimilarity	Cos	$u_{Cos}(x,y) = 1 - \frac{<x,y>}{\|x\|\|y\|}$
Canberra	Can	$u_{Can}(x,y) = \sum_{j=1}^{p} \frac{\lvert x_j - y_j \rvert}{\lvert x_j \rvert + \lvert y_j \rvert}$
Squared Chord	SC	$u_{SC}(x,y) = \sum_{j=1}^{p} (\sqrt{x_j} - \sqrt{y_j})^2$
Weighted Euclidean	WE	$u_{WE}(x,y) = \sqrt{\sum_{j=1}^{p} \alpha_i (x_j - y_j)^2}$
Chi-square	χ^2	$u_{\chi^2}(x,y) = \sum_{j=1}^{p} \frac{(x_j - m_j)^2}{m_j}$
Jeffrey Divergence	JD	$u_{JD}(x,y) = \sum_{j=1}^{p} (x_j \log \frac{x_j}{m_j} + y_j \log \frac{y_j}{m_j})$
Pearson's Correlation	ρ	$u_\rho(x,y) = 1 - \lvert \rho(x,y) \rvert$
Normalized Euclidean	NE	$u_{NE}(x,y) = \sqrt{\sum_{j=1}^{p} (\frac{x_j - y_j}{\sigma_j})^2}$

Where p is the dimension of space, $x = (x_j)_{j=1,\ldots,p}$ and $y = (y_j)_{j=1,\ldots,p}$ two points in R^p, $(\alpha_j)_{j=1,\ldots,p} \ge 0$, $\sum^{-1}$ the inverse of the variance and covariance matrix, σ_j^2 the variance, $\gamma > 0$, $m_j = \frac{x_j + y_j}{2}$ and $\rho(x,y)$ denotes the linear correlation coefficient of Bravais-Pearson.

In Table 1, we give a list of 13 conventional proximity measures. For our experiment and comparisons, we took Iris dataset from the UCI-repository.

2.1 Preorder equivalence

Two proximity measures, u_i and u_j generally lead to different proximity matrices. Can we say that these two proximity measures are different just because the resulting matrices have different numerical values? To answer this question, many authors,[7][8][18], have proposed approaches based on preordonnance defined as follows:

Definition 1. Equivalence in preordonnance: Let us consider two proximity measures u_i and u_j to be compared. If for any quadruple (x, y, z, t), we have: $u_i(x, y) \leq u_i(z, t) \Rightarrow u_j(x, y) \leq u_j(z, t)$, then, the two measures are considered equivalent.

In order to compare proximity measures u_i and u_j, we need to define an index that could be used as a similarity value between them. We denote this by $S(u_i, u_j)$. For example, we can use the following similarity index which is based on preordonnance.

$$S(u_i, u_j) = \frac{1}{n^4} \sum_x \sum_y \sum_z \sum_t \delta_{ij}(x, y, z, t)$$

$$\text{where} \quad \delta_{ij}(x, y, z, t) = \begin{cases} 1 \text{ if } [u_i(x, y) - u_i(z, t)] \times [u_j(x, y) - u_j(z, t)] > 0 \\ \quad \text{or } u_i(x, y) = u_i(z, t) \text{ and } u_j(x, y) = u_j(z, t) \\ 0 \text{ otherwise} \end{cases}$$

S varies in the range [0, 1]. Hence, for two proximity measures u_i and u_j, a value of 1 means that the preorder induced by the two proximity measures is the same and therefore the two proximity matrices of u_i and u_j are equivalent.

3 Topological equivalence

This approach is based on the concept of a topological graph which uses a neighborhood graph. The basic idea is quite simple: we can associate a neighborhood graph to each proximity measure (this is -our topological graph-) from which we can say that two proximity measures are equivalent if the topological graphs induced are the same. To evaluate the similarity between proximity measures, we compare neighborhood graphs and quantify to what extent they are equivalent.

3.1 Topological graphs

For a proximity measure u, we can build a neighborhood graph on a set of individuals where the vertices are the individuals and the edges are defined by a neighborhood relationship property. We thus simplify have to define the neighborhood binary relationship between all couples of individuals. We have plenty of possibilities for defining this relationship. For instance, we can use the definition of the Relative Neighborhood Graph (RNG) [9], where two individuals are related if they satisfy the following property: If $u(x, y) \leq \max(u(x, z), u(y, z))$; $\forall z \neq x, \neq y$ then, $V_u(x, y) = 1$ otherwise $V_u(x, y) = 0$.

Geometrically, this property means that the hyper-lunula (the intersection of the two hyper-spheres centered on two points) is empty. The set of couples that satisfy this property result in a related graph such as that shown in Figure 1. For the example shown, the proximity measure used is the Euclidean distance. The topological graph is fully defined by the adjacency matrix as in Figure 1.

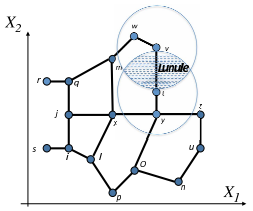

V_u	...	x	y	z	t	u	...
x	...	1	1	0	0	0	...
y	...	1	1	1	1	0	...
z	...	0	1	1	0	1	...
t	...	0	1	0	1	0	...
u	...	0	0	1	0	1	...

Fig. 1. RNG example for a set of points in R^2 and the associated adjacency matrix.

In order to use the topological approach, the property of the relationship must lead to a related graph. Of the various possibilities for defining the binary relationship, we can use the properties in a Gabriel Graph or any other algorithm that leads to a related graph such as the Minimal Spanning Tree, MST. For our work, we use only the Relative Neighborhood Graph, RNG, because of the relationship there is between those graphs [9].

3.2 Similarity between proximity measures in topological frameworks

From the previous material, using topological graphs (represented by an adjacency matrix), we can evaluate the similarity between two proximity measures via the similarity between the topological graphs each one produces. To do so, we just need the adjacency matrix associated with each graph.

Note that V_{u_i} and V_{u_j} are the two adjacency matrices associated with both proximity measures. To measure the degree of similarity between the two proximity measures, we just count the number of discordances between the two adjacency matrices. The value is computed as:

$$S(V_{u_i}, V_{u_j}) = \frac{1}{n^2} \sum_{x \in \Omega} \sum_{y \in \Omega} \delta_{ij}(x, y)$$

$$\text{where} \quad \delta_{ij}(x, y) = \begin{cases} 1 \text{ if } V_{u_i}(x, y) = V_{u_j}(x, y) \\ 0 \text{ otherwise} \end{cases}$$

S is the measure of similarity which varies in the range $[0, 1]$. A value of 1 means that the two adjacency matrices are identical and therefore the topological structure induced by the two proximity measures in the same, meaning that the proximity measures considered are equivalent. A value of 0 means that there is a full discordance between the two matrices ($V_{u_i}(x, y) \neq V_{u_j}(x, y)\ \forall \omega \in \Omega^2$). S is thus the extent of agreement between the adjacency matrices.

4 Comparison between topological and preordonnance equivalences

In this work, our goal is not to compare proximity matrices or the preorders induced but to propose a different approach which is the topological equivalence that we compare to the preordering equivalence. We propose to test whether the matrices are statistically different or not using Kendall's tau in preoder approach and Cohen's kappa coefficient in topological approach. These nonparametric tests compare proximity measures from their associated proximity matrices in preoder equivalence and from their associated adjacency matrices in topological equivalence.

4.1 Statistical Comparisons between two proximity measures

For the preorder equivalence, we propose to use a concordance index between preorders induced as a proximity measure between two measures u_i and u_j. To terminate this approach we can, like [11], use the generalized rate of Kendall based on the concordance of ranks. The ranks of the $n(n-1)$ pairs of proximity values between x and y by u_i are compared according to ones to u_j. We note $R_i(x,y)$ and $R_j(x,y)$ the respective ranks of $u_i(x,y)$ and $u_j(x,y)$.

$$D(u_i,u_j) = \frac{2}{n(n-1)} \sum_x \sum_{y \neq x} \delta_{ij}(x,y) \quad \text{where} \quad \delta_{ij} = \begin{cases} 0 & \text{if } R_i(x,y) = R_j(x,y) \\ 1 & \text{otherwise} \end{cases}$$

The comparison between indices of proximity measures has also been studied by [12], [13] from a statistical perspective. The authors proposed an approach that compares similarity matrices, obtained by each proximity measure, using Mantel's test [8], in a pairwise manner.

Let V_{u_i} and V_{u_j} adjacency matrices associated with two measures of near u_i and u_j. To compare the degree of the topological equivalence between two measures of proximity, we propose to test if the adjacency matrices associated are statistically different or not, using a non-parametric test of paired data. These matrices, and binary symmetric of order n, are unfolded in two vectors matched components, consisting of $n(n-1)/2$ values higher (or lower) the diagonal. The degree of topological equivalence between two proximity measures is estimated from the Kappa coefficient of concordance [3], calculated on the Table 2×2 contingency formed by the two vectors:

$$\kappa = \kappa(V_{u_i}, V_{u_j}) = \frac{\Pi_o - \Pi_e}{1 - \Pi_e} \qquad \text{with} \qquad \begin{cases} \Pi_o\text{: observed proportion} \\ \Pi_e\text{: random proportion} \end{cases}$$

We then formulate the null hypothesis $H_0 : \kappa = 0$ independence of agreement or concordance. The concordance is even higher than its value tends to 1, or perfect maximum if kappa = 1. It is equal to -1 in the case of a perfect discordance. The results of these comparison pair of proximity measures are given in Table 2.

Table 2. $\widehat{\rho}_s$ - Preorder (row) & $\widehat{\kappa}$ - Topologie (column)

	u_E	u_{Mah}	u_{Man}	u_{Min}	u_{Tch}	u_{Cos}	u_{Can}	u_{SC}	u_{WE}	$u_{\chi 2}$	u_{JD}	u_ρ	u_{NE}
u_E	**1**	.456	.845	.835	.767	.341	.588	.753	**1**	.753	.753	.400	.720
u_{Mah}	.633	**1**	.336	.456	.410	.378	.301	.301	.456	.222	.301	.357	.357
u_{Man}	.996	.635	**1**	.767	.705	.301	.689	.767	.845	.767	.767	.281	.811
u_{Min}	.998	.627	.992	**1**	.845	.258	.506	.670	.835	.670	.670	.400	.720
u_{Tch}	.990	.591	.981	.994	**1**	.378	.611	.767	.767	.767	.767	.432	.735
u_{Cos}	.876	.427	.858	.881	.893	**1**	.176*	.341	.341	.341	.341	.880	.240
u_{Can}	.912	.431	.903	.917	.926	.921	**1**	.753	.588	.753	.753	.080*	.640
u_{SC}	.967	.524	.957	.972	.979	.927	.975	**1**	.753	**1**	**1**	.320	.640
u_{WE}	**1**	.633	.996	.998	.990	.876	.912	.967	**1**	.753	.753	.400	.720
u_{χ^2}	.970	.530	.961	.974	.980	.928	.973	**1**	.970	**1**	**1**	.320	.640
u_{JD}	.963	.527	.959	.973	.980	.928	.974	**1**	.969	**1**	**1**	.320	.640
u_ρ	.977	.674	.979	.972	.953	.860	.899	.942	.977	.946	.944	**1**	.300
u_{NE}	.874	.434	.856	.881	.892	.985	.893	.914	.874	.916	.915	.856	**1**

*Not significant with risk of error $\leq 5\%$

The Kappa and Kendall's tau values between the 13 proximity measures in topological and preordonnance frameworks are given in Table 2.

The upper part of the diagonal of Table 2 present the exact values of the Kappa statistic test. We can conclude, with a risk error of 5%, that only measures of couples (u_{Cos}, u_{Can}) and (u_{Can}, u_ρ) are not significantly equivalent in topology. Note that measurements of couples (u_E, u_{WE}), (u_{SC}, u_{χ^2}), (u_{SC}, u_{JD}) and (u_{χ^2}, u_{JD}) are in perfect topological equivalence ($\kappa = 1$).

4.2 Classification of proximity measures

Let $D_{u_i}(E \times E)$ and $D_{u_j}(E \times E)$ the distance tables associated with proximity measures u_i et u_j. Each of these distances generates a topological structure of objects E. This structure is fully described by its adjacency matrix. To measure the degree of resemblance between graphs, simply count the number of discordances between the two adjacency matrices V_{u_i} and V_{u_j} associated with the two toplogical structures:

$$S(V_{u_i}, V_{u_j}) = \frac{1}{n^2} \sum_x \sum_y \delta_{ij}(x,y) \quad \text{with} \quad \delta_{ij}(x,y) = \begin{cases} 1 & \text{if } V_{u_i}(x,y) = V_{u_j}(x,y) \\ 0 & \text{otherwise} \end{cases}$$

The value 1 of the similarity measure S means that both adjacency matrices are identical and therefore, the topological structure induced by the two measures is the same. In this case, we talk about topological equivalence between the two proximity measures. The value 0 means that the topology is completely changed. From this measure S, we can compare and classifying proximity measures according to their degree of resemblance.

The topological and preorder similarity values between the 13 proximity measures are given in Table 3. The values of the similarities are quite close to 1 and proximity measures of couples (u_E, u_{WE}), (u_{SC}, u_{JD}) and (u_{χ^2}, u_{JD}) are in perfect topological and preordonnance equivalences. We can view these measures of proximity by applying, for example, an Ascendant Hierarchical Classification according to Ward's criterion [14], Figure 2.

Table 3. $S(V_{u_i}, V_{u_j})$ - Topologie (row) & $S(u_i, u_j)$ - Preorder (column)

S	u_E	u_{Mah}	u_{Man}	u_{Min}	u_{Tch}	u_{Cos}	u_{Can}	u_{SC}	u_{WE}	$u_{\chi 2}$	u_{JD}	u_ρ	u_{NE}
u_E	**1**	.776	.973	.988	.967	.869	.890	.942	**1**	.947	.945	.926	.863
u_{Mah}	.876	**1**	.773	.774	.752	.701	.707	.737	.776	.739	.738	.742	.703
u_{Man}	.964	.840	**1**	.964	.940	.855	.882	.930	.973	.933	.932	.924	.848
u_{Min_γ}	.964	.876	.947	**1**	.967	.871	.892	.946	.988	.950	.949	.925	.866
u_{Tch}	.947	.858	.929	.964	**1**	.865	.887	.940	.957	.942	.942	.914	.860
u_{Cos}	.858	.858	.840	.840	.858	**1**	.893	.898	.869	.899	.899	.830	.957
u_{Can}	.911	.840	.929	.893	.911	.822	**1**	.943	.890	.940	.942	.874	.868
u_{SC}	.947	.840	.947	.929	.947	.858	.947	**1**	.942	.957	**1**	.913	.884
u_{E_w}	**1**	.876	.964	.964	.947	.858	.911	.947	**1**	.947	.945	.926	.863
$u_{\chi 2}$	.947	.840	.947	.929	.947	.858	.947	**1**	.947	**1**	**1**	.912	.885
u_{JD}	.947	.840	.947	.929	.947	.858	.947	**1**	.947	**1**	**1**	.914	.884
u_{HIM}	.884	.813	.884	.867	.902	.884	.884	.920	.884	.920	.920	**1**	.825
u_ρ	.867	.849	.831	.867	.867	.973	.796	.849	.867	.849	.849	.876	**1**

*Not significant with risk of error $\leq 5\%$

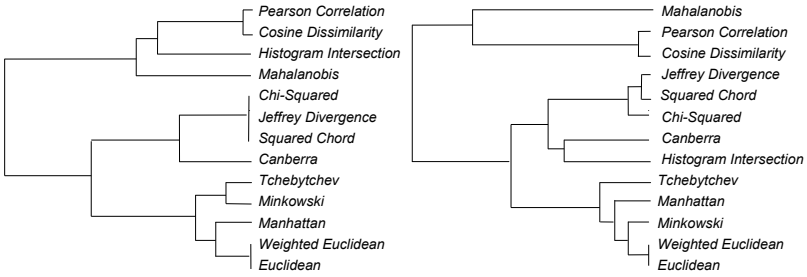

Fig. 2. a) Topological & b) Preorder hierarchical trees

Table 4. Contingency tables: preordonnance × topology

	$TC1$	$TC2$	$TC3$	$TC4$	Total
$PC1$	6	0	0	0	6
$PC2$	0	4	0	0	4
$PC3$	0	0	2	0	2
$PC4$	0	0	0	1	1
$Total$	6	4	2	1	13

$\widehat{\kappa} = 0.4348$; p-Value $= 5.74\%$

	$TC1$	$TC2$	$TC3$	Total
$PC1$	10	0	0	10
$PC2$	0	2	0	2
$PC3$	0	0	1	1
$Total$	10	2	1	13

$\widehat{\kappa} = 1$; p-Value $< 0.01\%$

	$TC1$	$TC2$	Total
$PC1$	10	2	12
$PC2$	0	1	1
$Total$	10	3	13

$\widehat{\kappa} = 1$; p-Value $< 0.01\%$

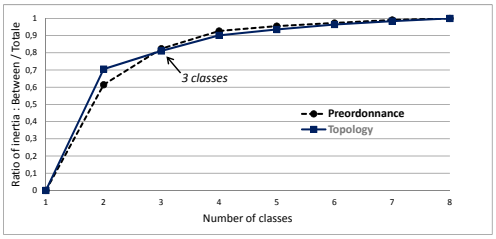

Fig. 3. Comparison of hierarchical trees

5 Conclusion and perspectives

This work proposes a new approach of topological equivalence between proximity measures, based on the notion of graphs neighborhood. The application

of the nonparametric test of Kappa on adjacency matrices associated with the proximity measures, has given statistical significance and validate or not the topological equivalence; really if they induce or not same neighborhood structure on the objects. The results of comparisons between topological and preordonnance equivalences are almost identical, both for the statistical test and classifications results. This topological approach extends to other data types (binary, qualitative). we plan to study the influence of the data and the neighborhood structure results and the effect of the choice a classification method of groups of proximity measures.

References

1. Batagelj, V., Bren, M.: Comparing resemblance measures. In Journal of classification **12** (1995) 73–90
2. Bouchon-Meunier, M., Rifqi, B. and Bothorel, S.: Towards general measures of comparison of objects. In Fuzzy sets and systems **2, 84** (1996) 143–153
3. Cohen, J.: A coefficient of agreement for nominal scales. Educ. Psychol Meas, 20, (1960) 27–46
4. Fagin, R., Kumar, R. and Sivakumar, D.: Comparing top k lists. In Proceedings of the fourteenth annual ACM-SIAM symposium on Discrete algorithms, Society for Industrial and Applied Mathematics (2003)
5. Lerman, I. C.: Indice de similarité et préordonnance associée, Ordres. In Travaux du séminaire sur les ordres totaux finis, Aix-en-Provence (1967)
6. Lesot, M. J., Rifqi, M. and Benhadda,H.: Similarity measures for binary and numerical data: a survey. In IJKESDP **1, 1** (2009) 63-84
7. Liu, H., Song, D., Ruger, S., Hu, R. and Uren, V.: Comparing dissimilarity measures for content-based image retrieval. In Information Retrieval Technology Springer 44–50
8. N. Mantel, *A technique of disease clustering and a generalized regression approach*, In Cancer Research, 27 (1967), pp. 209–220.
9. Preparata, F. P. and Shamos, M. I.: Computational geometry: an introduction. In Springer (1985)
10. Richter, M. M.: Classification and learning of similarity measures. In Proceedings der Jahrestagung der Gesellschaft fur Klassifikation, Studies in Classification, Data Analysis and Knowledge Organisation. Springer Verlag (1992)
11. Rifqi, M., Detyniecki, M. and Bouchon-Meunier, B.: Discrimination power of measures of resemblance. IFSA'03 Citeseer (2003)
12. Schneider, J. W. and Borlund, P.: Matrix comparison, Part 1: Motivation and important issues for measuring the resemblance between proximity measures or ordination results. In Journal of the American Society for Information Science and Technology **58 11** (2007) 1586–1595
13. Schneider, J. W. and Borlund, P.: Matrix comparison, Part 2: Measuring the resemblance between proximity measures or ordination results by use of the Mantel and Procrustes statistics. In Journal of the American Society for Information Science and Technology **11 58** (2007) 1596–1609.
14. Ward, J. R.: Hierarchical grouping to optimize an objective function. In Journal of the American statistical association JSTOR **58 301** (1963) 236–244

Probabilistic Strength Modeling of Flax-Fabric-Reinforced Polymer Composites

Jānis Andersons, Edgars Spārniņš, and Jānis Modniks

Institute of Polymer Mechanics, University of Latvia
Rīga LV-1006, Latvia
Email: janis.andersons@pmi.lv

Abstract: Reliability of a fiber-reinforced composite material in tension along fiber direction is governed by the strength distribution of the fibers and local load redistribution characteristics at broken fibers. Using flax fabric as the reinforcement introduces additional hierarchic level, that of fiber yarns. Such a composite material can be considered as a series of parallel systems with defects and two hierarchical levels of reinforcement. Strength distribution of a unidirectionally reinforced flax fabric/polymer matrix composite material is considered allowing for the stochastic character of fiber and yarn failure process. Failure stress of the composite is related to fiber strength characteristics, interfacial shear strength, geometrical characteristics and volume fraction of the reinforcement, and composite volume. The model is applied to strength prediction of flax/vinyl ester composite specimens of different sizes. The theoretical strength distribution is found to be in a reasonably good agreement with test results.
Keywords: Probabilistic strength modeling, Weibull distribution, flax fibers, unidirectional composite, Textile reinforcement

1 Introduction

Natural fibers of organic origin, such as flax, hemp, jute etc., are increasingly being used in such non-traditional applications as reinforcement of engineering materials. In order to efficiently exploit the mechanical properties of the fibers in a polymer-matrix composite, the fibers should be aligned, producing a unidirectionally reinforced (UD) composite. Since natural fibers are relatively short, spinning them into yarns, albeit with lower twist than for textile applications, produces fiber bundles that can be easily aligned. The resulting UD composite material thus possesses two hierarchical levels of reinforcement – a system of aligned yarns which, in their turn, consist of natural fibers. Due to the scatter in fiber strength, such composites undergo a stochastic fracture process when loaded in tension in the yarn direction, leading to the scale effect of strength, i.e. dependence of specimen strength on its size. In order to predict the strength of such a UD composite, a strength distribution of an impregnated yarn has to be determined and related to that of the composite.

Simple empirical models of the effect of yarn twist angle on the mean tensile strength of an impregnated natural fiber yarn have been proposed in [1, 2]. Probabilistic models for estimation of the strength of aligned-flax-fiber composites using fiber strength distribution have been derived and validated in [3, 4]. The purpose of the present paper is to combine the above approaches to develop a

probabilistic model of tensile strength and scale effect for oriented flax-fabric-reinforced polymer matrix composites in tension along the fiber direction.

2 Experimental

Non-crimp flax fiber fabric produced by Engtex from flax fibers provided by FinFlax was used as a reinforcement of the vinylester (VE) composite. The manufacture process is described in [5].
The fabric was made from unbleached, 570 tex, 58 t/m yarn. The flax yarns were warp-knitted transversely to the fiber direction, using 16 tex polyester yarn. Three layers of aligned fabric were stacked, impregnated with the resin, and cured, producing a composite material with structure shown schematically in Fig. 1.

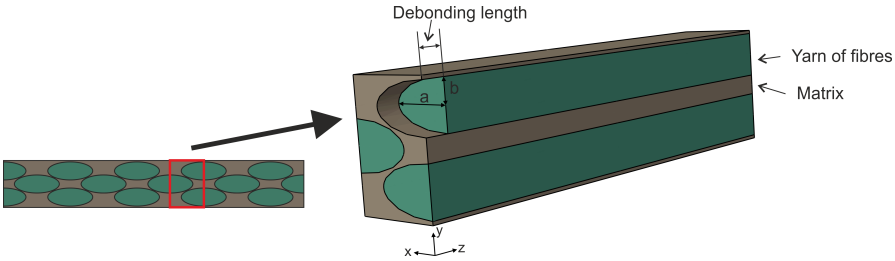

Fig. 1. Schematic of the cross-section of a three-ply flax fabrics/VE composite and the representative volume element used in FEM modeling

Rectangular specimens, aligned with the yarn direction, were prepared with gauge lengths of 25, 50, 100, and 150 mm. The width of the specimens was varied proportionally to the length. The specimens were tested in tension in the fiber direction at a strain rate of 1.33 %/min up to failure.

3 Strength model

We start by introducing a statistical model of strength of an aligned flax fiber composite [3], then apply the relation proposed in [2] to obtain the strength distribution of an impregnated twisted fiber yarn, and finally use this relation to predict the strength of multiple-yarn composite using the weakest link approach.
The tensile strength of elementary flax fibers has been shown [6] to follow the modified Weibull distribution:

$$P(\sigma) = 1 - \exp\left[-\left(\frac{l}{l_0}\right)^{\alpha} \left(\frac{\sigma}{\sigma_0}\right)^{\rho} \right] \tag{1}$$

Assuming that the only cause of composite strength variability is fiber strength scatter (i.e. neglecting the effect of reinforcement heterogeneity and limited length

of flax fibers), the strength model derived in [7] for continuous-fiber reinforced composites with a constant interfacial shear strength (IFSS) can be applied. This leads to a Weibull distribution of the cross-sectional average fiber stress, σ_f, at failure:

$$P_y(\sigma_f) = 1 - \exp\left[-\left(\frac{\sigma_f}{\tilde{\sigma}_y} \right)^{\tilde{\rho}} \right] \tag{2}$$

The relations expressing distribution Eq. (2) parameters via those of Eq. (1), IFSS, fiber radius, and the amount of fibers are provided in [7, 3].
Since the fiber yarns are twisted in the production process, Eq. (2) needs to be modified to allow for the reduction of strength due to twisting with respect to yarn axis characterized by angle φ of the fibers on the lateral surfaces of the yarn. According to [2], the effect of twist on strength can be described as follows:

$$\sigma_f^{\varphi} = \sigma_f \cos^2 2\varphi \tag{3}$$

Hence the cross-sectional average fiber stress in the twisted impregnated yarn at failure should have distribution of the same form as Eq. (2), but with a modified scale factor:

$$P_{y\varphi}(\sigma_f^{\varphi}) = 1 - \exp\left[-\left(\frac{\sigma_f^{\varphi}}{\tilde{\sigma}_y \cos^2 2\varphi} \right)^{\tilde{\rho}} \right] \tag{4}$$

A composite material contains multiple yarns, hence their gradual fracture and load distribution on the intact yarns has to be allowed for. However, for the there–ply composite material considered (see Fig. 1), failure of the first yarn is likely to trigger a fracture of the material. The plausibility of such scenario is checked in Section 4 below by evaluating the magnitude of the stress concentration factor on the intact yarns neighboring a failed one. Assuming a weakest-link fracture mechanism for the yarn-reinforced composite containing N yarns, the fiber contribution to its strength is as follows:

$$P_{cN}(\sigma_f^c) = 1 - \exp\left[-N\left(\frac{\sigma_f^c}{\tilde{\sigma}_y \cos^2 2\varphi} \right)^{\tilde{\rho}} \right] \tag{5}$$

Hence the average fiber stress at failure is given by

$$\left\langle \sigma_f^c \right\rangle = N^{-\frac{1}{\tilde{\rho}}} \tilde{\sigma}_y \cos^2 2\varphi \Gamma\left(1 + \frac{1}{\tilde{\rho}} \right) \tag{6}$$

Finally, the mean strength of the composite is expressed as a sum of the average fiber and matrix, σ_m, stresses at failure with the respective weights:

$$\sigma_c = \left\langle \sigma_f^c \right\rangle \nu_f + \sigma_m \left(1 - \nu_f\right) \tag{7}$$

where ν_f designates the fiber volume fraction. The stress born by the matrix at the failure of the composite can be evaluated by a product of matrix stiffness and composite failure strain, $\sigma_m = E_m \varepsilon_c$, or substituted by matrix strength.

4 Stress concentration at a broken yarn

The finite element calculations were performed using the commercial FEM code Abaqus. 3D model of a unit cell was built with a mesh of quadratic brick elements C3D20. The unit cell representing the yarn-reinforced composite material was chosen as shown in Fig. 1. Geometry and placement of the yarns were assessed using micrographs of cross-sections of the composite material. The shape of the yarn cross section was assumed elliptical. The yarns were modeled as a fiber-reinforced composite material with volume fraction of fibers of 0.38, which follows from the total fiber volume fraction of the composite ν_f = 0.23 [5] and the volume fraction of yarns of about 0.61. Fibers in the yarn are twisted about the axis of yarn by an angle varying form 0° at the axis to about φ=14° on the yarn surface. The average value of twist angle 9.4°, calculated by the formula $\varphi_{mean} = \varphi + \frac{\varphi}{\tan^2 \varphi} - \frac{1}{\tan \varphi}$ [8], was used to simplify the model.

The matrix behavior was assumed linear elastic with Young's modulus E_m = 3.4 GPa and Poissons' ratio ν_m = 0.3. The properties of the composite material representing the yarns were evaluated as follows. The modulus in longitudinal direction was calculated by the rule of mixtures using experimentally determined modulus of flax fibers E_f = 69 GPa [6] and matrix modulus. The remaining elasticity characteristics of the yarn were assumed to be equal to the respective matrix parameters.

The model was loaded by displacement in the longitudinal direction. Symmetric boundary conditions were applied on the planes parallel to *y-z* plane. The cases of broken yarn in the middle ply and broken yarn in the outer ply were considered. The stress concentration factor, defined as the ratio of average stress in a neighboring yarn in the failure plane in the broken and intact configurations, was estimated as a function of the debond length of the broken yarn.

It was determined that the stress concentration in the neighboring yarns depends on the debond length and has a maximum at l_d = 1.2*b* (*b* - minor radius of elliptical cross section of yarn) when a yarn in the middle ply is broken. In this case the stress concentration factor amounted to 1.2.

If a yarn close to composite edge is broken, the maximum overload is reached at a debond length l_d = 1.4*b* and the stress concentration factor value is 1.25.

5 Results and discussion

Elementary flax fiber strength distribution Eq. (1) parameters for ArcticFlax fibers produced FinFlax have been determined in [6] at $\alpha = 0.46$, $\rho = 2.8$, and $\sigma_0 = 1400$ MPa (at $l_0 = 1$ mm). The IFSS of flax fibers and VE matrix amounted to $\tau = 16.6$ MPa [9]. Using these data, the theoretical relations described in [3, 7] yielded the values of the strength distribution parameters Eq. (2) of an impregnated yarn as a function of yarn length presented in Table 1.

Table 1. Theoretical estimates of Eq. (2) parameters

Yarn length L, mm	25	50	100	150
$\tilde{\rho}$	67.4	69.3	71.1	72.1
$\tilde{\sigma}_y$, MPa	856.1	851.6	847.4	844.9

It is seen that the shape parameter values of the yarn strength distribution are rather large, therefore the overload experienced by intact yarns neighboring a broken yarn, reported in Section 4, are likely to trigger a catastrophic failure of the specimen. Therefore, the weakest-link relation Eq. (5) for the strength distribution should accurately represent the probabilistic fracture of a fabric-reinforced composite.

Fig. 2 shows the experimental dependence of the average tensile strength on the length of composite specimens. A notable reduction in strength with the increase in specimen size is seen.

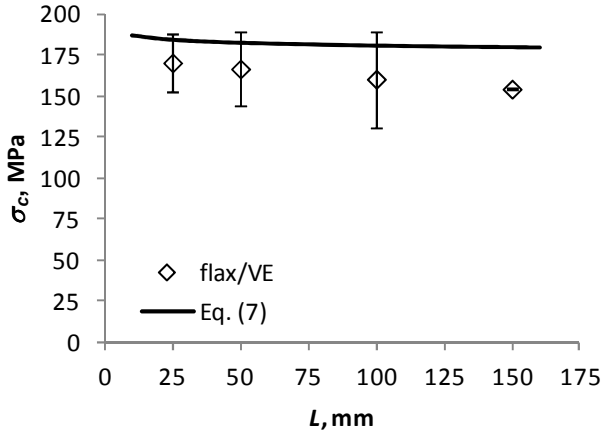

Fig. 2. Average tensile strength vs. specimen length

The predicted size effect of strength according to Eq. (7) is plotted by a solid line. In order to approximately allow for the matrix contribution to the stress at failure,

σ_m was evaluated assuming linear elastic matrix response and using the average experimental value of failure strain of 1.5%. The number of yarns N in a composite specimen was estimated based on specimen width and the measured average number of yarns per unit width.
The experimental strength is slightly but consistently overestimated by the theoretical relation Eq. (7). It should also be noted that the scale effect of strength inferred from the test results is considerably more pronounced than that following from the theoretical model. This is likely to be related to the assumption of fiber uniformity and continuity underlying the yarn strength model used. Since flax fibers are of limited length, their ends may form stress concentration sites that could lead to premature failure [10]. Moreover, the disorder in fiber geometry, alignment, and spacing, neglected by the present model, should also increase strength scatter of an impregnated yarn and, hence, promote the scale effect of strength.

6 Conclusions

A simple probabilistic model of the tensile strength of flax-fabric-reinforced composite has been developed allowing for fiber strength scatter, twist of the reinforcing yarns, and the size of a specimen. The model provides an upper limit of the tensile strength.

7 Acknowledgement

This work has been funded by ESF via project 2009/0209/1DP/1.1.1.2.0/09/APIA/ VIAA/114.

References

1. Ma, H., Li, Y., and Luo Y., The effect of fiber twist on the mechanical properties natural fiber reinforced composites, in: *18th International Conference on Composite Materials*, Jeju, South Korea (2011).
2. Shah, D. U., Schubel, P. J., and Clifford, M. J., Modelling the effect of yarn twist on the tensile strength of unidirectional plant fibre yarn composites, *J. Compos. Mater.*, http://dx.doi.org/10.1177/0021998312440737 (2012).
3. Andersons, J. and Joffe, R., Estimation of the tensile strength of an oriented flax fiber-reinforced polymer composite, *Compos. A*, **42**, 1229–1235 (2011).
4. Andersons, J., Joffe, R., Spārniņš, E., and Weichert, D., Modeling the effect of reinforcement discontinuity on the tensile strength of UD flax fiber composites, *J. Mater. Sci.*, **46**, 5104–5110 (2011).
5. Andersons, J., Spārniņš, E., Nyström, B., and Joffe, R., Scale effect of the tensile strength of flax-fabric-reinforced polymer composites, *J. Reinf. Plast. Compos.*, **30**, 1969–1974 (2011).
6. Andersons, J., Spārniņš, E., Joffe, R., and Wallström, L., Strength distribution of elementary flax fibres, *Compos. Sci. Technol.*, **65**, 693-702 (2005).

7. Curtin, W.A., Tensile strength of fiber-reinforced composites: III. Beyond the traditional Weibull model for fiber strengths, *J. Compos. Mater.*, **34**, 1301-1332 (2000).
8. Madsen, B., Hoffmeyer, P., Thomsen, A.B., and Lilholt, H., Hemp yarn reinforced composites - I. Yarn characteristics, *Compos. A*, **38**, 2194-2203 (2007).
9. Spārniņš, E., Nyström, B., Andersons, J., Interfacial shear strength of flax fibers in thermoset resins evaluated via tensile tests of UD composites, *Int. J. Adhes. Adhes.*, http://dx.doi.org/10.1016/j.ijadhadh.2012.03.006 (2012).
10. Andersons, J., Joffe, R., Spārniņš, E., Weichert, D., Modeling the effect of reinforcement discontinuity on the tensile strength of UD flax fiber composites, *J. Mater. Sci.*, **46**, 5104–5110 (2011).

Forecasting TSO marginal price by neuro-fuzzy techniques.

Atsalakis George
Department of Production Engineering and Management, Technical University of Crete, Chania, Greece 73100, email:atsalak@otenet.gr

Tsakalaki Katerina
Department of Production Engineering and Management, Technical University of Crete, Chania, Greece 73100, email:kattsak_89@hotmail.com

Plokamakis George
Public Power Corporation S.A. email: gplok@yahoo.gr

Abstract: The aim of this study is to demonstrate the effectiveness of an adaptive neuro-fuzzy inference system (ANFIS) to forecast the marginal price that Greek Transmission System Operator (TSO - DESMIE) pays for electricity supply. The technique involvedthe use of a hybrid model to forecast the marginal price per hour. Adevelopment of 24 neuro-fuzzyderivedtechniques for modelingthe marginal price for each hour of a day is described. Each model is implemented using an adaptive neuro-fuzzy inference system (ANFIS), where automatic adjustment of the system parameters is effected by aneural network based on prior knowledge. Historical data of hourly delay prices are used as inputs to the models. One step ahead forecasting ismodeled on the basis of these inputs. Another one model that forecasts the average marginal price of the 24 hours is developed.

The models derived using the above techniques were validated using test data that had not been used during training. The ANFISmodels were shown to achieve an improved accuracy compared to well-known statistical errors.

Keywords: Electricity forecasting, Anfis forecasting, marginal price forecasting, fuzzy forecasting.

1. Introduction

The Greek Transmission System Operator (DESMIE) is an anonymous company that gives access to those people that produce or supply the system with electricity, plans and distributes the loads of electricity at the production systems, arranges the deviations between production and demand and ensures the safety, the efficiency and the reliability of the system (http://www.ypeka.gr/Default.aspx?tabid=276). The marginal price of the system is defined as the bid price of the last unit that enters the system in the daily electricity market (Press conference of the syndicalist of Public Power Corporation, 2007). Every marginal price of the system should reflect the marginal cost in order to cover the real consumption (www.rae.gr). The marginal price is measured in €/MWh every hour for every day

(www.energylink.gr). The daily energy planning executes for every hour of the distribution day, the following tasks (Bakirtzis, 2009):

- Submission of injection bids and cargo declarations.
- Classification of injection bids in ascending order (supply curve).
- Classification of cargo declarations in descending order (demand curve).
- Determination of the marginal price of the system from the section of the supply curve and the demand curve.

So, the unit for which the supply is equated with the demand is called the marginal unit of the system and the cost of this unit is called the marginal price of the system (Press conference of the syndicalist of Public Power Corporation, 2007).

Artificial neural networks (ANNs) have received more and more attention in financial time series forecasting in recent years. This popularity springs from their capability of performing highly complex mappings on nonlinear data. Nonetheless, they have some significant drawbacks such as the lack of any restrictive assumptions about the functional relationships between the predictor variables and the predicated variable, the difficulty to deal with qualitative information and the 'black box' syndrome. On the other hand, fuzzy inference systems incorporate human knowledge by using the if-then rules and expertise for inferencing and decision making. However, the disadvantage of fuzzy logic is the lack of self-learning capability. This is the reason why the integration of these two approaches is preferred in order to overcome the disadvantages not only of the neural networks but also of the fuzzy systems and results in neuro-fuzzy system models.

The purpose of this paper is to forecast the marginal price that Greek Transmission System Operator (TSO - DESMIE) pays for electricity supply, therefore taking advantage of the benefits of both a neural network and a fuzzy inference system. The rest of the paper is organized as follows: Section 2 reviews related research and Section 3 discusses the proposed methodology. Section 4 outlines the data and reports the empirical findings, while Section 5 includes the conclusions and some further discussions about the future research in this sector.

2. Literature review and related work

Remarkable research has been done in the field of electricity as far as marginal price forecasting is concerned. The methods used in the published papers vary from artificial neural networks, fuzzy logic, and stochastic models to integration of one or more methods. These related researches are the following:

Azevedo and Vale (2006) have forecasted electricity prices with historical statistical information and using neural networks and K-means clustering

method in order to find clusters.Amjady and Keynia (2009) have forecasted price of electricity markets one day ahead combining a mutual information technique and cascaded neuro-evolutionary algorithm.Aggarwal et al. (2009) have reviewed and evaluated the techniques used so far to forecast electricity price in deregulated markets, including stochastic time series, causal models and artificial intelligence based models.Catalao et al. (2007) have forecasted short-term electricity prices in a competitive market using a neural network approach.Nwulu and Fahrioglu (2012) have forecasted locational marginal price using artificial neural networks and support vector machines.Li et al. (2010) have reviewed the existing techniques to forecast electricity price in a grid environment and have showed a forecasting system, which combines fuzzy inference system and least-squares estimation.Esfahani (2011) has forecasted short-term electricity price using a neuro-fuzzy approach, which was developed through a Matlab-based software.Ercan and Soto (2011) have forecasted long term electricity price for France using a deterministic and a stochastic model.Zareipour et al. (2006) have forecasted the hourly Ontario energy price using multivariate adaptive regression splines.Kourtis et al. (2011) have reviewed the various methodologies used to forecast electricity price and load demand.Haghi and Tafreshi (2007) have reviewed and verified the different models used to forecast electricity price and have proposed Hidden Markov Models as a forecasting method.Aggarwal et al. (2008) have forecasted electricity pricein Australian electricity market using wavelet transform and LSE based mixed model.Torbaghan (2010) has forecasted medium term electricity price in Ontarioand Nord pool electricity market using dataand various models, such as Linear Regression Model, Radial Basis Function Neural Network, Support Vector Machine and Weighted Nearest Neighbor.Aggarwal et al. (2009) have reviewed statistical models and key issues as far as short term price forecasting in deregulated electricity markets is concerned.Dias (2009) has forecasted hourly electricity prices in the Portuguese power market using ARIMA models.Al-Shakhs (2011) has forecasted marginal price of electric power spot market one day ahead using an innovated forecasting approach, which combines Multiple Linear Regression and Artificial Neural Networks.Szkuta et al. (1999) have forecasted short-term electricity price using artificial neural networks.Pindoriya et al. (2008) have forecasted energy price in electricity markets using an adaptive wavelet neural network.Hong and Lee (2005) have forecasted locational marginal prices in deregulated electricity markets using a neuro-fuzzy method.Amjady (2006) has forecasted short-term prices of electricity markets one day ahead using a fuzzy neural network.

3. ANFIS architecture

This paper considers the development of a of an adaptive neuro-fuzzy inference system (ANFIS) to forecast the marginal price that Greek Transmission System Operator (TSO - DESMIE) pays for electricity supply based on the innovative neuro-

fuzzy methodology of Jang (Jang, 1993), which differs from the traditional ANN(Artificial Neural Networks) in that it is not fully connected and not all the weights or nodal parameters are modifiable.Essentially, the fuzzy rule base is encoded in a parallel fashion so that all the rules are activated simultaneously, so as to allow network training algorithms to be applied.As in Jang's original work, the model uses a hybrid learning algorithm to identify the parameters for the Sugeno-type fuzzy inference systems. It applies a combination of the least-squares method and the back-propagation gradient descent method for training the Fuzzy Inference System (FIS) membership function parameters to emulate the given training data set. Specifically, a back-propagation algorithm is used to optimize the fuzzy sets of the premises and a least-squares procedure is applied to the linear coefficients in the consequent terms.In addition, it uses a testing data set for checking the model over fitting. ANFIS is a multilayer neural network-based fuzzy consisted of five layers, in which the training and predicted values are represented by the input and output nodes and the nodes functioning as membership functions (MFs) and rules are presented in the hidden layers. Its topology is shown in Figure 1. During the learning phase of ANFIS, the parameters of the membership functions are changing continuously in order to minimize the error function between the target output and the calculated values.This architecture has the benefit that it eliminates the disadvantage of a normal feed forward multilayer network, where it is difficult for an observer to understand or modify the network.

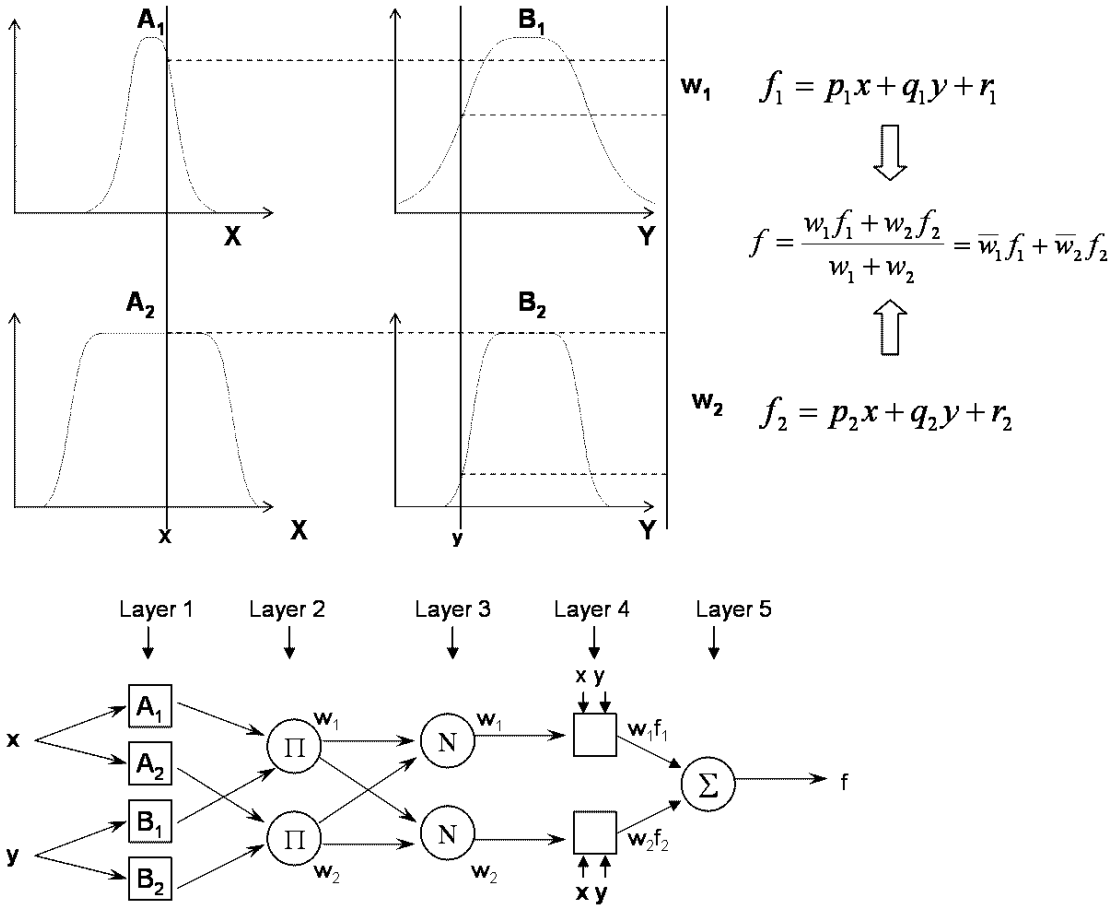

Figure 1: An illustration of the reasoning mechanism for a Sugeno-type model and the corresponding ANFIS architecture (Jang, 1997)

As seen from Figure1, different layers of ANFIS have different nodes. Each node in a layer is either fixed or adaptive (Jang 1993).For simplicity, it is assumed that the examined fuzzy inference system has two inputs, x and y, and one output. For the first-order Sugeno fuzzy model, a typical fuzzy rule set in this model, with two fuzzy If-Then rules, has the following form:

$$\text{Rule1: If } x \text{ is } A_1 \text{ and } y \text{ is } B_1 \text{ then } f_1 = p_1 \cdot x + q_1 \cdot y + r_1 \qquad (2)$$

$$\text{Rule2: If } x \text{ is } A_2 \text{ and } y \text{ is } B_2 \text{ then } f_2 = p_2 \cdot x + q_2 \cdot y + r_2 \qquad (3)$$

This architecture develops an adaptive network that is functionally equivalent to a two inputs first-order Sugeno fuzzy model with four rules, where each input has two membership functions. The error measure to train the aforementioned ANFIS is defined as:

$$E = \sum_{k=1}^{n} (y_k - \hat{y}_k)^2 \quad (4)$$

where y_k and $\hat{y}_k$ are the kth desired and estimated output, respectively, and n is the total number of pairs (inputs–outputs) of data in the training set. Due to its efficiency and transparency, ANFIS is outperforming other models.

4. Experimental data and performance of the model

The experimental data concerns the marginal pricesof the Greek Operator System and consists of daily time series of the average marginal prices, ranging from 1/1/2011 to 21/10/11, in total 290 samples. The model forecasts the marginal prices one step ahead. The 260 samples have been used as training data for training the model and the remaining 30 have been used as evaluation data to test the prediction performance of the resulting model. The structure of ANFIS consist one input and one output, which means that the forecasting system is used to forecast the next daymarginal prices value based on the previous values. The method of trial and error is used in order to decide the type and number of membership functions, the number of epochs and the step size that best describe the model and provide the lowest error. The optimal fuzzy inference is achieved after 2000 epochs with two membership functions of gauss2 shape and the step size set in 0.01. Figure 2 depicts the initial MFs of each input variable before the training of the model and figure 3 depicts the final MFs after the completion of the training process. The comparison between the initial and the final MFs of the input data indicates important differences and the model resulted in remarkable deviation between the initial and the final MFs.

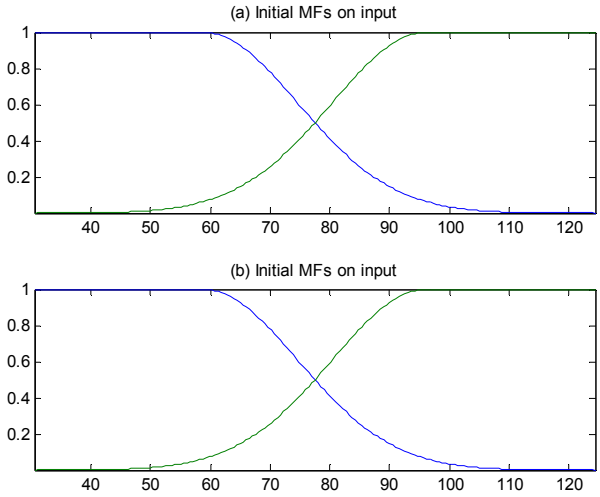

Figure 2: Form of Membership Functions before training

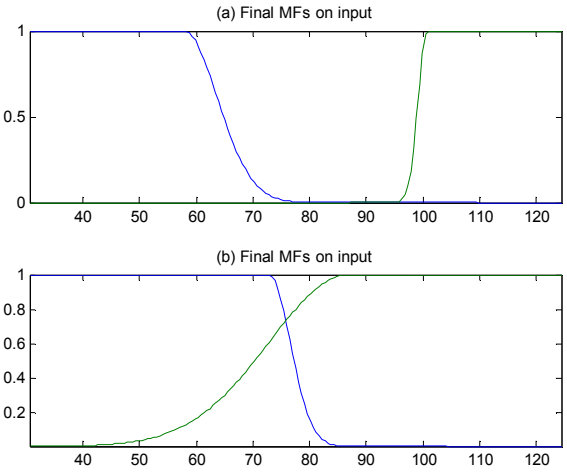

Figure 3: Form of Membership Functions aftertraining

Moreover, figure 4 depicts the out of sample results produced by the Adaptive-Network-based Fuzzy Inference System (ANFIS). It can be seen that the actual values and the values from the ANFIS prediction are almost identical, which means that the model is performing satisfactory.

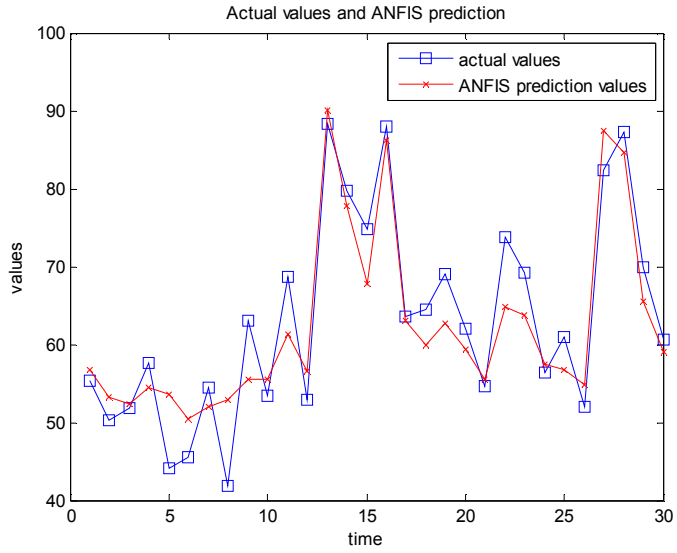

Figure 3: ANFIS out of sample forecasting results

Lastly, figure 4 shows the ANFIS error curves and the ANFIS step size curve.

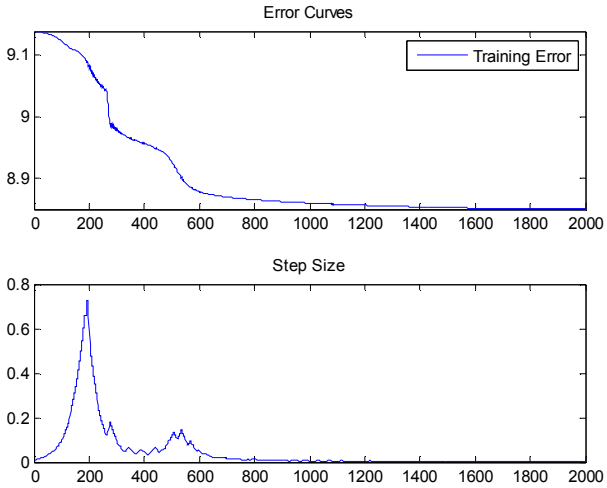

Figure 4: ANFIS error curves and ANFIS step size curve

The network applies 4 rules and there is one input and one output. Table 1 describes the type and values of the ANFIS parameters.

Table 1:ANFIS parameter types and their values used for training

ANFIS parameter type	**Value**
MF type	Gauss2 function
Number of MFs	2
Output MF	Linear
Number of Nodes	21

Number of linear parameters	12
Number of nonlinear parameters	16
Total number of parameters	28
Number of training data pairs	260
Number of evaluating data pairs	30
Number of fuzzy rules	4

During the evaluation phase, the out of sample data is carried out and the output of the model is compared with the actual data of the next day. The performance of the model is examined using the main statistical criteria of: Mean square error(MSE), Root mean square error(RMSE), Mean absolute error(MAE) and Mean absolute percentage error(MAPE). Table 2 summarizes the results of the statistical analysis.

Table 2: Statistical performance of the ANFIS model

	ANFIS
MSE	23.6824
RMSE	4.8665
MAE	4.0055
MAPE	6.7508

The results indicate that the forecasting performance of ANFIS is satisfactory and acceptable both in research and in practice.

5. Conclusion

This paper presents a Fuzzy Inference System for the prediction of daily marginal prices of the Greek Operator System. The model is developed using Matlab software. The results of the prediction are satisfactory and encouraging. Fuzzy logic theory could predict well, as far as modeling on uncertain data is concerned. ANFIS and its use to forecast the marginal price that Greek Transmission System Operator (TSO - DESMIE) pays for electricity supplyhave the following advantages:

a) ANFIS is simple to maintain and apply on forecast practically.

b) It combines the capabilities of fuzzy systems and neural networks.

c) Fuzzy rule based system incorporates the flexibility of human decision making by means of the use of fuzzy set theory and makes use of fuzzy linguistic terms described by MFs.

d) It requires fewer and simpler trials and errors for optimization of their architecture.

e) It is nonlinear and capable of adapting and learning fast from numerical and linguistic knowledge.

f) ANFIS is a model-free, easy to implement approach. In contrast to traditional time series methods, little training is needed to calculate predictions with ANFIS. It implements a single-fitting procedure to nonlinear situations, without the need of establishing a formal model for the problem being resolved. Thus, no a priori information is required to determine the empirical relationship between explanatory and predicted variables and the method suitability is always tested a posteriori.

g) The transparent rule structure of ANFIS allows the researcher to extract information about the empirical relationship between the inputs and the outputs over time and to provide concise explanations.

In conclusion, these prediction results can provide useful information and guidance for electricity market analysts and managers of the Greek Operator System. Yet, further research is recommended in order to improve the forecast results, such as the introduction of more inputs to the model, the introduction of data not only for the year 2011 but also for previous years, the comparison of the forecast results with the forecast results of other models or the comparison of the forecast results with the forecast results of the same or other models for other countries.

6. References

1. Aggarwal S.K., L.M. Saini, Ashwani Kumar (2008), Price forecasting using wavelet transform and LSE based mixed model in Australian electricity market, International Journal of Energy Sector Management, Vol. 2, Issue 4, pp. 521-546
2. AggarwalKumar Sanjeev, L.M. Saini, Ashwani Kumar (2009), Short term price forecasting in deregulated electricity markets: A review of statistical models and key issues
3. Aggarwal Kumar Sanjeev, Lalit Mohan Saini, Ashwani Kumar (2009), Electricity price forecasting in deregulated markets: A review and evaluation, Electrical Power and Energy Systems, Vol. 31, Issue 1, pp. 13-22
4. Al-Shakhs H. Mohammed (2011), Day-ahead marginal price forecasting of electric power spot market using innovated forecasting approaches, Master Thesis, Dalhousie University, Department of Electrical and Computer Engineering, Halifax, Nova Scotia

5. AmjadyNima and FarshidKeynia (2009), Day-ahead price forecasting of electricity markets by mutual information technique and cascaded neuro-evolutionary algorithm, IEEE Transactions on Power Systems, pp. 306-318
6. AmjadyNima (2006), Day-ahead price forecasting of electricity markets by a new fuzzy neural network, IEEE Transactions on Power Systems, Vol. 21, No. 2, pp. 887-896
7. Azevedo Filipe and Zita A. Vale (2006), Forecasting electricity prices with historical statistical information using neural networks and clustering techniques, Power Systems Conference and Exposition, PSCE, IEEE, pp. 44-50
8. Bakirtzis G. Anastasios (2009), Marginal price of the Greek Transmission Operator System, Conference on Networks, Interconnections and Supply of Electricity in Greece, Conference and Culture Center of Patrai University
9. Catalao J.P.S., S.J.P.S. Mariano, V.M.F. Mendes, L.A.F.M. Ferreira (2007), Short-term electricity prices forecasting in a competitive market: A neural network approach, Electric Power Systems Research, Vol. 77, Issue 10, pp. 1297-1304
10. Dias Vasconcellos Antonio (2009), Forecasting hourly prices in the Portuguese power market with ARIMA models, Master Thesis, ISCTE Business School, Lisbon
11. ErcanPelin and Javier Soto (2011), A model for long term electricity price forecasting for France, Master Thesis, School of Electrical Engineering KTH, Royal Institute of Technology, Stockholm
12. Esfahani M. (2011), Neuro-fuzzy approach for short-term electricity price forecasting developed MATLAB-based software, Fuzzy Information and Engineering, Springer, Vol. 3, No. 4, pp. 339-350
13. HaghiValizadehHamed and S. M. MoghaddasTafreshi (2007),An overview and verification of electricity price forecasting models, International Power Engineering Conference, IPEC, IEEE, pp. 724-729
14. Hong Ying-Yi, Chuan-Fang Lee (2005), A neuro-fuzzy price forecasting approach in deregulated electricity markets, Electric Power Systems Research, Vol. 73, Issue 2, pp.151-157
15. Jang J. S.R., C.T. Sun and E. Mizutani (1997), Neuro-Fuzzy and Soft Computing, Prentice-Hall
16. Jang J. S.R. (1993), ANFIS: Adaptive network-based fuzzy inference system, IEEE Trans Systems, Man Cybern, Vol. 23, No. 3, pp. 665-685
17. Kourtis George, IoannisHadjipaschalis, Andreas Poullikkas (2011), An overview of load demand and price forecasting methodologies, International Journal of Energy and Enviroment, Vol. 2, Issue 1, pp. 123-150
18. Li Guang, Jacques Lawarree and Chen-Ching Liu (2010), State-of-the-Art of electricity price forecasting in a grid environment, Handbook of Power Systems II, Energy Systems, Springer
19. Ministry of Enviroment Energy and Climate Change, http://www.ypeka.gr/Default.aspx?tabid=276&locale=en-US&language=el-GR
20. Nwulu I. Nnamdi and Murat Fahrioglu (2012), A soft computing approach to projecting locational marginal price, Neural Computing and Applications, Springer

21. Pindoriya N. M., S. N. Singh, S. K. Singh (2008), An adaptive wavelet neural network-based energy price forecasting in electricity markets, IEEE Transactions on Power Systems, Vol. 23, No. 3, pp. 1423-1432
22. Press conference of the syndicalists of Public Power Corporation, 2007, www.genop.gr
23. Regulatory Authority For Energy, www.rae.gr
24. Szkuta B.R., L.A. Sanabria, T.S. Dillon (1999), Electricity price short-term forecasting using artificial neural networks, IEEE Transactions on Power Systems, Vol. 14, No. 3, pp. 851-857
25. TorbaghanShariatShahab (2010), Master Thesis, Department of Energy and Enviroment, Division of Electric Power Engineering, Chalmers University of Technology, Goteborg, Sweden
26. Zareipour H., K. Bhattacharya, C.A. Canizares (2006), Forecasting the hourly Ontario energy price by multivariate adaptive regression splines, Power Engineering Society General Meeting, IEEE, page 7

A Unifying Approach to Importance Measures for Nonrepairable Components of Binary Coherent Systems

Frank Beichelt

School of Statistics and Actuarial Science
University of the Witwatersrand
Johannesburg, Republic of South Africa
Email: Frank.Beichelt@wits.ac.za

Abstract: The components (subsystems) of a complex system usually have different degrees of influence on its failure behavior and on its availability. For the reliability engineer, it is important to quantify this influence. Corresponding analytical criteria are called *importance measures*. Importance measures for components have been among else introduced by *Birnbaum*, *Butler*, *Vesely* and *Fussel*, *Arndt* and *Kirstein*, *Meng*, *Barlow* and *Proschan*, *Natvig*, *Bergman,* and *Xie*. This paper proposes and discusses a general importance measure for components, which contains some of the established ones as special cases.

Keywords: Binary systems, availability, reliability, importance measures, yield importance.

1 Introduction

We consider a binary coherent system S with components $c_1, c_2, ..., c_n$. The corresponding *indicator variables* for the two states 1 (*available*) and 0 (*unavailable*) are

$$z_i = \begin{Bmatrix} 1 \text{ if } c_i \text{ is available} \\ 0 \text{ otherwise} \end{Bmatrix}, \; i = 1,2,...,n; \quad z_S = \begin{Bmatrix} 1 \text{ if } S \text{ is available} \\ 0 \text{ otherwise} \end{Bmatrix}.$$

In a coherent system, the states z_i of the components uniquely determine the state of the system. Hence there exists a function φ with property $z_S = \varphi(\mathbf{z})$ with $\mathbf{z} = (z_1, z_2, ..., z_n)$. Function φ is called the *structure function* of S, and n is its *order*. Usually, φ is not uniquely defined. Throughout the paper we assume that $z_1, z_2, ..., z_n$ are independent random variables. The probabilities $p_S = P(z_S = 1)$ and $p_i = P(z_i = 1), i = 1,2,...,n,$ are the *availabilities* of the system and its components, respectively. They refer to a fixed or a variable time point t or to the stationary regime (given that failed components are renewed after failures in finite time intervals). If we need to explicitly characterize the time dependencies of the components and the system, we write $p_i = p_i(t)$ and $p_S = p_S(t)$. Then, in case without renewal of failed components, the $p_S(t)$ and $p_i(t)$ are the *survival probalilities* ('*reliabilities*') of the system and its components, respectively. Since we

only consider systems without renewal, we will generally refer to p_S and p_i as '*reliabilities'*. The system reliability is given by $p_S = E((\varphi(z_1, z_2, ..., z_n))$. Since the components operate independently, p_S is only a function of the vector of the component reliabilities $\mathbf{p} = (p_1, p_2, ..., p_n)$: $p_S = h(\mathbf{p})$. The crucial, but easily to verify *pivotal decomposition formula* for $h(\mathbf{p})$ with *pivotal component* c_i is

$$h(\mathbf{p}) = p_i h((1_i, \mathbf{p})) + (1 - p_i)\, h((0_i, \mathbf{p}))\,, \tag{1}$$

where the vectors $(r_i, \mathbf{p})$ are defined as

$$(r_i, \mathbf{p}) = (p_1, p_2, ..., p_{i-1}, r, p_{i+1}, ..., p_n), \quad r = 0 \text{ or } 1,\ i = 1, 2, ..., n. \tag{2}$$

Apart from series and parallel systems with identical components, components have different degrees of influence on the failure behavior of *S*. For the reliability engineer, this influence is interesting with regard to the following questions:

1. What is the contribution of a component to the system availability?
2. How varies the system availability in dependence on the availability of a component?
3. What maximum increase in system availability can be achieved if the availability of a component is increased?
4. What component causes most likely a system failure?
5. What components contribute most likely to a system failure?

The significance of the influence of components with regard to one or more of these or related questions is quantified by so-called *importance measures*. Knowledge of these measures is a key information for the design and possible upgrading of systems from the reliability point of view as well as for their efficient maintenance. For instance, if the availability of a system has to be increased by upgrading its components, then ordering the components with regard to importance measures, which refer to questions 1 to 3, is crucial. On the other hand, if the order of the components with regard to importance criteria referring to questions 4 and/or 5 is known, then this will facilitate the search for the cause of a system failure. Importance measures have not only be defined for components, but also for subsets of components, e.g. minimal path- and cut sets.

In section 2, some important importance measures will be summarized, and in section 3 they are formally seen to be special cases of a general and fairly flexible importance measure called *reliability* or *availability yield importance*. For a more comprehensive survey, see e.g. *Beichelt* and *Tittmann* (2012).

2 Importance Measures for Components

Birnbaum-Importance The first, most simple, but nevertheless up to now crucial importance measure is due to *Birnbaum* (1969). The *Birnbaum-importance* (*B-importance*) $I_B(i, \mathbf{p})$ of component c_i is defined as

$$I_B(i,\mathbf{p}) = h((1_i,\mathbf{p})) - h((0_i,\mathbf{p})). \tag{3}$$

An equivalent definition is

$$I_B(i,\mathbf{p}) = P(\varphi((1_i,\mathbf{z})) - \varphi((0_i,\mathbf{z})) = 1), \tag{4}$$

where the vectors $(r_i,\mathbf{z})$, $r = 0,1,$ are defined analogously to (2). Thus, $I_B(i,\mathbf{p})$ can be interpreted as the probability that the renewal of only the failed component c_i, when the system is unavailable, restores the availability of the system. Since the sum of the B-importances generally does not add up to 1, a *standardized B-importance* $I_{B,S}(i,\mathbf{p})$ may be a more useful importance measure:

$$I_{S,B}(i,\mathbf{p}) = \frac{I_B(i,\mathbf{p})}{\sum_{k=1}^{n} I_B(k,\mathbf{p})}, \quad i = 1,2,...,n. \tag{5}$$

Reliability Improvement Potential The *B*-importance of elements only answers question 3. This is because $I_B(i,\mathbf{p})$ is the maximally possible increase in system reliability due to c_i, namely if the reliability of c_i is increased from 0 to 1, i.e. if a new, absolute reliable component is introduced into the system. Such an increase is, however, a hypothetical parameter, since normally a component comes with a positive reliability. Instead, the actual changes in system reliability are of interest, which are induced by changing the reliability of a component. Helpful for solving this problem and in answering questions 1 and 2 in the introduction are the following two modified *B*-importance measures, also proposed by *Birnbaum* (1969)

$$I_0(i,\mathbf{p}) = h(\mathbf{p}) - h((0_i,\mathbf{p})), \quad I_1(i,\mathbf{p}) = h((1_i,\mathbf{p})) - h(\mathbf{p}). \tag{6}$$

By making use of the decomposition formula (1),

$$I_0(i,\mathbf{p}) = p_i I_B(i,\mathbf{p}), \quad I_1(i,\mathbf{p}) = (1-p_i) I_B(i,\mathbf{p}). \tag{7}$$

A significant advantage to $I_B(i,\mathbf{p})$ is that $I_0(i,\mathbf{p})$ and $I_1(i,\mathbf{p})$ depend on p_i. The measures I_0 (I_1) linearly increase (decrease) with increasing p_i. Their interpretation is obvious. Again, standardized versions of I_0 and I_1 can be defined.

Barlow-Proschan Importance We now consider time-dependent component availabilities $p_i = p_i(x)$. Let L_i be the lifetime of c_i with distribution function $F_i(x)$ and density $f_i(x)$. Then $p_i(x) = 1 - F_i(x)$, and by (3) and (4), the probability that c_i causes a system failure in $(x, x+\Delta x]$ is $I_B(i,\mathbf{p}(x))\, f_i(x)\Delta x + o(\Delta x)$. Therefore, the probability that c_i causes as system failure in $(0,t]$ is

$$\int_0^t I_B(i,\mathbf{p}(x))\, f_i(x)dx.$$

The *Barlow-Proschan-importance* (*BP-importance*) of c_i is

$$I_{BP}(i,t,\mathbf{p}) = \frac{\int_0^t I_B(i,\mathbf{p}(x))\, f_i(x)dx}{\sum_{k=1}^n \int_0^t I_B(k,\mathbf{p}(x))\, f_k(x)dx}. \tag{8}$$

Thus, given the system fails in $(0,t]$, $I_{BP}(i,t,\mathbf{p})$ is the probability that the failure of c_i has triggered this system failure. Hence, the *BP*-importance refers to question 4. As a special case, if $t \to \infty$, then $I_{BP}(i,t,\mathbf{p})$ simply becomes the probability that the system failure occurring anytime in $(0,\infty)$ has been triggered by the failure of c_i :

$$I_{BP}(i,\mathbf{p}) = \int_0^\infty I_B(i,\mathbf{p}(x))\, f_i(x)dx. \tag{9}$$

Natvig-Importance *Natvig* (1979, 1985) (for extensions see *Natvig* and *Gåsemyr* (2010)), considered that component most important, the failure of which reduces the expected residual system lifetime most. Let $\overline{F}_i(t) = 1 - F_i(t)$ be the survival function of c_i, and $L_R(i)$ be the residual system lifetime from the time point at which component c_i fails. Then the *Natvig-importance* of c_i is

$$I_N(i) = \frac{E(L_R(i))}{\sum_{k=1}^n E(L_R(k))}, \tag{10}$$

where

$$E(L_R(i)) = -\int_0^\infty I_B(i,\mathbf{p}(x))\, \overline{F}_i(x) \ln \overline{F}_i(x)dx.$$

Bergman's Importance In case of time-dependent component reliabilities, *Bergman* (1985) proposed a powerful generalization of the transition from $I_B(i,\mathbf{p})$ to $I_1(i,\mathbf{p})$. He considered the increase in the expected system lifetime if $\overline{F}_i(x)$ is replaced by a survival function $\overline{G}_i(x)$ with property $\overline{G}_i(x) > \overline{F}_i(x)$ for $x > 0$. Let

$$\mathbf{p} = \left(\overline{F}_1, \overline{F}_2, ..., \overline{F}_n\right) \text{ and } \left(\overline{G}_i, \mathbf{p}\right) = (p_1, p_2, ..., p_{i-1}, \overline{G}_i, p_{i+1}, ..., p_n).$$

Then this increase is

$$\Delta_{Be}(i,\overline{\mathbf{G}},\mathbf{p}) = \int_0^\infty h((\overline{G}_i(x),\mathbf{p}(x)))\, dx - \int_0^\infty h((\mathbf{p}(x))\, dx.$$

Formulas (1) and (3) yield

$$\Delta_{Be}(i,\overline{\mathbf{G}},\mathbf{p}) = \int_0^\infty \left[\overline{G}_i(x) - \overline{F}_i(x)\right] I_B(i,\mathbf{p}(x))\, dx. \tag{11}$$

With regard to $\overline{\mathbf{G}} = (\overline{G}_1, \overline{G}_2, ..., \overline{G}_n)$, component c_i has the *Bergman-importance*

$$I_{Be}(i,\overline{\mathbf{G}},\mathbf{p}) = \frac{\Delta_{Be}(i,\overline{\mathbf{G}},\mathbf{p})}{\sum_{k=1}^{n}\Delta_{Be}(k,\overline{\mathbf{G}},\mathbf{p})},\ i=1,2,...,n. \tag{12}$$

Xie's Lifetime Yield Importance Bergman's importance concept is based on a yield (increase) in the expected system lifetime. He already suggested that a more general yield concept could serve as a basis for a more general importance measure, which may take into account other than reliability aspects as well, e.g. economical ones. To construct such a criterion, *Xie* (1987) introduced a *yield function* $Y(x)$ with properties $Y(+0)=0$ and $Y(\infty)<\infty$ as a function of the system lifetime $L_s = x.$ If $Y(x)$ is differentiable, the corresponding *yield rate* is $y(x) = dY(x)/dx.$ Since $F_s(x) = P(L_s \le x) = 1 - h(\mathbf{p}(x))$, the expected yield in $[0, L_s)$ due to the operation of the system is

$$E(Y(L_s)) = \int_0^\infty Y(x)\,dF_s(x) = \int_0^\infty h(\mathbf{p}(x))y(x)dx.$$

Analogously to the derivation of (11), the expected yield increase if replacing $\overline{F}_i(x)$ with $\overline{G}_i(x)$, $\overline{G}_i(x) > \overline{F}_i(x)$ for $i=1,2,...,n,$ is seen to be

$$\Delta_X(i,Y,\overline{\mathbf{G}},\mathbf{p}) = \int_0^\infty [\overline{G}_i(x) - \overline{F}_i(x)]y(x)I_B(i,\mathbf{p}(x))\,dx,\ i=1,2,...,n. \tag{13}$$

Xie's lifetime yield importance of component c_i is defined as

$$I_X(i,Y,\overline{\mathbf{G}},\mathbf{p}) = \frac{\Delta_X(i,Y,\overline{\mathbf{G}},\mathbf{p})}{\sum_{k=1}^{n}\Delta_X(k,Y,\overline{\mathbf{G}},\mathbf{p})},\ i=1,2,...,n.$$

For a thorough discussion of this importance measure see *Xie* and *Bergman* (1991).

3 Reliability Yield Importance

Instead of relating a yield to the system lifetime, it may frequently be a more adequate approach to assign a yield to the system reliability. Let $Y = Y(z)$ be a real-valued, nonnegative, and increasing function on $[0, 1],$ and

$$I_R = \int_0^\infty Y(h(\mathbf{p}(x))\,dx < \infty.$$

Note that $\widetilde{Y}(x) = Y(h(\mathbf{p}(x)))$ is a decreasing function in $x,\ 0 \le x < \infty.$ I_R is the total *reliability yield* due to the work of the system to its failure. Analogously to the derivation of (12), the increase in I_R if $\overline{F}_i(x)$ is replaced with $\overline{G}_i(x),$ is seen to be

$$\Delta_R(i,Y,\overline{\mathbf{G}},\mathbf{p}) = \int_0^\infty \left[\overline{G}_i(x) - \overline{F}_i(x)\right] I_{B,Y}(i,\mathbf{p}(x))\,dx,\ i=1,2,...,n, \tag{14}$$

where the Birnbaum-yield-importance $I_{B,Y}(i,\mathbf{p})$ of c_i is (compare to (1))

$$I_{B,Y}(i,\mathbf{p}) = Y(h((1_i,\mathbf{p})) - Y(h((0_i,\mathbf{p}))), \quad i = 1,2,...,n. \tag{15}$$

$I_{B,Y}(i,\mathbf{p})$ can be interpreted as the economical or any other profit arising from installing the absolute reliable component c_i in the system. (For a somewhat related idea see *Samaniego* and *Shaked* (2008)). Now, with regard to a vector of survival functions $\overline{\mathbf{G}} = (\overline{G}_1, \overline{G}_2, ..., \overline{G}_n)$, the *reliability yield importance* of component c_i if $\overline{F}_i$ is replaced with $\overline{G}_i$ is defined as

$$I_R(i,Y,\overline{\mathbf{G}},\mathbf{p}) = \frac{\Delta_R(i,Y,\overline{\mathbf{G}},\mathbf{p})}{\sum_{k=1}^{n}\Delta_R(k,Y,\overline{\mathbf{G}},\mathbf{p})}, \quad i = 1,2,...,n. \tag{16}$$

If only an importance ranking of the components is required, then the calculation of the $\Delta_R(i,Y,\overline{\mathbf{G}},\mathbf{p}),\ i = 1,2,...,n,$ is sufficient. By suitable choice of the yield function Y as well as $\overline{F}_i$ and $\overline{G}_i$, it can be established that the time-dependent importance measures introduced in section 2 are formally special cases of the reliability yield importance:

1. *Standardized B-importance*: $I_{B,S}(i,\mathbf{p})$ as given by (5) is obtained from the reliability yield importance (16) by letting there $Y(x) \equiv 1,\ \overline{F}_i(x) \equiv 0,\ \overline{G}_i(x) \equiv 1.$

2. *Bergman-importance*: $I_{Be}(i,\overline{\mathbf{G}},\mathbf{p})$ as given by (12) is obtained from the reliability yield importance (16) by letting there $Y(x) \equiv 1.$

3. *Barlow-Proschan importance*: $I_{BP}(i,\mathbf{p})$ as given by (9) is seen to be a special case of (16) when replacing the yield function $\widetilde{Y}(x) = Y(h(\mathbf{p}(x)))$ with

$$\widetilde{Y}(x) = h(\mathbf{p}(x))\frac{f_i(x)}{\overline{G}_i(x) - \overline{F}_i(x)}, \quad \overline{G}_i(x) - \overline{F}_i(x) > 0, \quad 0 < x < \infty.$$

The more general BP-importance (8) we get from (16) by replacing the yield function $\widetilde{Y}(x) = Y(h(\mathbf{p}(x)))$ with

$$\widetilde{Y}(x) = \left\{ \begin{matrix} h(\mathbf{p}(x))\dfrac{f_i(x)}{\overline{G}_i(x) - \overline{F}_i(x)} & \text{for } 0 < x \le t, \\ 0, & \text{otherwise} \end{matrix} \right\}.$$

4. *Natvig-importance*: $I_N(i,\mathbf{p})$ we get from (16) by replacing $\widetilde{Y}(x) = Y(h(\mathbf{p}(x)))$ by

$$\widetilde{Y}(x) = h(\mathbf{p}(x))\frac{\overline{F}_i(x)\ln\overline{F}_i(x)}{\overline{G}_i(x) - \overline{F}_i(x)}.$$

5. *Xie's lifetime yield importance*: $I_N(i,\mathbf{p})$ we get from (16) by replacing the yield function $\widetilde{Y}(x) = Y(h(\mathbf{p}(x)))$ with

$$\widetilde{Y}(x) = h(\mathbf{p}(x))\, y(x).$$

Thus, the importance measures **1** to **4** are special cases of Xie's yield importance.

Example Let us consider a 3-component series-parallel-system the reliability block diagram of which is given by the following figure:

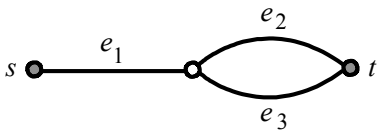

The components are assumed to operate independently of each other and have at a fixed time point the reliabilities $p_1, p_2,$ and p_3. Then the reliability of the system is

$$p_s = h(\mathbf{p}) = p_1p_2 + p_1p_3 - p_1p_2p_3.$$

In particular, for $p = p_i$, $i = 1, 2, 3,$ we have

$$h(1_1,\mathbf{p}) = 2p - p^2,\ h(0_1,\mathbf{p}) = 0,$$
$$h(1_2,\mathbf{p}) = h(1_3,\mathbf{p}) = p,\ h(0_2,\mathbf{p}) = h(0_3,\mathbf{p}) = p^2.$$

Now, let us assume that the lifetimes of the components are identically exponentially distributed with parameter λ: $p_i(x) = e^{-\lambda x}$, $\lambda > 0$, $x \geq 0$, $i = 1,2,3,$ Then, for a quadratic yield function $\widetilde{Y}(x) = (h(\mathbf{p}(x)))^2$ the corresponding time-dependent Birnbaum-yield importances are

$$I_{B,Y}(1,\mathbf{p}(x)) = 4e^{-2\lambda x} - 4e^{-3\lambda x} + e^{-4\lambda x}, \tag{17}$$
$$I_{B,Y}(2,\mathbf{p}(x)) = I_{B,Y}(3,\mathbf{p}(x)) = e^{-2\lambda x} - e^{-4\lambda x}. \tag{18}$$

Let the replacement survival probabilities of the components be $\overline{G}_i(x) = e^{-\mu x}$ for $0 < \mu < \lambda,\ x \geq 0.$ Then $\overline{G}_i(x) > \overline{F}_i(x),\ x > 0,\ i = 1,2,3.$ From (14), (17) and (18),

$$\Delta_R(1,Y,\overline{\mathbf{G}},\mathbf{p}) = \frac{4}{2\lambda+\mu} - \frac{4}{3\lambda+\mu} + \frac{1}{4\lambda+\mu} - \frac{8}{15\lambda},$$

$$\Delta_R(2,Y,\overline{\mathbf{G}},\mathbf{p}) = \Delta_R(3,Y,\overline{\mathbf{G}},\mathbf{p}) = \frac{1}{2\lambda+\mu} - \frac{1}{4\lambda+\mu} - \frac{2}{15\lambda}.$$

In particular, for $\mu = \lambda/2,$

$$I_R(1,Y,\overline{\mathbf{G}},\mathbf{p}) = 0.6216, \quad I_R(2,Y,\overline{\mathbf{G}},\mathbf{p}) = I_R(3,Y,\overline{\mathbf{G}},\mathbf{p}) = 0.1892.$$

As expected, if emphasis is on the reliability yield rather than the increase in the expected system lifetime:

$$I_R(1,Y,\overline{\mathbf{G}},\mathbf{p}) = 0.6216 > I_{Be}(1,\overline{\mathbf{G}},\mathbf{p}) = 0.5714.$$

Remark The total reliability yield due to the work of the system in the finite interval $[0,t]$ is $I_R(t) = \int_0^t Y(\mathbf{p}(x))dx$. $I_R(t)$ can serve as the base for defining importance measures $I_R(i,t,Y,\overline{\mathbf{G}},\mathbf{p})$ for the components analogously to (16).

References

1. Arndt, K. and B. Kirstein, An importance ranking for systems with highly reliable components. *Elektron. Informationsverarb.&Kybernetik* 19: 535-545 (1983).

2. Beichelt, F. and P. Tittmann, *Reliability and Maintenance: Networks and Systems.* Chapman & Hall/CRC: Boca Raton, London, New York (2012).

3. Barlow, R.E. and F. Proschan, Importance of systems and fault tree events. *Stochastic Processes and Applications* 3: 153-173 (1975).

4. Bergman, B., On some new reliability importance measures. *Proceedings of the IFAC SAFECOMP*'85 (ed.: J. Quirk), Como: 61-64 (1985).

5. Birnbaum, Z., On the importance of different components in a multi-component system. In: *Multivariate Analysis II*. New York: Academic Press (1969).

6. Natvig, B., A suggestion of a new measure of importance of system components. Stochastic Processes and their Applications 9: 319-330 (1979).

7. Natvig, B., New light on measures of system components. *Scandinavian Journ. of Statistics* 12: 43-54 (1985).

8. Natvig, B., On the reduction in remaining system lifetime due to the failure of a specific component. *Journal of Applied Probability* 19: 642-652 (1987).

9. Natvig, G. and J. Gåsemyr, New results on the Barlow–Proschan and Natvig measures of component importance in nonrepairable and repairable systems, *Methodology and Computing in Applied Probability*, Springer: Berlin-London-NewYork, 1-15 (2009).

10. Samaniego, F.J. and M. Shaked, Systems with weighted components. *Statistics and Probability letters* 78: 815-823 (2008).

11. Xie, M., On some importance measures for system components. *Stochastic Processes and their Applications* 25: 273-278 (1987).

12. Xie, M. and B. Bergman, On a general measure of component importance. Journal *of Statistical Planning and Inference* 29: 211-220 (1991).

Using Demographically Stochastic Modeling to Study the Effects of Cub Survival on Amur Leopard Population Trends

Sergey S. Berg

Conservation Biology Graduate Program, University of Minnesota
St. Paul, Minnesota, USA
Email: berg1546@umn.edu

Abstract: The Amur or Far Eastern leopard (*Panthera pardus orientalis*) survives today as a small relict population of a sub-species once abundant across a large portion of Eastern Asia. Demographically stochastic population modeling can help provide novel insights into the ecology and extinction risk of the remaining 30-40 individuals confined to the Russian Far East; thereby aiding the ongoing conservation of this critically endangered species in an anthropogenic landscape. I developed an individual-fate stage-specific population model to evaluate what role cub survival to independence plays in predicting observed population trends of Amur leopards from 2000 to 2007. Use of demographically stochastic models is particularly appropriate for this species because they explicitly incorporate dependent cub mortality as a response to mother mortality. I used litter-size estimates of Amur leopards and published estimates of adult mortality rates from populations of African leopards (*P. p. pardus*) to model population dynamics over the eight-year period. My results suggest that the maximum survival to independence of one cub per litter documented in other leopard sub-species fails to explain observed population trends in Amur leopards. To achieve equivalent overall population growth of 1.18, cub survival-to-independence rates had to be increased to an average of 1.39 per litter (± 0.13 SD) in our models. I suspect this reflects a facultative response to relatively superabundant resources when compared to other leopard populations. Reduced adult mortality rates and an increased female breeding probability were also considered, but provided less accurate predictions of population trends over the eight-year period. Collectively, these model results suggest that cub survival rates in Amur leopards may be higher than those documented for any other *P. pardus* sub-species.
Keywords: Cub survival, Resource limitation, Maternal dependence, Demographic stochasticity, *Panthera pardus*

1 Introduction

The Amur or Far Eastern leopard (*Panthera pardus orientalis*) is a critically endangered felid endemic to the temperate forests of southeastern Russia and is of high conservation concern (Pikunov et al., 2003; Jackson and Nowell, 2008). Until the late 19th century, Amur leopards were numerous and distributed across a large portion of eastern Asia. However, ongoing habitat loss and hunting during the 20th century severely decreased their distribution and numbers in the wild. Currently, the remaining 30-40 individuals are confined to an area of approximately 4600 km^2 in the southwest portion of Primorski Krai in Russia. Monitoring the number, age structure, and distribution of this remaining population is an explicit priority of the Russian National "Strategy for Conservation of the Far Eastern Leopard", and

understanding observed population trends through demographic modeling is an important goal in their conservation (Uphyrkina et al., 2002; Pikunov et al., 2003).

I evaluated the validity of current cub survival-to-independence rates in *P. pardus* in predicting recent population trends of Amur leopards. Snow-track population surveys conducted by the Wildlife Conservation Society (WCS) consistently reported a higher number of cubs than females with cubs, leading me to question the maximum survival to independence of one leopard per litter observed in all other leopard sub-species (Stevenson-Hamilton, 1947; Turnbull-Kemp, 1968; Bailey, 1993). I combined the results of these surveys with the best estimates of leopard mortality and reproductive characteristics using an individual-fate, stage-specific population model and determined cub survival-to-independence rates required to predict population trends observed from 2000 to 2007 (Pikunov et al., 2003; ALTA, 2007).

2 Model description

To investigate the effect of cub survival to independence in Amur leopards, I designed an individual-fate age-structured population model with post-mortality censusing, partitioning the life cycle into five underlying biological age-classes of variable length (Table 1; Bailey, 1993; Pikunov et al., 2003). This approach provides several advantages over traditional, aggregate population models by 1) describing population traits and demographic parameters with distributions rather than means values (DeAngelis and Rose, 1992), and 2) explicitly accounting for maternally-dependent cub mortalities that are associated with mother mortality (Turnbull-Kemp, 1968; Laurenson, 1994). Post-mortality censusing was selected in accordance with the timing of the aforementioned snow-track surveys conducted in Primorski Krai (Pikunov et al., 2003).

For each demographic parameter – mortality rate (Fig. 1), breeding rate (0.337 ± 0.031), and litter size (Fig. 2) – we estimated a mean and standard deviation from studies of Amur leopards and, where data were lacking, closely-related African leopards (*P. p. pardus*; Bailey, 1993). Age- and sex-specific mortality and breeding rates for each year were determined by independently sampling from these normal distributions, truncated to a 0:1 span, thereby introducing environmental stochasticity into the model. An individual of a given age and sex died and was removed from the population if a random sample from a 0:1 uniform distribution was less than the corresponding year's mortality rate for that age-class and sex. Individuals reached reproductive maturity at 2.75 years of age (Sunquist, 1983; Martin and DeMeulenaer, 1988), and a similar approach as that described above was used to determine if an adult female without dependent cub(s) produced a litter that year (Turnbull-Kemp, 1968; Martin and DeMeulenaer, 1988; Bailey, 1993). The size of each litter was determined by randomly sampling from the multinomial distribution of litter size.

The model uses a seasonal time step (3 months) and is configured for both males and females, each of which is given a unique ID tag at the time they are born and

enter into the population. Dead or alive status, age, sex, breeding status, presence and ID(s) of dependent cub(s), and ID of mother (for dependent cubs) is recorded and updated for every living leopard at each time step. Breeding and cub dispersal occurred in June, with cubs being born three months (1 time step) later in September and dependent on their mother for 21 months (7 time steps). Mortalities were determined 1 time step later during the winter, and censuses were performed in March.

Although individuals are certainly able to die at any time throughout the year, most populations of wild felids experience the majority of their mortalities during the winter. This can be caused by several factors, including heightened weather severity, decreased prey abundance, and increased hunting pressure (Crowe, 1975; Knopff et al., 2010). For this reason, many demographic models treat mortality as a single yearly event, a strategy known as mortality-pulse modeling (Crowe, 1975; Bender et al., 2007).

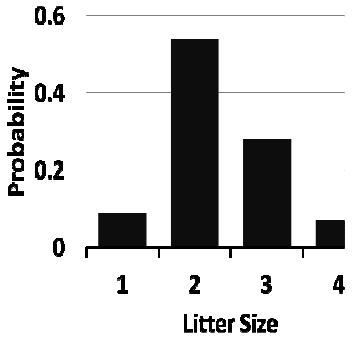

Fig 1. Multinomial probability distribution of litter size.

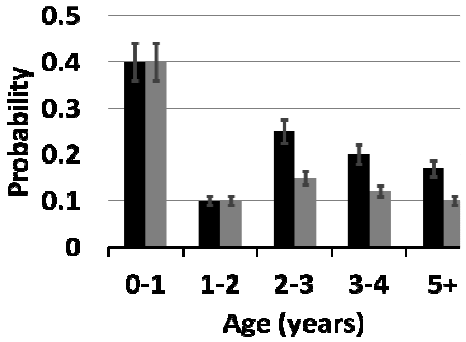

Fig 2. Age-specific mortality probabilities for males (black) and females (gray) (mean ± SD).

3 Initial conditions, model output, and survival scenarios

I used an initial population size, sex ratio, number of females with cubs, and age-class distribution based on the number of individuals of each sex and age-class observed in the 2000 snow-track survey (Pikunov et al., 2003). Each simulation was based on 1000 iterations using identical starting conditions. The primary results reported here are the mean and 95% confidence interval of the population size projections in 2000, 2003, and 2007, based on 1000 independent simulations.

Model results were validated by comparing them to the results of the snow-track surveys conducted during those years (Table 2) using a chi-squared goodness-of-fit test (Zar, 1999). I also compared the predicted age-class- and sex-distributions, as well as the number of females with cubs to those estimated for the Amur leopard population in Primorski Krai.

I analyzed two main scenarios in regard to cub survival-to-independence rates. The first limited survival to a maximum of one individual per litter, as has been documented for all other leopard sub-species (Stevenson-Hamilton, 1947; Turnbull-Kemp, 1968; Bailey, 1993). The second scenario placed no limitation on survival and used the best current estimates of yearly mortality rates of cubs to determine how many individuals per litter survived to independence.

Table 1. Definitions of Amur leopard age-classes.

Age-Class	Range (yrs)
Small cub	0-1
Large cub	1-2
Young sub-adult	2-3
Old subadult	3-4
Adult	5+

Table 2. Population dynamics of Amur leopards between 2000 and 2007.

Category	2000	2003	2007
Males	4-5	9	7-9
Females w/o cubs	8-9	7	3-7
Females with cubs	1-2	4-5	4
Cubs of unkn. sex	1-3	4-5	5-6
Adults of unkn. sex	8-9	4	6-8
Total	22-28	28-30	27-32

4 Results

Limiting the number of cubs that survived to independence to a maximum of one per litter decreased population growth rates (Fig. 3) and resulted in an overall population decline of 13% across the eight-year-period. Use of current estimates of cub mortality rates without limiting survival to independence (Fig. 4) improved the accuracy of the model in recreating trends in population size ($X^2 = 0.007$, $p < 0.01$, $df = 3$) as estimated from snow-track surveys conducted between 2000 and 2007. This approach resulted in an average survival to independence of 1.39 (± 0.13 SD) leopards per litter, as compared to the 0.94 (± 0.04 SD) survival rate seen in the first scenario (n = 2.78 litter/year ± 1.19 SD).

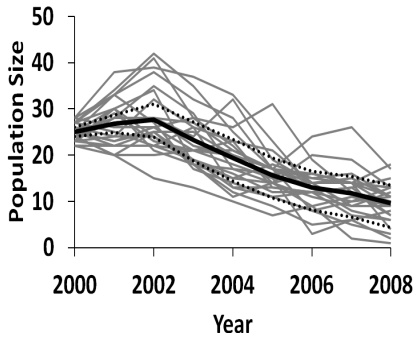

Fig 3. Mean (solid line) and 95% CI (dotted line) for 1000 simulations with limited survival to independence.

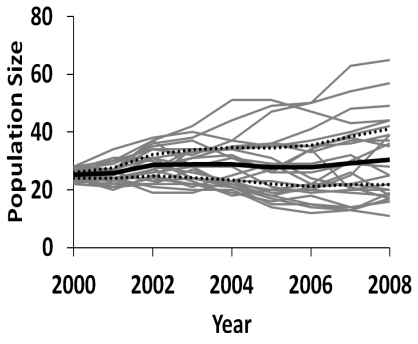

Fig 4. Mean (solid line) and 95% CI (dotted line) for 1000 simulations with non-limited survival to independence.

5 Discussion

Given current best estimates of *P. p. orientalis* adult mortality and breeding rates, my results suggest that the maximum survival to independence of one individual per litter documented in all other leopard sub-species (Stevenson-Hamilton, 1947; Turnbull-Kemp, 1968; Bailey, 1993) is insufficient to account for observed population trends in Amur leopards. To achieve equivalent population growth, survival-to-independence rates had to be increased to 1.39 (± 0.13 SD), a rate supported by cub mortality rates of other felids (0.4-0.42; Martin and DeMeulenaer, 1988; Chapron et al., 2008). This level of survival predicts a fluctuating but relatively stable population consistent with the results of ongoing population monitoring.

Alternatively, adult mortality rates needed to be reduced to levels lower than that published for any other wild felid. Reductions on the order of 20-40% for all non-cub age-classes resulted in equivalent population sizes during the eight-year period but with an older age structure than commonly seen in wild populations. This scenario also predicts a steady population decline of 3% per year if projected beyond 2007, leading me to reject it as a possible alternative.

Another approach was to increase breeding rates to levels significantly higher than that documented in other leopard populations. Increases on the order of 50-60% resulted in equivalent population sizes but a significantly higher number of females with cubs each year (an additional 3-6) than that estimated from the snow track surveys. Based on this discrepancy with current population estimates, I also rejected this scenario in favor of the higher cub survival one.

I hypothesize that this higher survival-to-independence rate in Amur leopards reflects a lack of individual resource limitation caused by low population density. Demographic parameters can be strongly affected by food abundance and nutritional quality, and populations experiencing high food abundance per individual can exhibit significant increases in reproductive rates, time to maturity, and cub survival to independence (Owen et al., 2010). The Primorski Krai population of Amur leopards is currently estimated to have a density of 1.1-2.2 individuals per 100 km^2 (Pikunov et al., 2003), which is significantly lower than that documented for those populations from which the notion of a maximum survival of one cub per litter originated (4.5-6.7 individuals per 100 km^2; Bailey, 1993; Jenny, 1996; Oli, 1994). This lower density may be linked to higher average resource abundance per individual than that experience by other leopard populations, resulting in the higher survival-to-independence rate suggested by my results.

Demographic parameters such as survival to independence and breeding rates strongly influence population growth. Knowing how these parameters affect populations can help managers more accurately predict future population trends and consequences of different management prescriptions. Although more work is needed to confirm and determine the true cause of the higher cub survival-to-

independence rate in Amur leopards suggested by my result, it does offer encouragement for their ongoing conservation and proposed re-introduction into other areas in Primorski Krai, Russia (Miquelle et al., 2010).

6 Conclusion

The situation of the Amur leopard is representative of many other endangered carnivores (Gaona et al., 1998). Their historical range has been fragmented and their population size reduced as a consequence of anthropogenic activities. My results support a re-evaluation of cub survival-to-independence rates in Amur leopards in an effort to better understand this small population and to prevent its extinction.

7 Acknowledgements

I am grateful to J. Forester, P. Kapfer, and Y. Cohen for contributions and suggestions at every stage. I thank D. Miquelle for comments on earlier drafts of my manuscript and his hard work in managing Amur leopards. This material is based upon work supported by the National Science Foundation Graduate Research Fellowship under Grant No. 00006595 and the University of Minnesota Conservation Biology Graduate Program Travel Grant Award for 2011-2012.

References

1. Amur Leopard and Tiger Alliance [ALTA]. (2007). ALTA Conservation Update. London: ALTA.
2. Bailey, T.N. (1993). *The African Leopard: Ecology and Behavior of a Solitary Felid*. New York: Columbia University Press.
3. Bender, L., L. Lomas, and J. Browning. (2007). Condition, survival, and cause-specific mortality of adult female mule deer in North-Central New Mexico. *J. Wild Mgmt.* **71**, 1118-1124.
4. Chapron, G., D. Miquelle, A. Lambert, J. Goodrich, S. Legendre, and J. Clober. (2008). The impact on tigers of poaching versus prey depletion. *J. Appl. Ecol.* **45**, 1667-1674.
5. Crowe, D. (1975). A model for exploited bobcat populations in Wyoming. *J. Wild. Mgmt.* **39**, 408-415.
6. DeAngelis, D. and K. Rose. (1992). Which individual-based approach is most appropriate for a given problem? In: DeAngelis, D. And L. Gross (Eds), *Individual-Based Models and Approaches in Ecology: Populations, Communities, and Ecosystems.* New York: Chapman and Hall.
7. Gaona, P., P. Ferreras, and M. Delibes. (1998). Dynamics and Viability of a Metapopulation of the Endangered Iberian Lynx (Lynx pardinus). *Ecol. Mono.* **68**, 349-370.
8. Jackson, P. and K. Nowell. (2008). Pantera pardus ssp. Orientalis. In: IUCN, IUCN Red List of Threatened Species. Version 2010.4.

9. Jenny, D. (1996). Spatial organization of leopards Panthera pardus in Tai National Park, Ivory Coast: is rainforest habitat a ‚tropical haven'? *J. Zool., Lond.* **234**, 387-408.
10. Knopff, K., A. Knopff, and M. Boyce. (2010). Scavening makes cougars susceptible to snaring at wolf bait stations. *J. Wild. Mgmt.* **74**, 664-653.
11. Martin, R. And T. DeMeulenaer. (1988). *Survey of the status of the leopard (Panthera pardus) in Sub-Saharan Africa*. Lausanne: CITES Secretariat.
12. Miquelle, D., Y. Darman, V. Aramilev, M. Hotte, S. Bereznyuk, A. Myslenkov, V. Solkin, D. Pikunov, A. Kostyria, S. Christie, and J. Lewis. (2010). A program for reintroduction of the Far Eastern leopard into southern Sikhote-Alin, Primorsky Krai, Russian Far East. Vladivostok: Ministry of Natural Resources, Russian Federation.
13. Nowell, K. and P. Jackson. (1996). *Wild Cats: Status Survey and Conservation Action Plan*. Switzerland: International Union for Conservation of Nature and Natural Resources (IUCN).
14. Oli, M. (1994). Snow leopards and blue sheep in Nepal: densities and predator:prey ratios. *J. Mammal.* **75**, 998-1004.
15. Owen, C., S. Niemann, and R. Slotow. (2010). Copulatory parameters and reproductive success of wild leopards in South Africa. *J. Mammal.* **91**, 1178-1187.
16. Pikunov, D., D. Miquelle, V. Abramov, I. Nikolaev, I. Seredkin, A. Murzin, and V. Korkishko. (2003). A Survey of Far Eastern Leopard and Amur Tiger Populations in Southwest Primoski Krai, Russian Far East. Attachment to: Tigris Foundation, Habitat Assessment and Land-use Planning for Siberian Tigers and Amur Leopards in the Russian Far East. Vladivostok: Wildlife Conservation Society.
17. Stevenson-Hamilton, J. (1947). *Wildlife in South Africa*. London: Cassell.
18. Sunquist, M. (1983). Independence of three radiotagged leopards. *J. Mammal.* **64**, 337-341.
19. Turnbull-Kemp, P. (1968). *The Leopard*. London: Bailey Bros & Swinfen.
20. Uphyrkina, O. D. Miqueele, H. Quigley, C. Driscoll, and S. O'Brien. (2002). Conservation Genetics of the Far Eastern Leopard (Panthera pardus orientalis). *J. Hered.* **93**, 303-311.
21. Zar, J.H. (1999). *Biostatistical Analysis, Fourth Edition*. New Jersey: Prentice-Hall.

A Bayesian Mixture Coffin-Manson Approach to Predict Semiconductor Lifetime

Olivia Bluder[1,2], Jürgen Pilz[2], Michael Glavanovics[1], and Kathrin Plankensteiner[1,2]

[1] KAI - Kompetenzzentrum für Automobil- und Industrieelektronik GmbH
Europastraße 8, 9524 Villach, Austria
(e-mail: olivia.bluder@k-ai.at)
[2] Alpen-Adria University of Klagenfurt
Universitätsstraße 65-67, 9020 Klagenfurt, Austria

Abstract. Based on physical failure inspection, known physical relationships, correlation analysis and posterior predictive distributions, a valid model for semiconductor lifetime is developed. It is shown that the data follow a mixture of two normal distributions and that the mixture weights depend on the destruction level. The mean lifetime of each component is modeled with an extended Coffin-Manson model. As priors, a combination of normal and hierarchical inverse gamma distributions is used. Since the given data show censoring, this is not a conjugate setting and the posterior distributions are simulated with MCMC methods. Model verification, based on the posterior predictive distribution, confirms good prediction quality for interpolations and shows potential for improving extrapolations.
Keywords: Semiconductor reliability, lifetime prediction, Bayesian model, Coffin–Manson model, Mixtures-of-Experts model.

1 Introduction

In automotive applications power semiconductors are applied in subsystems that concern the passenger's safety (e.g. ABS, airbags, engine), therefore the reliability demands are especially high. To define valid operating conditions, measurements and device testing are necessary. Usually, failure rates equal to parts per million (ppm) quantiles under certain stress test conditions are expected. The shortage of resources, namely limited testing time and number of stressed devices, demands for accurate modeling and prediction methods.

One approach to obtain reliable ppm values is to analyze each test separately (normally one test consists of 16 devices under test (DUTs) tested under the same test conditions). This means estimating the moments of the underlying distribution and extrapolating the ppm values [1]. The main limitation of this method is that predicting the outcome of future tests is impossible. Another approach is to use the results from various tests and include prior beliefs, engineering experience and results from previous tests to develop an accurate prediction model. This combination implies using a Bayesian model [2].

2 Data characteristics and available information

In this paper semiconductor lifetime data from a cycle stress test [6] are used. The DUTs are tested under different accelerated electrical and thermal stress conditions. For each DUT the stress test system provides the following information:

- Applied stress pulses: The pulses are defined by voltage (V), current (I), pulse width (t_p) and the time between two stress pulses (t_{rep}).
- Ambient temperature (T_{amb}): The DUTs are tested in a climate chamber with a fixed, predefined ambient temperature.
- Time to failure (TTF) and Cycles to Failure (CTF): The TTF is measured exactly and the CTF are calculated based on the applied t_{rep}.
- Failure event: The software distinguishes between two failure events, short circuit and open load; non-failed devices are called survivors.

To develop a semiconductor lifetime model, the results of 11 tests are used. In detail, this means that CTF of 161 DUTs, tested under 10 different test conditions (one condition was tested twice) are available. All DUTs originate from the same technology and equal designs. The test conditions are chosen with a 2^{4-1} fractional factorial design [10]. The levels of the factors V, I, t_p and t_{rep} are selected based on a reference test. Previous investigations (see Bluder [1]) indicate that the logarithmic CTF (logCTF) follow a normal distribution, hence a normal probability plot with a logarithmic x-axis can be used to get a first impression of the data (see Figure 1).

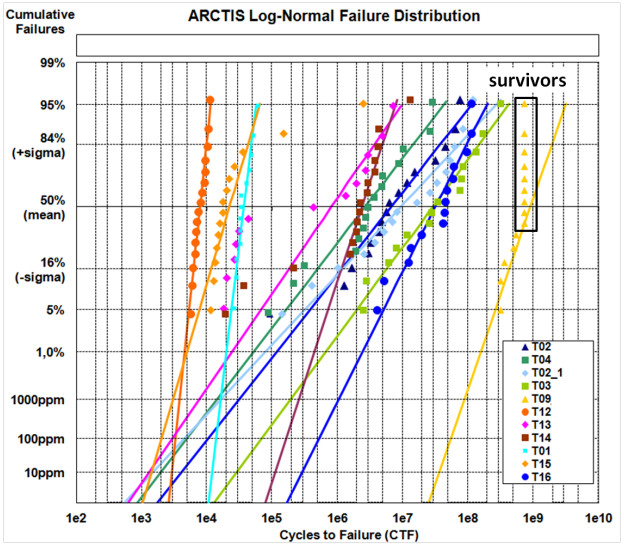

Fig. 1. Semiconductor lifetime probability plots of 11 tests [3].

Each color in Figure 1 represents one test (group of DUTs tested under equal test conditions). Test $T09$ is located isolated from the others, because the applied stress is significantly lower than the one of the adjacent tests. This is the reason why more than 50% of the DUTs did not fail, consequently they are censored. Tests $T02$ and $T02\_1$ have the same test conditions, they serve as reference tests. At the first glance, the results are reasonable, since the mean lifetime is inversely proportional to the applied stress. A closer look at the plot shows that the DUTs appear to be divided into two branches with a transition zone between 10^5 and 10^6 CTF. This gap is not caused by missing stress levels, therefore it is assumed that two dominating failure mechanisms are present. The distributions of the CTF of e.g. test $T13$ underlines this hypothesis. Even though the applied test conditions are equal for all DUTs, nearly 50% fail in the first branch ($< 10^5$ CTF), one DUT fails in the transition zone and the rest fails in the second branch ($\geq 10^6$ CTF).
Physical failure inspection confirms this assumption (see Figure 2). All analyzed devices from the first branch show no visible failure spot, indication for a so called "soft" short circuit in the lower metal layers. Devices from the second branch show visible power metal lift-offs and burn marks at the failure location.

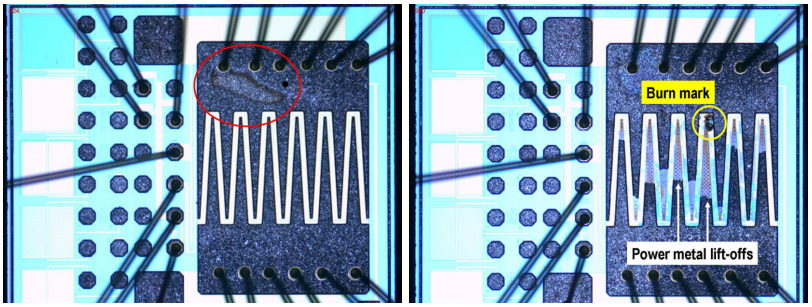

Fig. 2. Optical micrographs of partially opened devices. DUT of 1^{st} branch shows no visible failure spot, only remains of the etching process (left). DUT of 2^{nd} branch shows power metal lift-offs and a burn mark (right) [2].

3 Model to predict semiconductor reliability

To create a valid lifetime model, the observations of two dominant failure mechanisms need to be considered. This can be done by using a mixture of two normal distributions [5]

$$p(\mathbf{logCTF}|\boldsymbol{\vartheta}) = \eta\,\phi(\mathbf{logCTF}|\mu_1,\sigma_1^2) + (1-\eta)\,\phi(\mathbf{logCTF}|\mu_2,\sigma_2^2). \quad (1)$$

The plots in Figure 1 show that the means (μ_1, μ_2) vary within the two branches, dependent on the applied test conditions. Also the variances (σ_1^2, σ_2^2) differ, they are smaller in the first and larger in the second branch. These observations can be included into the model given in (1) by expanding it to a heteroscedastic mixture regression model.

Heteroscedasticity is achieved by assuming $\sigma_1^2 \neq \sigma_2^2$. To find the appropriate regression model for the mean lifetime, additional information from semiconductor physics is applied. The Coffin-Manson power law [4] is commonly known to describe semiconductor lifetime under accelerated thermal stress

$$N = A \cdot \Delta T^{-\beta} \tag{2}$$

where the number of cycles to failure N is modeled dependent on the temperature rise ΔT. However, modeling the mean lifetime of given data with this relationship leads to poor results. Significant improvement can be achieved by using an extended Coffin-Manson model [4], also known as Norris-Landzberg model. With this, the regression model for e.g. the first component of the mixture model can be expressed as

$$E(\log \mathrm{CTF}_i) = \mu_1 = \log(A_1) + \alpha_1 \cdot \log(t_{rep_i}) - \beta_1 \log(\Delta T_i) + \frac{\Delta H_1}{k T_{peak_i}}, \tag{3}$$

where ΔH is the activation energy and k is the Boltzmann constant. Approximated values for ΔT and the peak temperature T_{peak} can be calculated based on the applied test conditions [7].

Furthermore, it can be observed that the amount of devices failing within the first branch (η) is proportional to the stress level. Therefore, η needs to be modeled dependent on test parameters, leading to a Mixtures-of-Experts model [2]. Good results ($R^2 = 0.89$) can be achieved by using a logit model dependent on T_{peak} (see Bluder [2]). Further investigations (see Plankensteiner [13]) suggest using a cumulative beta distribution function dependent on the destruction level L_{SOA}

$$\eta(L_{SOA}) = \int_0^{L_{SOA}} \frac{\Gamma(a+b)}{\Gamma(a) \cdot \Gamma(b)} \cdot \xi^{a-1} \cdot (1-\xi)^{b-1} d\xi, \tag{4}$$

where a and b are estimated by least squares minimization and $0 < L_{SOA} < 1$. For each test condition L_{SOA} can be calculated by

$$L_{SOA} = \frac{T_{peak} - T_{case}}{T_{dest} - T_{case}} = \frac{\Delta T}{T_{dest} - T_{case}}. \tag{5}$$

For the investigated devices the destruction temperature T_{dest} is 339°C and the case temperature T_{case} is 150°C. Applying this model to the 11 test conditions yields an $R^2 = 0.97$.

On the one hand, at this point a model for semiconductor lifetime is defined and point estimates can be calculated. On the other hand, additional information on the regression parameters α, β and ΔH is provided in literature and from internal experts. This important and valuable knowledge can be considered by defining the Mixtures-of-Experts model within a Bayesian framework. Hence, in place of point estimates the posterior distribution of the model parameters is used, which is proportional to the likelihood $L(\cdot)$ times the prior distribution $p(\boldsymbol{\vartheta})$

$$p(\boldsymbol{\vartheta}|\mathbf{logCTF}) \propto L(\boldsymbol{\vartheta}|\mathbf{logCTF})p(\boldsymbol{\vartheta}). \tag{6}$$

Within the likelihood function, censored data points can be considered by using the survivor function instead of the probability density function. Additional information for the model parameters is included into the prior distributions. For the regression parameters normal prior distributions are selected. Table 1 lists the available prior information from company internal

information for			
α	β	ΔH	information source
-0.333	2	1.25	NIST [12]
	$[5, 8]$	$[0.4, 0.8]$	internal experts
	5	$[0.3, 1.5]$	Nelson [11]
	7.1		Lecuyer et al. [9]

Table 1. Available prior information for Coffin-Manson parameters.

experts and literature. The given intervals and point estimates can be combined to the following joint prior distributions for the three parameters

$$\begin{aligned} \alpha_{1,2} &\sim \mathcal{N}(-0.333, 1) \\ \beta_{1,2} &\sim \mathcal{N}(5.15, 0.893) \\ \Delta H_{1,2} &\sim \mathcal{N}(0.917, 0.355). \end{aligned} \tag{7}$$

For the scaling parameters (A_1, A_2) no prior information is available, therefore flat normal priors ($\sim \mathcal{N}(10, 5)$) are used.
The priors of the variances are hierarchical inverse gamma distributions. This means that the inverse variances (precisions) are gamma distributed, where the scale, in turn, is a unknown hyperparameter following a gamma distribution.

$$\sigma^2_{1,2} \sim \mathcal{G}^{-1}(c_0, C_0) \qquad C_0 \sim \mathcal{G}(g_0, G_0). \tag{8}$$

The advantage of using hierarchical priors for the variances is that a slight data dependency can be introduced by choosing the scale parameter G_0 dependent on the sample variance s^2_y. Due to the lack of prior information

for the variances, values suggested by S. Frühwirth-Schnatter [5] are used ($c_0 = 3, g_0 = 0.5, G_0 = g_0((c_0 - 1) \cdot 0.5 \cdot s_y^2)^{-1}$).

Due to censoring and mixture behavior, no analytical solution for the posterior distributions exists, therefore a combination of data augmentation and Slice-within-Gibbs sampler [2] is used. The summary statistic of the posterior distributions is given in Table 2.

			quantiles					quantiles	
	mean	*std*	5%	95%		*mean*	*std*	5%	95%
$\log(A_1)$	-3.17	1.56	-5.75	-0.59	$\log(A_2)$	-9.81	1.99	-13.47	-6.96
α_1	-1.37	0.17	-1.60	-1.13	α_2	-2.13	0.84	-3.52	-0.79
β_1	4.87	0.89	6.31	3.39	β_2	6.08	0.92	7.57	4.54
ΔH_1	0.41	0.085	0.271	0.55	ΔH_2	0.89	0.10	0.74	1.08
σ_1^2	0.028	0.023	0.017	0.044	σ_2^2	0.449	0.079	0.334	0.583

Table 2. Summary statistic for the mixture of Coffin-Manson models.

The results are satisfactory and indicate good model quality because

- all regression parameters are significant
- the means of the regression parameters (β and ΔH) lie in the a-priori expected intervals (compare with Table 1)
- all model parameters show Bayesian learning because the posterior standard deviations are smaller than a-priori assumed (compare to distributions given in (7))
- as assumed a-priori, the variance of the first branch is smaller than the one of the second branch.

4 Evaluation of the model quality

The model presented in the previous section fits the data well, but the aim of this work is to make reliable predictions. To validate the prediction quality, the posterior predictive distribution is used. This is the probability of a new data point (y_{new}) conditional on the already measured data ($\boldsymbol{y} = \mathbf{logCTF}$) and is defined as

$$p(y_{new}|\boldsymbol{y}) = \int p(y_{new}, \boldsymbol{\vartheta}|\boldsymbol{y}) d\boldsymbol{\vartheta} = \int p(y_{new}|\boldsymbol{\vartheta}) p(\boldsymbol{\vartheta}|\boldsymbol{y}) d\boldsymbol{\vartheta}. \tag{9}$$

To judge the prediction quality of the model, the posterior predictive distribution for each of the 11 tests is sampled in a leave-one-out cross validation [8] style.

Figure 3 displays the posterior predictive distributions for the 11 tests. The prediction quality of the model is good since only slight deviations are

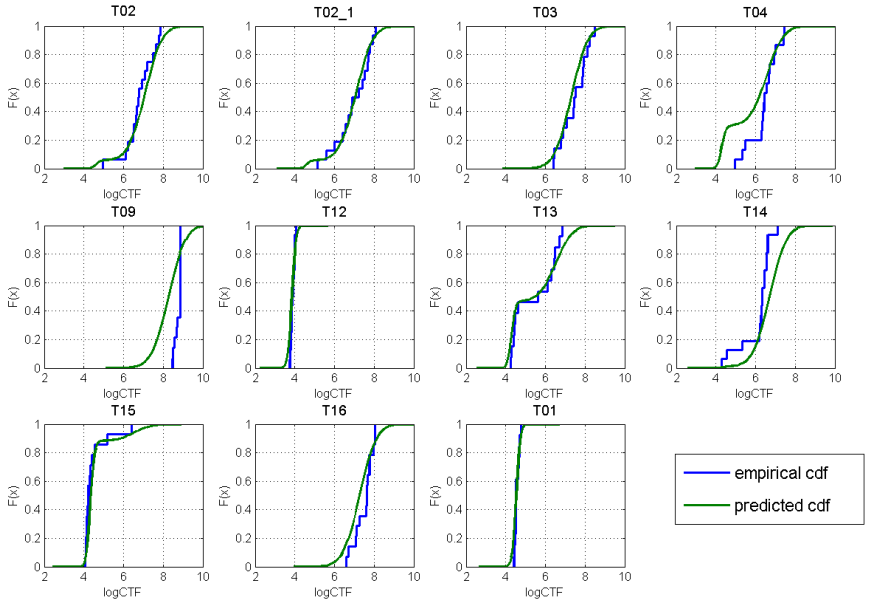

Fig. 3. Posterior predictive distributions for mixture Coffin-Manson model. Empirical CDFs are based on kernel smoothing estimates.

observable for two tests: the estimated mean lifetime of the first branch from test $T04$ is too low, but the predicted weights are acceptable. Test $T09$, the test with significantly lower stress, shows a shift in mean lifetime. This inaccuracy can be explained by the fact that it is an extrapolation based on tests with significantly higher stress levels. No deviation can be seen for the test with the highest stress level, $T12$. For $T12$ the difference to the adjacent stress levels is not as large as for test $T09$, consequently it can be inferred that "slight" extrapolations are permitted, but must be handled with care.

5 Conclusion

In this paper a Mixtures-of-Experts model based on the Coffin-Manson relationship, with mixture weights dependent on the destruction level is proposed to model semiconductor lifetime. Due to the fact that prior knowledge for the Coffin-Manson parameters is available, the model is used within a Bayesian framework. The posterior distributions of the model parameters show only small variations, indicating a good fit. Evaluating the posterior predictive distributions demonstrates that reliable predictions can be achieved for interpolated stress test conditions, but there is still room for improvement regarding extrapolated conditions.
With the proposed model, stress testing time can be reduced to a minimum,

since semiconductor lifetime can be predicted based on test conditions defined by a fractional factorial design. Furthermore, valid parameter ranges for future applications can be defined. However, testing is not replaced completely, because for each design variation the model parameters need to be evaluated again.

Acknolewdgement

The authors would like to thank Alfred Waukmann and Roland Sleik for the measurement support, as well as Horst Lewitschnig and Michael Nelhiebel for valuable discussions on the topic.
This work was jointly funded by the Federal Ministry of Economics and Labor of the Republic of Austria (contract 98.362/0112-C1/10/2005) and the Carinthian Economic Promotion Fund (KWF) (contract 18911|13628|19100)

References

1. Bluder, O., Statistical analysis of Smart Power Switch life test results, Master thesis, Alpen-Adria University of Klagenfurt (2008).
2. Bluder, O., Prediction of Smart Power device lifetime based on Bayesian modeling, PhD thesis, Alpen-Adria University of Klagenfurt (2011).
3. Bluder, O., Glavanovics, M. and Pilz, J., Applying Bayesian Mixtures-of-Experts models to statistical description of smart power semiconductor reliability, *Microelectronics Reliability*, 51, 1464–1468 (2011).
4. Escobar, L. A. and Meeker, W. Q., A review of accelerated test models, *Statistical Science*, 21(4), 552–577 (2006).
5. Frühwirth-Schnatter, S., *Finite mixture and Markov switching models*, First edition: Springer, Berlin (2006).
6. Glavanovics, M., Köck, H., Kosel, V. and Smorodin, T., A new cycle test system emulating inductive switching waveforms, In *Proceedings of the 12th European Conference on Power Electronics and Applications 2007*, 1–9 (2007).
7. Glavanovics, M. and Zitta, H., Thermal destruction testing: an indirect approach to a simple dynamic thermal model of Smart Power Switches, In *Proceedings of ESSCIRC2001* (2001).
8. Kohavi, R., A study of cross-validation and Bootstrap for accuracy estimation and model selection, In *Proceedings of the International Joint Conference on Artificial Intelligence (IJCAI)*, Morgan Kaufmann, 1137–1143 (1995).
9. Lecuyer, P., Fremont, H., Landesman, J.-P. and Bahi, M.-A., Wearout estimation using the robustness validation methodology for components in 150 °C ambient automotive applications, *Microelectronics Reliability*, 50, 1744–1749 (2010).
10. Montgomery, D. C, *Design and analysis of experiments*, 5th edition: John Wiley & Sons, New York / Chichester (2001).
11. Nelson, W. B., *Accelerated testing: statistical models, test plans, and data analyses*, John Wiley & Sons, Hoboken, New Jersey (1990).
12. NIST, NIST handbook, http://www.itl.nist.gov/div898/handbook (06/2010).
13. Plankensteiner, K., Prediction of Smart Power device lifetime based on Bayesian modeling, Master thesis, Alpen-Adria-University of Klagenfurt (2011).

An unified approach to simple correspondence analysis

Ida Camminatiello, Eric J. Beh and Luigi D'Ambra

Dept of Business Strategies and Quantitative Methodologies Second University of Naples, Italy
Email: camminat@unina.it
School of Mathematical & Physical Sciences, University of Newcastle, Australia
Eric.Beh@newcastle.edu.au
Department of Biological Sciences, University of Naples Federico II, Italy
dambra@unina.it

Abstract: In this paper we present an unification to the methods for graphically summarising the association between two categorical variables that form a two-way contingency table. In particular we focus on following methods based on the decomposition of a known index: correspondence analysis (CA) based on the decomposition of Pearson's chi-squared statistic; non symmetrical correspondence analysis (NSCA) based on the decomposition of the Goodman-Kruskal tau index; singly ordered cumulative correspondence analysis based on the decomposition of Taguchi's statistic; doubly ordered cumulative correspondence analysis based on the decomposition of the doubly cumulative chi-squared statistic.
Keywords: correspondence analysis, doubly cumulative chi-squared statistic, Goodman-Kruskal tau index, Taguchi's statistic.

1 Introduction

There are several methods that can be used to graphically summarise the association between two categorical variables that form a two-way contingency table. Here, we focus on those based on the decomposition of a known index. The most popular method is correspondence analysis (CA) which is based on the decomposition of Pearson's chi-squared statistic. There are a number of variations of the classical approach including D'Ambra and Lauro (1989) who introduced non-symmetrical correspondence analysis (NSCA) using the decomposition of the Goodman-Kruskal tau index. For a two-way contingency table consisting of an ordinal variable and a nominal variable, Beh, D'Ambra and Simonetti (2007, 2011) presented an approach to CA based on the decomposition of Taguchi's statistic. Cuadras (2002) proposed another approach to CA based on double cumulative frequencies (however, such an approach does not lead to the decomposition of any known association index). Finally D'Ambra, Beh, Camminatiello (2012) explore the development of CA taking into account the presence of two ordered variables by partitioning the doubly cumulative chi-squared statistic.
This aim of this paper is to present a simple unification to these, and other, methods of correspondence analysis of a two way contingency table.

2 Some approaches to simple correspondence analysis

2.1 Correspondence analysis

Let $\mathbf{N} = (n_{ij})$ be a two-way contingency table that cross-classifies n units according to I ordered row categories and J ordered column categories. The matrix of proportions (referred to as the correspondence matrix in CA) is denoted by $\mathbf{P} = n^{-1}\mathbf{N}$. The marginal relative frequency of the *i*th row and *j*th column of $\mathbf{N}$ is $p_{i\bullet}$ and $p_{\bullet j}$ and they may be represented in vector or matrix form. In this paper, the vector $\mathbf{r}$ consists of $p_{i\bullet}$, for i = 1, 2, . . . , *I* as elements while $\mathbf{D}_r$ is the diagonal matrix of these quantities. Similarly, $\mathbf{c}$ is the vector of $p_{\bullet j}$ values, for *j* = 1, 2, . . . , *J*, with $\mathbf{D}_c$ being the diagonal matrix of these values.
There are a number of ways in which CA may be performed. One approach is to consider (Greenacre, 1984)

$$\mathbf{D}_r^{-1/2}\left(\mathbf{P} - \mathbf{r}\mathbf{c}^T\right)\mathbf{D}_c^{-1/2} = \mathbf{U}\mathbf{D}_\alpha\mathbf{V}^T \qquad (1)$$

where $\mathbf{U}$ is a column matrix containing the left singular vectors of the left hand side (LHS) of (3) such that $\mathbf{U}^T\mathbf{U} = \mathbf{I}$. Similarly, $\mathbf{V}$ is the column matrix containing the right singular vectors of the LHS of (3) where $\mathbf{V}^T\mathbf{V} = \mathbf{I}$. The matrix $\mathbf{D}_\alpha$ is diagonal where the *(k, k)*th element is the *k*'th singular value α_k.
It is known that

$$X^2 = n\ trace\left(\mathbf{D}_r^{-1/2}\left(\mathbf{P} - \mathbf{r}\mathbf{c}^T\right)\mathbf{D}_C^{-1}\left(\mathbf{P} - \mathbf{r}\mathbf{c}^T\right)^T\mathbf{D}_R^{-1/2}\right) = n\sum_{k=1}^{K}\overline{\alpha}_k^2$$

where X^2 is the Pearson's chi-squared statistic.

2.2 Non symmetrical correspondence analysis

When the variables are asymmetrical related D'Ambra and Lauro (1989) introduced the NSCA which involves the following singular value decomposition (SVD)

$$\mathbf{D}_r^{-1/2}\left(\mathbf{P} - \mathbf{1}_r\mathbf{c}^T\right)\mathbf{D}_c^{1/2} = \mathbf{U}\mathbf{D}_\alpha\mathbf{V}^T \qquad (2)$$

It is easy to verify that

$$N_\tau = trace\left(\mathbf{D}_r^{-1/2}\left(\mathbf{P}-\mathbf{1}_r\mathbf{c}^T\right)\mathbf{D}_c\left(\mathbf{P}-\mathbf{1}_r\mathbf{c}^T\right)^T\mathbf{D}_r^{-1/2}\right) = n\sum_{k=1}^{K}\overline{\alpha}_k^2$$

where N_τ is the numerator of the Goodman–Kruskal tau index, $\tau = \dfrac{\sum_{i=1}^{I}\sum_{j=1}^{J} p_{i\bullet}\left(\dfrac{p_{ij}}{p_{i\bullet}} - p_{\bullet j}\right)^2}{1-\sum_{j=1}^{J} p_{\bullet j}^2} = \dfrac{N_\tau}{1-\sum_{j=1}^{J} p_{\bullet j}^2}$ that is a measure of predictability of the rows by the columns. When, for each column, the distribution of the response categories across each of the rows is identical to the overall marginal proportion there is no relative increase in predictability and thus τ is zero. Similarly, $\tau = 1$ only when there is perfect predictability of the response categories (columns) given the predictor categories (rows). To assess the statistical significance of dependence, a test criterion called *C* has been developed (Light and Margolin, 1971) that is asymptotically approximated as a $\chi^2_{(I-1)(J-1)}$ random variable under the null hypothesis that the joint probabilities pr_{ij} are equal to the column marginal probabilities $pr_{\bullet j}$, i.e. $H_0 : pr_{ij} = pr_{\bullet j}$.

2.3 Singly ordered cumulative correspondence analysis

If one of the two categorical variables of a two-way contingency table have an ordered structure, we can consider the cumulative CA approach proposed by Beh, D'Ambra and Simonetti (2011).

For row *i*, consider the cumulative frequencies $z_{i1} = n_{i1}$, $z_{i2} = n_{i1} + n_{i2}, \Lambda$, $z_{iJ} = n_{i1} + \Lambda + n_{iJ}$ and the relative cumulative frequencies $d_1 = n_{\bullet 1}/n$, $d_2 = \left(n_{\bullet 1} + n_{\bullet 2}\right)/n$, Λ, $d_J = \left(n_{\bullet 1} + \Lambda + n_{\bullet J}\right)/n$. Let $\mathbf{W}$ be the $(J-1)\times(J-1)$ diagonal matrix of weights $w_j = \left(d_j\left(1-d_j\right)\right)^{-1}$. Also, let $\mathbf{A}$ be the $(J-1)\times J$ matrix involving the cumulative column proportions d_j and $\mathbf{M}_{-J}$ be a $(J-1)\times J$ matrix formed from the upper triangular matrix of 1's with the last (*J*'th) row removed, singly cumulative CA involves the following SVD

$$\mathbf{D}_r^{-1/2}\left(\mathbf{P}-\mathbf{r}\mathbf{c}^T\right)\mathbf{M}_{-J}^T\mathbf{W}^{1/2} = \mathbf{U}\mathbf{D}_\alpha\mathbf{V}^T \qquad (3)$$

It can be shown that

$$T = n\times trace\left(\mathbf{D}_r^{-1/2}\left(\mathbf{P}-\mathbf{r}\mathbf{c}^T\right)\mathbf{M}_{-J}^T\mathbf{W}\mathbf{M}_{-J}\left(\mathbf{P}-\mathbf{r}\mathbf{c}^T\right)^T\mathbf{D}_r^{-1/2}\right)$$

where $T = \sum_{j=1}^{J-1} w_j \left(\sum_{i=1}^{I} n_{i\bullet} \left(\frac{z_{ij}}{n_{i\bullet}} - d_j \right)^2 \right)$ is the Taguchi's statistic (1974). It is as a measure of the uni-directional association between the row and ordered column variables instead of the two-way association structure that the Pearson chi-squared statistic considers. Note that Taguchi's statistic is a cumulative version of the numerator of the Goodman–Kruskal tau index.

Let $\mathbf{M}$ be a $J \times J$ matrix formed from the upper triangular matrix of 1' and $\mathbf{W}_J$ the $J \times J$ diagonal matrix of weights $w_j = 1/J$. Cuadras (2008) replaced $\mathbf{M}_{-J}$ with $\mathbf{M}$ and $\mathbf{W}$ with $\mathbf{W}_J$ in (3) obtaining

$$\mathbf{D}_r^{-1/2}\left(\mathbf{P} - \mathbf{r}\mathbf{c}^T\right)\mathbf{M}^T\mathbf{W}_J^{1/2} = \mathbf{U}\mathbf{D}_\alpha\mathbf{V}^T$$

However, Nair (1987) showed the link between Pearson's chi-squared statistic and Taguchi's statistic is $T = \sum_{j=1}^{J-1} \overline{X}_j^2$ for the weight $w_j = \left(d_j\left(1 - d_j\right)\right)^{-1}$. Here, $\overline{X}_j^2$ is the Pearson chi-squared statistic for the $I \times 2$ contingency table obtained by aggregating column categories 1 to j, and aggregating the column categories $j+1$ to J. For this reason, Nair (1987) referred to T as a cumulative chi-squared statistic and showed that the distribution of T can be approximated using Satterthwaite's (1946) method. It is bounded such that $0 \le T \le n(I-1)$.

2.4 Doubly ordered cumulative correspondence analysis

Let $\mathbf{L}$ be the $I \times I$ upper triangular matrix of ones. Cuadras (2008) proposed an approach to CA based on double cumulative frequencies:

$$\mathbf{D}_r^{-1/2}\mathbf{L}\left(\mathbf{P} - \mathbf{r}\mathbf{c}^T\right)\mathbf{M}^T\mathbf{W}_J^{1/2} = \mathbf{U}\mathbf{D}_\alpha\mathbf{V}^T \qquad (4)$$

This approach presents some disadvantages. First, it does not lead to the decomposition of any known association index. Second, the matrices $\mathbf{L}$ and $\mathbf{M}$ pool the rows and the columns of original table in a successive manner, so they do not lead to $2(I-1)\times 2(J-1)$ 2x2 tables.

By considering the singly-ordered cumulative CA approach of Beh, D'Ambra and Simonetti (2007, 2011) as a starting point, D'Ambra, Beh and Camminatiello (2012) presented an alternative cumulative CA technique based on the row and column cumulative frequencies. The advantage of doing so is that they overcome the above problems inherent in Cuadras' (2008) approach.

Let $\mathbf{R}$ be the $2(I-1)\times I$ matrix obtained by alternating the rows of an $(I-1)\times I$ lower triangular matrix of one's (by first removing the row consisting of all one's) with the rows of an $(I-1)\times I$ upper triangular matrix of one's (by first removing the row consisting of all one's). That is

$$\mathbf{R}=\begin{bmatrix} 1 & 0 & 0 & \Lambda & 0 \\ 0 & 1 & 1 & \Lambda & 1 \\ 1 & 1 & 0 & \Lambda & 0 \\ 0 & 0 & 1 & \Lambda & 1 \\ \Lambda & \Lambda & \Lambda & \Lambda & \Lambda \\ 1 & 1 & 1 & \Lambda & 0 \\ 0 & 0 & 0 & \Lambda & 1 \end{bmatrix}$$

Similarly, let $\mathbf{C}$ be the $J\times 2(J-1)$ matrix obtained by alternating the columns of an $J\times(J-1)$ upper triangular matrix of one's (by first removing the column consisting of all one's) with the columns of a $J\times(J-1)$ down triangular matrix of one's (by first removing the column consisting of all ones). That is

$$\mathbf{C}=\begin{bmatrix} 1 & 0 & 1 & 0 & \Lambda & 1 & 0 \\ 0 & 1 & 1 & 0 & \Lambda & 1 & 0 \\ 0 & 1 & 0 & 1 & \Lambda & 1 & 0 \\ \Lambda & \Lambda & \Lambda & \Lambda & \Lambda & \Lambda & \Lambda \\ 0 & 1 & 0 & 1 & \Lambda & 0 & 1 \end{bmatrix}$$

Let $\mathbf{H}=\mathbf{RPC}$ be the $2(I-1)\times 2(J-1)$ doubly cumulative table, with $h_{i\bullet}$ and $h_{\bullet j}$ the *i*th row and *j*th column cumulative marginal relative frequencies, respectively. Let $\mathbf{D}_R$ and $\mathbf{D}_C$ be the diagonal matrices with the marginal relative frequencies of the doubly cumulative table $\mathbf{H}$.
D'Ambra, Beh and Camminatiello (2012) proposed a generalisation of the Taguchi decomposition based on cumulative frequencies for the rows and columns by considering

$$\mathbf{S}=\mathbf{D}_R^{-1/2}\mathbf{R}\left(\mathbf{P}-\mathbf{r}\mathbf{c}^T\right)\mathbf{C}\mathbf{D}_C^{-1/2}=\mathbf{U}\mathbf{D}_\alpha\mathbf{V}^T \qquad (5)$$

This approach is equivalent to the CA on the matrix H

$$\mathbf{D}_R^{-1/2}\left(\mathbf{H}-\mathbf{R}\mathbf{r}\mathbf{c}^T\mathbf{C}\right)\mathbf{D}_C^{-1/2}=\mathbf{U}\mathbf{D}_\alpha\mathbf{V}^T$$

One may note that, by considering (5), a measure of association between the ordered row categories and ordered column categories is

$$\begin{aligned} X^{**2} &= n(I-1)(J-1)\,trace\left(\mathbf{S}\mathbf{S}^T\right) \\ &= n(I-1)(J-1)\,trace\left(\mathbf{D}_R^{-1/2}\mathbf{R}\left(\mathbf{P}-\mathbf{r}\mathbf{c}^T\right)\mathbf{C}\mathbf{D}_C^{-1}\mathbf{C}^T\left(\mathbf{P}-\mathbf{r}\mathbf{c}^T\right)^T\mathbf{R}^T\mathbf{D}_R^{-1/2}\right) \\ &= n(I-1)(J-1)\sum_{k=1}^{K}\overline{\alpha}_k^2. \end{aligned}$$

where $X^{**2}=\sum_{i=1}^{I-1}\sum_{j=1}^{J-1}X_{ij}^{**2}$ is doubly cumulative chi-squared statistic introduced by Hirotsu (1994) and X_{ij}^{**2} is the chi-squared statistic for the 2×2 contingency table obtained by pooling the original table $I\times J$ data at the i th row and j th column.

Therefore, the doubly ordered cumulative chi-squared statistic can be partitioned into the sum of squares of the singular values of the LHS of (5) in much the same way as classical CA involves partitioning Pearson's chi-squared statistic.

Hirotsu (1994) showed that the null distribution of the statistic X^{**2} is approximated by $d\chi_v^2$ with $d=d_1d_2$ and $v=(I-1)(J-1)/(d_1d_2)$ where

$$d_1=1+\frac{2}{J-1}\left(\frac{\lambda_1}{\lambda_2}+\frac{\lambda_1+\lambda_2}{\lambda_3}+\Lambda+\frac{\lambda_1+\Lambda+\lambda_{J-2}}{\lambda_{J-1}}\right),$$

$$d_2=1+\frac{2}{I-1}\left(\frac{\gamma_1}{\gamma_2}+\frac{\gamma_1+\gamma_2}{\gamma_3}+\Lambda+\frac{\gamma_1+\Lambda+\gamma_{I-2}}{\gamma_{I-1}}\right),$$

$\lambda_j=(n_{\bullet 1}+\Lambda+n_{\bullet j})/(n_{\bullet,j+1}+\Lambda+n_{\bullet J})$ and $\gamma_i=(n_{1\bullet}+\Lambda+n_{i\bullet})/(n_{i+1,\bullet}+\Lambda+n_{I\bullet})$.

2.5 An unified approach.

In this section we present an unification to the methods above described by using suitable parameters.

In order to represent the rows and columns of **N** we can consider the following SVD depending on four matrices $\mathbf{F},\mathbf{B},\mathbf{D},\mathbf{E}$ and the vector **a**

$$\mathbf{F}\mathbf{B}\left(\mathbf{P}-\mathbf{a}\mathbf{c}^T\right)\mathbf{D}^T\mathbf{E}=\mathbf{U}\mathbf{D}_\alpha\mathbf{V}^T \tag{6}$$

By modifying these parameters in a appropriate way, we obtain the six methods above described. Table 1 summarizes suitable parameters, the obtained methods and decomposed indices.

Weights	Centered	Matrix for cumulating the rows	Matrix for cumulating the columns	Metrics	Approach	Index
$\mathbf{F}=\mathbf{D}_r^{-1/2}$	$\mathbf{a}=\mathbf{r}$	$\mathbf{B}=\mathbf{I}$	$\mathbf{D}^T=\mathbf{I}$	$\mathbf{E}=\mathbf{D}_c^{-1}$	CA	Pearson's chi-squared statistic
$\mathbf{F}=\mathbf{D}_r^{-1/2}$	$\mathbf{a}=\mathbf{1}_r$	$\mathbf{B}=\mathbf{I}$	$\mathbf{D}^T=\mathbf{I}$	$\mathbf{E}=\mathbf{D}_c$	NSCA	Goodman-Kruskal tau index
$\mathbf{F}=\mathbf{D}_r^{-1/2}$	$\mathbf{a}=\mathbf{r}$	$\mathbf{B}=\mathbf{I}$	$\mathbf{D}^T=\mathbf{M}_{-J}^T$	$\mathbf{E}=\mathbf{W}$	singly ordered cumulative CA	Taguchi's statistic
$\mathbf{F}=\mathbf{D}_r^{-1/2}$	$\mathbf{a}=\mathbf{r}$	$\mathbf{B}=\mathbf{I}$	$\mathbf{D}^T=\mathbf{M}^T$	$\mathbf{E}=\mathbf{W}_J$	Cuadras approach	No index
$\mathbf{F}=\mathbf{D}_r^{-1/2}$	$\mathbf{a}=\mathbf{r}$	$\mathbf{B}=\mathbf{L}$	$\mathbf{D}^T=\mathbf{M}^T$	$\mathbf{E}=\mathbf{W}_J$	Cuadras approach	No index
$\mathbf{F}=\mathbf{D}_R^{-1/2}$	$\mathbf{a}=\mathbf{r}$	$\mathbf{B}=\mathbf{R}$	$\mathbf{D}^T=\mathbf{C}$	$\mathbf{E}=\mathbf{D}_C^{-1}$	doubly ordered cumulative CA	doubly cumulative chi-squared statistic

Table1. An unified approach to simple correspondence analysis

References

Beh, E. J., D'Ambra, L., Simonetti, B., Cumulative correspondence analysis for ordered categorical data using Taguchi's Statistic, *Communication in Statistics – Theory and Methods* **40**, 1620-1632 (2011).

Beh, E. J., D'Ambra, L., Simonetti, B., Ordinal correspondence analysis based on cumulative chi-squared test, *CARME 2007*. Rotterdam 25-27 June

Cuadras, C.M.; Cuadras i Pallejà, D., A unified approach for representing rows and columns in contingency tables, *A CODAWORK'08*. Girona: La Universitat (2008).

D'Ambra, L., Beh, E. J., Camminatiello I., Cumulative Correspondence Analysis of Two-Way Ordinal Contingency Tables, *Communication in Statistics - Theory and Methods* (forthcoming) (2012).

Goodman, L. A., Kruskal, W. H., Measures of association for cross classifications, *Journal of the American Statistical Association* **49**, 732-764 (1954).

Greenacre, M. J. (1984). *Theory and Application of Correspondence Analysis*. London Academic Press.

Hirotsu, C., Modelling and analysing the generalized interaction, *Proceedings of the Third IEEE Conference on Control Applications*, ISBN-10: 0780318722 (1994).

Light, R. J., Margolin B. H., *An* analysis of variance for categorical data, *Journal of the American Statistical Association* **66,** 534 - 544 (1971).

Nair, V. N., Chi-squared type tests for ordered alternatives in contingency tables, *Journal of the American Statistical Association* **82**, 283-291 (1987).

Satterthwaite, F. E., An approximate distribution of estimates of variance components, *Biometr. Bull.* **2**, 110 - 114 (1946).

Taguchi, G., A new statistical analysis for clinical data, the accumulating analysis, in contrast with the chi-square test, *Saishin Igaku* **29**, 806-813 (1974).

Compartment based modeling and particle filter observer for urban travel time traffic estimation: Sensitivity analysis and case study

Matthieu Canaud[1], Nour-Eddin El Faouzi[1], and Jacques Sau[2]

[1] Transport and Traffic Engineering Laboratory, Université de Lyon, IFSTTAR, ENTPE, 25 avenue François Mitterrand Case 24 69675 Bron Cedex, France
e-mails: matthieu.canaud@ifsttar.fr and nour-eddin.elfaouzi@ifsttar.fr
[2] Fluids Mechanics and Acoustics Laboratory, LMFA, Université de Lyon, 43 boulevard du 11 novembre 1918 69622 Villeurbanne, France
e-mail: jacques.sau@univ-lyon1.fr

Abstract. In this paper, we propose a simple but robust model in order to estimate and predict travel time in urban areas. This model is coupled with particle filter engine which enables real-time urban state traffic estimation, from which travel time can be derived. To validate the proposed model and to test its robustness, an analysis of model sensitivity has been carried out using experimental design method. Such an approach enables factor effects characteristics, even if input data are subject to uncertainties and biases and also highlights the main influence of the downstream supply as well as the role of interactions.

Keywords: Urban traffic modeling, Travel time estimation, Sequential Monte–Carlo, Experimental design, Sensitivity analysis.

1 Introduction

Challenges of a better understanding of travel time, whether in urban or interurban, are manifolds. This indicator is useful (i) for monitoring the performance of a road network; (ii) as an indicator of decision support for tactical strategies; (iii) to communicate to users in real time for helping route choices. In urban areas, these issues are more critical because of the growth in mobility needs, the significant increase in vehicle traffic and the high sensitivity of traffic condition to perturbations. Despite this, few works have focused on the estimated travel times on signalized urban roads, mainly due to methodological issues.

In this paper we propose a robust traffic model to estimate and predict travel time in urban areas. The model is based on space-time discretization of traffic quantities associated with flow exchanges in terms of upstream demand and downstream supply. Due to the high nonlinearity of the model, particle filter (PF) has been chosen as the estimated method. The model, coupled

with PF, enables real-time urban traffic state estimation (Sau *et al.* [17]) and therefore urban travel time estimation.

Thus, this approach allows the state of the system to be reconstructed given the observed measures. Then, we have to test its performance in terms of estimation quality of travel time and its relevance to the evolution and behavior of traffic flows. In this respect, a considerable effort is devoted to the sensitivity study of the model, thanks to the experimental design method.

This paper is structured as follows. The first part is dedicated to the modeling framework description, by providing more details on the first order macroscopic model used in our case. The second part presents PF that provides an efficient solution to state vector estimation. Finally, we present the sensitivity analysis based on experimental design. The results prove the validity of the chosen model.

2 Urban Traffic State-Space Modeling

It is known in dynamic system theory (Chien and Kuchipudi, [6]; Chen, [5]; Chui and Chen, [7]; Doucet *et al.*, [10]; Ristic *et al.*, [15]) that knowledge about a system's model, even approximately, enables estimation of all important information, here travel time, from the measured quantities.

In urban network settings, traffic modeling with signalized intersections is a complex task given the spatial and temporal variability of the phenomenon and the number of data to be processed.

In several European cities, information on travel time in real time is provided on highways and main roads. However, in many urban roads, reliable travel time information in real time is still missing, due to the complex nature of urban traffic dynamics, composed of so many turning movements and interruption. In this section we present a dynamic model able to reproduce the main features of traffic flows in urban areas.

2.1 Compartment based urban traffic model

Travel time estimation can be calculated from simulations and traffic measurements from sensors (video, probe vehicles, ...). These simulations, based on simple and robust models, can provide estimates and forecasts relevant enough either *a posteriori*, or in real time. A simple and robust model reflecting the main characteristics of urban traffic is required when it comes to travel time estimation. To this end the urban network was split into segments serving as interconnected compartments. We attribute a maximum capacity to each one (noted $n_{j,\max}$ for compartment j) and the link between two connected compartments is characterized by a maximum flow (noted $q_{j,\max}$ between compartment j and $j+1$). Thus, flow exchanges between compartments are established in terms of supply and demand, a demand function

of upstream compartment and a supply function of the compartment downstream. Hence, this modeling framework is consistent with the well-known LWR macroscopic model ([14] [12]). This approach allows us to implement a dynamic model, able to reproduce the main features of urban traffic.

More specifically, at time t_k, the system is characterized by the number of vehicles in each compartment, their output flow and the input flow in the first one. Thus, the system is composed of N compartment populations and $N+1$ vehicle flows between them, e.g. variables of the model are $n_{k,j}$, the number of vehicles in compartment j at time t_k, $j = 1, \ldots, N$, $q_{k,j}$, vehicles flow between compartment j and $j+1$ at time t_k, $q_{k,0}$, vehicle flow entering in the first compartment.

Having defined a structure of the urban traffic system and the variables that characterize it, the dynamic model can be written at time t_k as follows:

1. demand of compartment j: $\Delta_{k,j} = \min(n_{k,j}, q_{j,\max}\Delta t)$,
2. supply of compartment $j+1$: $\Omega_{j,j+1} = n_{j+1,\max} - n_{k,j+1}$,
3. vehicle transfer from compartment j to $j+1$: $P_{k,j} = \min(\Delta_{k,j}, \Omega_{k,j})$.

With these three equations, we can deduce the update of the system state from time k to time $k+1$:

$$\begin{array}{l} n_{k+1,j} = n_{k,j} - P_{k,j} + P_{k,j-1} \\ q_{k,j} = P_{k,j}/\Delta t \end{array} . \tag{1}$$

As a system, a compartment k is subject to external actions including its upstream demand D_k and its downstream supply S_k, lateral inflows and outflows and events such as incidents, crashes, ... Without loss of generality[1], we adopt here a simpler version in which lateral inflows and outflows are neglected and consider only the actions of the first two input parameters, namely D_k and S_k (figure 1).

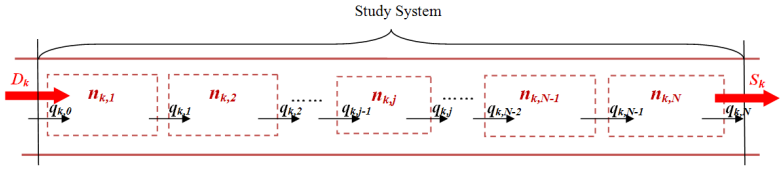

Fig. 1. Urban system schematization of N compartment populations and $N+1$ flows

All system features are defined in the state vector x_k, which contains the N compartment populations and the $N+1$ flows, e.g.

$$x_k = (n_{k,1}, \ldots, n_{k,N}, q_{k,0}, q_{k,1}, \ldots, q_{k,N}). \tag{2}$$

[1] More complex case needs more sophisticated method like for example the augmented state vector approach

Equations (1) are the dynamic equations of the system that can be symbolically represented by a function f. The state equation can be formally written as follows:

$$x_{k+1} = f(x_k, u_k), \tag{3}$$

where f is a complex and highly nonlinear function with no straightforward analytical form, and u_k is the (D_k, S_k) pair.

The state equation (3) is completed by an (linear) observation equation, which maps measurements, y_k, and the state vector of the system:

$$y_k = Cx_k, \tag{4}$$

where C is a real matrix consisting of rows whose elements are all zero except the element corresponding to the position of the sensor delivering a measurement. In our case, the measured quantities are the flow and occupancy rates of each compartment.

As there are uncertainties for both measurements and the model, the complete dynamical model is given by

$$\begin{cases} x_k = f(x_{k-1}, u_{k-1}) + w_{k-1} \\ y_k = Cx_k + v_k \end{cases} \tag{5}$$

where v_k and w_k are Gaussian noises of null mean and (positive) variance-covariance matrix respectively Q_k and R_k.

2.2 Urban travel time derivation

Since the state vector encompasses all the dynamic characteristics of the system, its knowledge is used to derive all the appropriate quantities. We assume that we know the time dependence of $x(t)$ of the state vector. It first determines the duration $T_j(t_{e_j})$, that is the time that a vehicle entering compartment j at time t_{e_j} needs to cross it. Let's $x_j(t)$ be the vector that gives the evolution over time, of compartment j population, while the element $x_{N+j+1}(t)$ gives the evolution over time of the flow leaving same compartment. The number of vehicles ahead a vehicle entering compartment j at time t_{e_j} is given by the component $x_j(t_{e_j})$.

Thus, $T_j(t_{e_j})$ is the solution of the equation:

$$x_j(t_{e_j}) = \int_{t_{e_j}}^{t_{e_j}+T_j(t_{e_j})} x_{N+j+1}(t)dt. \tag{6}$$

This vehicle enters then compartment $j+1$ at time $t_{e_{j+1}} = t_{e_j} + T_j(t_{e_j})$. Equation (6) can be used to determine $T_{j+1}(t_{e_{j+1}})$, the travel time of compartment $j+1$, and so on for all N compartments in the system.

Thus we can derive the travel time needed for a vehicle entering the first compartment at time t_{e_1}, to travel all compartments by: $T(t_{e_1}) = \sum_{j=1}^{N} T_j(t_{e_j})$.

3 Particle filter method

The data assimilation process combines two types of heterogeneous information: data and a mathematical model to achieve the model state variables. It is a technique to estimate the actual state x_t of the system given the measurements $y_{0:t}$ up to time t. In this Bayesian spirit it consists of the recursive calculation of the posterior $\mathbb{P}(x_t|y_{(0:t)})$.

Among the data assimilation techniques, there are sequential methods such as Kalman filter and its extended versions (extended, ensemble or unscented). Due to the high nonlinearity of our dynamic model, the Bayesian filtering based on Monte-Carlo methods is used (Mihaylova and Boel [13]). It consists of sophisticated techniques for estimating models based on simulation, generally with the assumption of a Markov behavior of the physical system.

The underlined theory has been extensively described in the works of Doucet, [9] [10]; Arulampalam *et al.*, [1]; Ristic *et al.*, [15] and Chen, [5]. We briefly recall the main ingredients of the PF.

The aim of the Monte-Carlo approach is to use a proxy sample of size m of $\mathbb{P}(x_{0:t-1}|y_{0:t-1})$, also called particles, to derive estimates of unknown distributions $\mathbb{P}(x_{(0:t)}|y_{(0:t)})$. However, sampling along the aforementioned law is difficult, and the conventional technique is to use an importance sampling, where a distribution $\pi(x_{0:t}|y_{0:t})$, called the importance function is chosen. Under these conditions, any average value is written:

$$\begin{aligned} I(h_t) &= \int h_t(x_{0:t}) \frac{\mathbb{P}(x_{0:t}|y_{0:t})}{\pi(x_{0:t}|y_{0:t})} \pi(x_{0:t}|y_{0:t}) dx_{0:t}, \\ &= \mathbb{E}_{\pi(\cdot|y_{o:t})}[h_t(x_{0:t})\omega(x_{0:t})], \end{aligned} \tag{7}$$

where $\omega(x_{0:t})$ correspond to the weight affected to each sample or particle, and are expressed by:

$$\omega(x_{0:t}) = \frac{\mathbb{P}(x_{0:t}|y_{0:t})}{\pi(x_{0:t}|y_{0:t})}. \tag{8}$$

The distribution $\mathbb{P}(x_{(0:t)}|y_{(0:t)})$ is approximated by a set of random state vector samples of size m with associated normalized weights $\{\omega_{(0:t)}^{(j)} : j = 1, \ldots, m\}$. The importance functions are selected to be appropriate to the Markov process and so lead to a sequential algorithm for updating samples and associated weights. Doucet [8] has shown that $\mathbb{P}(x_t|x_{t-1}^{(j)}, y_t)$, where (j) denotes the j^{th} sample, is the optimal importance function that minimizes the importance weight variance $\omega_t^{(j)}$ knowing the past $x_{t-1}^{(j)}$ and y_t, but of no practical use in general case.

The recurrence relation of the weights is simplified and written:

$$\omega_t^{(j)} = \omega_{t-1}^{(j)} \mathbb{P}(y_t|x_{t-1}^{(j)}). \tag{9}$$

In our application, we measure directly the components of the state vector, the observation equation is linear and the Gaussian assumption is reasonable. With the model defined in section 2.1, the partial Gaussian state space case, where the optimal importance function is available, (Doucet, [8], Arulampalam *et al.* [1]) is a well-founded approximation, defined by

$$\begin{cases} x_t = f(x_{t-1}, u_{t-1}) + w_{t-1}, w_t \sim \mathcal{N}(0, R_t) \\ y_t = Cx_t + v_t, v_t \sim \mathcal{N}(0, Q_t) \end{cases}, \tag{10}$$

with $f : \mathbb{N}^n \to \mathbb{N}^n$, C a real matrix and v_t and w_t are Gaussian noise, with Q_t and R_t positive definite matrices.

Using the two following equations:

$$\begin{aligned} S_t^{-1} &= Q_t^{-1} + C^t R_t^{-1} C, \\ \mu_t &= S_t Q_t^{-1} f(x_{t-1}, u_{t-1}) + C^t R_t^{-1} y_t, \end{aligned} \tag{11}$$

samples and weights update equations for the sequential algorithm become:

$$\begin{aligned} x_t &= \mathbb{P}(x_t | x_{t-1}, u_{t-1}, y_t) \sim \mathcal{N}(\mu_t, S_t), \\ \omega_t^{(j)} &= \omega_{t-1}^{(j)} \mathbb{P}(y_t | x_{t-1}^{(j)}, u_{t-1}), \end{aligned} \tag{12}$$

where

$$\mathbb{P}(y_t | x_{t-1}^{(j)}, u_{t-1}) \sim \exp\left(-1/2 \; \upsilon_t^t (R_t + C Q_t C^t)^{-1} \upsilon_t\right), \tag{13}$$

with $\upsilon_t = y_t - C f(x_{t-1}, u_{t-1})$.

Thus, with those new samples and weights, the estimation of the state vector at time t is

$$\hat{x}_t = \sum_{j=1}^{m} \omega_t^{(j)} x_t^{(j)}. \tag{14}$$

4 Sensitivity analysis of the model

4.1 Experimental design

Experimental design methods are widely used in research as well as in industrial settings (Fang *et al.*, [11] and Santner *et al.*, [16]). The primary goal in the research area is usually to show the statistical significance of an effect that a particular factor induces on the dependent variable of interest.

In many cases, it is sufficient to consider the factors affecting the process under considerations at two levels (screening design) or three levels (surface response design). The experimenter would like to determine whether any of these changes affect the results of the production process.

The most intuitive approach to study those factors would be to vary the factors of interest in a full factorial design, i.e. consider all possible combinations of settings. That is the implemented strategy of our problem. The next step is how to analyze the result of the design. To this end, the

ANalysis Of VAriance (ANOVA) and Pareto chart are well adapted (other tools existed like effects estimates, regression coefficients, surface response, curves of iso-response, ...). Some of them are presented, used and described in the following sections.

4.2 Study case and considerations

Travel time analysis is very useful, since it enables to know how travel time varies with the factor variations and the importance and nature of the effects of factors on the travel time. For this purpose we were inspired by the study case introduced in Bousquet *et al.* [2]. The data used in this study were collected on an urban road axis in Toulouse (South of France). The urban axis on which the experiment was performed is composed of 7 consecutive sections of approximately 2 km with 6 traffic signal controlled intersections. In this site we have selected the five last sections which have the advantage of minor lateral inflows and outflows at the crossroads (which is consistent with our modeling framework), the compartment-based modeling is well adapted.

From previous analyses (Canaud *et al.* [4]), the experimental factors are chosen as the variables that act directly on real travel time. Hence, the chosen factors are the maximum capacity of cells (label A), the maximum flows between cells (B), the upstream demand (C) and the downstream supply (D). For each of these factors, we assign a nominal value and a physical variation, defining their high level and low level. The other input variables of the model are kept constant. With the four selected factors and their two levels, one can perform a $2^4(= 16)$ full factorial design in order to analyze the factors affecting travel time. This was done in Canaud *et al.* [3]. This screening experimental design enables a better understanding of system behavior. Furthermore, thanks to an analysis of travel time accuracy and also a study of missing data recovery capability, authors show that the model provides accurate estimates of travel time even with noisy measurements, as well as a reconstruction of missing data.

The purpose of this work is to extend the previous findings in order to highlight the behavior of interactions, leading to some recommendation for the improvement of traffic operators. In this aim we performed a full factorial design with three levels. The main advantage compared to what has been investigated in Canaud *et al.* [3] is that surface response design can identify some quadratic factors effect, and hence, better interpret the role of interactions.

4.3 Analysis of factors affecting travel time

With four selected factors and their three levels, we performed a $3^4(= 81)$ full factorial design. Results are shown in figure 2. As one can see some interactions are missing. This is explained by the fact they are not significant based on to their p-value.

The figure on the right side is the Pareto diagram, a graphical representation of the factors (and interactions) standardized effects, in decreasing order. The factor is significant if it goes beyond the vertical dashed line (95% confident threshold). So figure 2 exhibits the interaction between maximum flow and downstream supply (BD) which is found to be the most significant interaction. The downstream supply has a highest impact, followed by the maximum flow. We can note also that the sign of their standardized effect are negatives, meaning that the less downstream supply and maximum flow are, the longer the travel time is. Finally, the adjusted R-squared underlines the adequacy of the model. An adjusted R-squared of 91.41% means that our model is efficient to represent the study response, i.e. travel time.

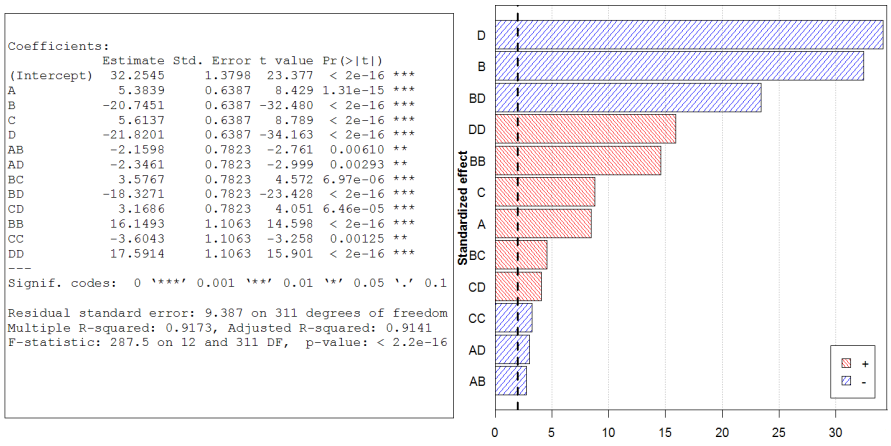

```
Coefficients:
            Estimate Std. Error t value Pr(>|t|)
(Intercept)  32.2545     1.3798  23.377  < 2e-16 ***
A             5.3839     0.6387   8.429 1.31e-15 ***
B           -20.7451     0.6387 -32.480  < 2e-16 ***
C             5.6137     0.6387   8.789  < 2e-16 ***
D           -21.8201     0.6387 -34.163  < 2e-16 ***
AB           -2.1598     0.7823  -2.761  0.00610 **
AD           -2.3461     0.7823  -2.999  0.00293 **
BC            3.5767     0.7823   4.572 6.97e-06 ***
BD          -18.3271     0.7823 -23.428  < 2e-16 ***
CD            3.1686     0.7823   4.051 6.46e-05 ***
BB           16.1493     1.1063  14.598  < 2e-16 ***
CC           -3.6043     1.1063  -3.258  0.00125 **
DD           17.5914     1.1063  15.901  < 2e-16 ***
---
Signif. codes:  0 '***' 0.001 '**' 0.01 '*' 0.05 '.' 0.1

Residual standard error: 9.387 on 311 degrees of freedom
Multiple R-squared: 0.9173, Adjusted R-squared: 0.9141
F-statistic: 287.5 on 12 and 311 DF,  p-value: < 2.2e-16
```


Fig. 2. Coefficient estimations and significativity (left) and Pareto chart (right) of the estimated travel time

The response surfaces (figures 3) offer a graphical visualization of the interactions between factors. In the following, only three interactions are provided namely BC, BD and CD, since interactions with factors A are not significant. Moreover, factor A is the less influent factors among simple effects. Hence, one can conclude that the model is less sensitive to the maximum compartment population.

Regarding the interaction figures, we can first conclude that as expected maximum flow and downstream supply (middle figure) have relatively the same impact on travel time and the optimal combination for travel time reduction is when both are at their higher level. This is consistent with the study case since there are no lateral inputs, meaning that this configuration is more or less equal to one compartment, with free flow in it, which is not realistic.

Second point shown by left and right side figures is that travel time is almost no sensitive to demand but highly sensitive to factors B and D. These

two figures also highlight the fact that the minimum of travel time could be obtained (on these two figures) not with the higher level of flow and supply, but with an intermediate value (0.5). This information is helpful for traffic operators in order to act on the traffic conditions.

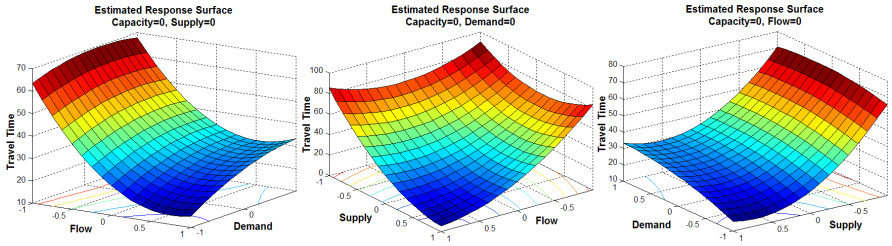

Fig. 3. Response surfaces of interaction BC (left), BD (middle) and CD (right)

For those three figures, the factors that are not explored were fixed at the nominal value (level 0). The other interaction figures with higher or lower level for those factors bring also useful information in order to have a complete understanding of the system behavior.

5 Conclusion

In this paper, we have proposed a dynamic compartment-based traffic model that has been coupled with a PF method in order to provide real time travel time estimation. The model has been implemented on a real-world operational section and the estimates have been analyzed to validate it. We conclude that this model can provide a good estimation even if input data are subject to uncertainties and biases. An analysis of factors affecting real travel time was performed to link time variation with variables. This study concluded that the travel time decreases together with an increase of both downstream supply and maximum flow. Regarding the interactions, one can see how to act on traffic conditions in order to reduce travel time in the study case site.

Among the perspectives, it appears logical to make the scenarios more complex (e.g. taking into account lateral inputs and so on, see Canaud *et al.* [4]) and to perform the study in order to have better understanding of system behavior in other situations. More generally, the goal is to highlight how travel time is affected by different factors in urban network and how to improve traffic conditions.

References

1. Arulampalam, M., Maskell, S., Gordon, N. and Clapp, T. "A tutorial on particle filters for online nonlinear/non-Gaussian Bayesian tracking". *IEEE Transactions on Signal Processing* 50(2):174–188 (2002)
2. Bousquet, A., Sau, J., El Faouzi, N-E. and Billot, R. "Frequency analysis and particle filtering modelling of urban traffic for arterial travel time estimation". *5th IMA Conference on Mathematics in Transport*, London, UK (2010)
3. Canaud, M., El Faouzi, N-E. and Sau, J. "Reservoir-based urban traffic modeling for travel time estimation: sensitivity analysis and case study". *Proceedings of the 91th Transportation Research Board Annual Meeting (TRB)*, Washington D.C., USA, (22-26 January 2012)
4. Canaud, M., El Faouzi, N-E., Sau, J. and Billot, R. "Urban traffic modeling and particle filter for travel time estimation: experimental design for sensitivity analysis". *Technical report IFSTTAR-ENTPE*, Lyon (2012)
5. Chen, Z. "Bayesian filtering: From Kalman filters to particle filters, and beyond". *Tech. Rep. of Adaptive Systems Lab., McMaster University, ON, Canada* (2003)
6. Chien, S.I and Kuchipudi, C.M. "Dynamic travel time prediction with real-time and historic data". *Journal of Transportation Engineering* 129(6):608–616 (2003)
7. Chui, C. K. and Chen, G., *Kalman filtering with real-time applications*, Springer-Verlag, New York (1987).
8. Doucet, A. "Monte Carlo methods for Bayesian estimation of hidden Markov models. Application to radiation signals". *PhD of University Paris-Sud, Orsay* (1997)
9. Doucet, A. "On sequential simulation-based methods for Bayesian filtering". *Tech. Rep. of Departement of Engineering, Cambridge University* (1998)
10. Doucet, A., De Freitas, J.F.G. and Gordon, N.J., *Sequential Monte Carlo methods in practice*, Springer, New-York (2001)
11. Fang, K.T., Li, R. and Sudjinato, A., *Design and Modeling for computer experiments*, Chapman and Hall (2005)
12. Lighthill, M.J. and Whitham, G.B. "On Kinematic waves II: A theory of traffic flow on long crowded roads". *Proc. of The Royal Society A: Mathematical, Physical and Engineering Sciences* 229:317–345 (1955).
13. Mihaylova, L., Boel, R. "A particle filter for freeway traffic estimation". *Proceedings of the 43rd IEEE CDC Conference 2004* 2106–2111, Nassau, Bahamas (2004).
14. Richards, P.I. "Shock-waves on the highway". *Operations Research* 4:45–51 (1956).
15. Ristic, B., Arulampalam, M. and Gordon, N., *Beyond the Kalman Filter: Particle Filters for Tracking Applications*, Artech House, Boston (2004)
16. Santner, T.J., Williams, B.J. and Notz, W.I., *The design and analysis of computer experiments*, Springer-Verlag, New York (2003)
17. Sau, J., El Faouzi, N-E., Ben Aissa, A. and De Mouzon, O., "Sequential Monte Carlo for real time traffic condition estimation and prediction". *Recent Advances in Stochastic Modelling and Data Analysis*, World Scientific Publishing, 12th International Symposium on ASMDA, Chania, Crete (2007)

Multi-scale PCA on ECG signal diagnostic

Chaouch H., Ouni K. and Nabli L.

Automatic and Signal processing and Image Laboratory, National school of engineering, Monastir, Tunisia.
Email: hanenchaouc8@gmail.com
Email: ouni_khaled@yahoo.fr
Email: lotfinabli@yahoo.fr

Abstract: In this paper, a method of ECG diagnostic is proposed. This method is based on three parts: the simplification using multi-scale PCA, the default detection and localization by classic linear PCA. The obtained results are efficient by comparing with the expert results.
Keywords: Diagnostic, ECG, Multi-scale PCA, linear PCA, default detection, default location, calculating contributions.

1 Introduction

The electrocardiogram (ECG) is the biological signal the most introduced in the signal treatment researches .Many approach of detection and classification were applied on the ECG [1, 2, 3 and 4]. This work comes in this context, in which a method of ECG diagnostic method is proposed using the multi-scale principal components analysis (MSPCA). This method was proposed by Bakshi [5] in 1998, it enabling to combine modelling through PCA of every wavelet cofficient issued of multi-scaled decomposition. The signal will be re-built on the scale which an abnormal event is observed so as to reduce the number of entity to be watched over. The projection of the re-built signal on the linear PCA model is then applied [6]. The PCA method is based on three parts. The first step is to determine the number to keep in the PCA model by introducing various techniques [7 and 8]. The choice of the method of determining of the principal components has a significant impact on the rest of the PCA steps. In this work, we use the cumulative variance percent to determine the number of principal components [9]. The second step is the detection of defects that uses the PCA to follow the process behavior at a normal state. On comparing the observed behavior with that given by the PCA, the defects are detected. Many methods have been used to detect the defect, and the frequent ones are the square prediction error (SPE) and Hotteling statistic T^2 [10], which will be introduced also in this approach. To localize the defected variables, many methods have been introduced. In this paper, the defects are localized by the method of calculating contributions [11]. The set of defected parameters on the ECG, and with the intervention of the expert, allowing to give the existing pathology in the subject matter.

2 Wavelet Transform and Multi-Scale Analysis

The wavelet transform is a mathematic tool which allows decomposing signal into frequencies by maintaining a space location. The original signal is projected on asset of basic functions that vary in frequency and space. These basic functions adapt to the frequencies of the signal which will be analyzed. The wavelet transform allows having a location in time and frequency. The wavelet analysis adapts to a prototype function of wavelets called “mother wavelet”. This wavelet generates by recursive translation and dilatation a set of basic function called “daughter wavelet”. The principal of the mother wavelet is given by the following equation:

$$\Psi(\tau, s) = \frac{1}{\sqrt{s}} \Psi(\frac{t-\tau}{s})$$

with τ and s are respectively the translation factor and the dilatation factor. We can find infinity of values for these two factor, we can vary it continuously: this is the principal of the continuous wavelet transform (CWT). This transform as defined is redundant because it gives more wavelet coefficient that it is necessary to describe the signal exhaustively. Practically, we are often deal with discrete signal. That is why we are interested to discretize the values of τ and s, we are talking here about the discrete wavelet transform (DWT). This transform is easier then the CWT in implementation. In this paper, we introduce the DWT in the multi-scale analysis. The discrete wavelet transform allows translating and dilating the wavelet within discrete values.

The coefficients are dicretized as follow:

$s = s_0^j$ et $\tau = k\tau_0$ with s_0 f 1 et τ_0 f 0 fixed and belong to Ä.

The DWT is given by the following equation :

$$DWT(\tau_0, s_0) = \frac{1}{\sqrt{s_0^j}} \int_{-\infty}^{+\infty} x(t)\Psi(\frac{t - ks_0^j\tau}{s_0})dt$$

with s_0^j is the scale factor, τ_0 is the translation factor, k and j are integer.

$\Phi(t)$ and $\Psi(t)$ are the respectively the scale function and the wavelet function defined as follow :

$$\Phi(t) = 2^{-j/2}\Phi(2^{-j}t - k)$$

$\Psi(t) = 2^{-j/2}\Psi(2^{-j}t - k)$ with $k, j \in$ Ä

The projection on the scale function gives the scale coefficients or approximation coefficients a_j. While, the projection on the wavelet function is known as the wavelet coefficient d_j and called the signal detail passing from one scale to another larger.

$$a(j) = \sum_{k=-\infty}^{k=+\infty} x(k)g(2j-k)$$

$$d(j) = \sum_{k=-\infty}^{k=+\infty} x(k)h(2j-k)$$

with h and g are respectively the scale function coefficients (low-pass filter) and the wavelet function coefficients (high-pass filter).

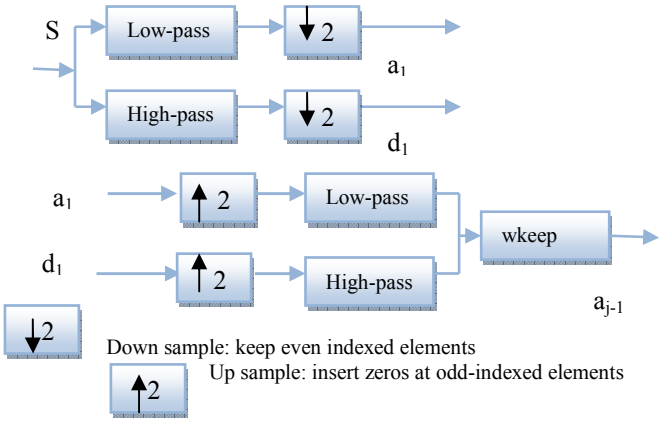

Fig. 1. Multi-scale decomposition and reconstruction

3 Linear Principal components analysis (LPCA)

The method of default detection and location has a great contribution in biological and industrial signal monitoring. This approach rests on three steps: determining the number of principal component, detection and location of defaults. Determining the number of the principal components l is based on the benchmark proposed by Qin.S[12] which integrates the principal of minimizing the variance of reconstruction error. Consider a process whose normal functioning is presented by a matrix of data X with n measures and m variables. The reconstruction error variance of the nth component of $x(k) = [x_1 \ldots\ldots x_m]^T \in \Re^m$ is given by:

$$\rho_i = \mathrm{var}\left\{\zeta_i^T (x(k) - x(k)^i) \right\}$$

with ζ_i is the ith column of the identity matrix and $x(k)$ represents the measurement vector whose ith component has been reconstructed in the following way:

$$x(k)_i = \frac{\left[C_{-i}^T 0 C_{+i}^T\right]}{1 - C_{ii}} x(k)$$

with $C = \rho_1 \rho_1^T = [C_1 C_2 \ldots\ldots C_m]$, C_i the ith column of the matrix C . The vectors made up by the first (i-1) and the last (m-i) elements are presented by the signs (+i) et (-i).

The determining of the number of principal components is based on the minimization criterion explained as follow:

$$J(1) = \sum_{i=1}^{m} \frac{\rho_i}{\mathrm{var}\left\{\zeta_i^T x_k\right\}} = \sum_{i=1}^{m} \frac{\rho_i}{\zeta_i^T \Sigma \zeta_i}$$

The second part of the PCA approach is the default detection. Two methods are introduced at this step, the Hotteling statistic T² and the SPE method (Squared Prediction Error) which are defined as follow:

$$T^2(k) = \sum_{i=1}^{l} \frac{t_i^2(k)}{\lambda_i}$$

$$SPE(k) = \sum_{j=1}^{m} (e_j(k))^2$$

with $e_j(k)$ is the j[th] residue.

The detection of a default is true if one of these following conditions is found:

$$SPE \text{ p } \delta_\alpha^2$$

$$T^2 \text{ p } \chi_\alpha^2(1)$$

where δ_α^2 and $\chi_\alpha^2(1)$ are respectively the thresholds of T² and SPE.

For determining the defected variables we introduce the localization method of the PCA approach. We use here the principle of calculating contributions of variables at the principal component. In fact, every principal component is expressed as follow:

$$t_i = \rho_i^T x = \sum_{j=1}^{m} \rho_{ij} x_j$$

with ρ_i as the proper vector corresponding to the value λ_i .

The total contribution of the variable x_j on the q highest components is given by:

$$Cont_j = \sum_{i=1}^{q} Cont_{ij}$$

$$Cont_{ij} = \frac{t_i}{\lambda_j} \rho_{ij} x_j$$

ρ_{ij} is j[th] component of the proper vector ρ_i .

4 Multi-Scale LPCA

The proposed approach is based on the multi-scale linear principal components analysis (MSLPCA). This method developed by Bakshi in 1998, allows combining the PCA modeling of each wavelet coefficient. In this paper, we use the wavelet toolbox of matlab for the application of MSPCA. The multi-scale principal component generalizes the usual PCA of a multivariate signal seen as a matrix by performing simultaneously a PCA on the matrices of details of different levels. In addition, a PCA is performed also on the coarser approximation coefficients matrix in the wavelet domain as well as on the final reconstructed matrix. By selecting

conveniently the numbers of retained principal components, interesting simplified signals can be reconstructed as shown in fig.2.

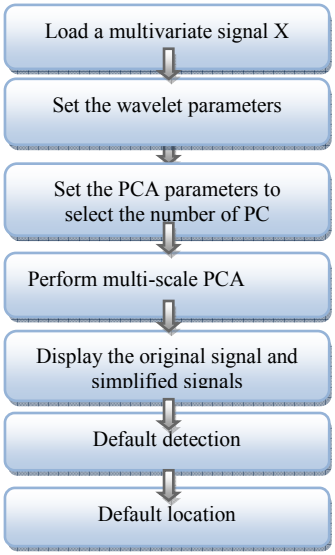

Fig. 2. MSPCA algorithm

5 ECG signal diagnostic

5.1 ECG signal simplification

The first step in the diagnostic ECG approach is the application of the MSPCA to simplify the studied signal. The following figures show the result of the ECG simplification. The studied signal is a multi-varied one, composed by 9 variables as shown in figure 3. These variables are determined from the ECG characteristic waves, the R wave amplitude (RA), the P wave amplitude (PA), the Q wave amplitude (QA) and the S wave amplitude (SA). The rest of variables describe the ECG segments which are: QS, QP, RR and ST intervals. The application of the MSPCA allows simplifying the multi-varied signal. In fact, after decomposing the signal into wavelet coefficient using the discrete wavelet transform (DWT) we apply the linear PCA approach on each variable to find the number of principal component. These variables are reconstructed using only the retained principal components. The reconstructed signal is called simplified as shown in figure 4.
This signal will be used in the rest of the proposed study.

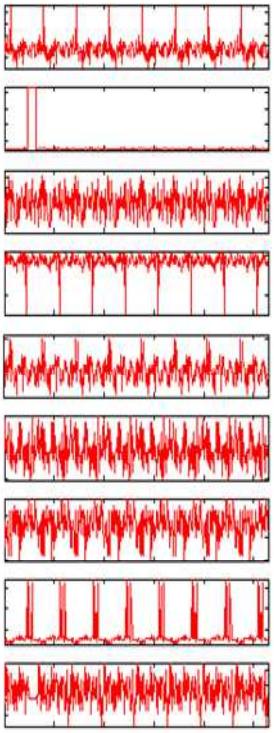

Fig. 3. Original Signal

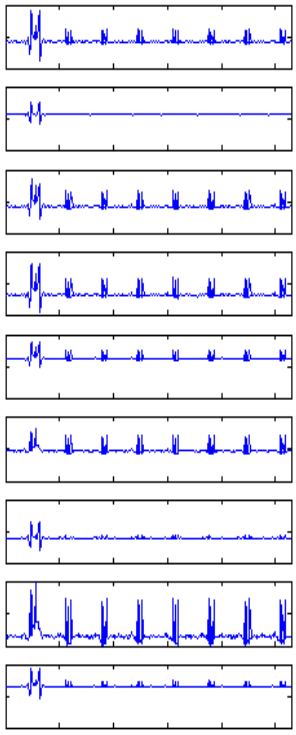

Fig. 4. Simplified Signal

5.2 Default detection and location

In the detection part, we introduce the method of squared predictive error SPE to identify defaults on the studied signal. Figures 5 shows that there is no detected default using the SPE method. That can be explained by the normal functioning of the ECG. In fact, we have to generate some default on the signal for effective assessment of our study. We increase a dozen of measures using the same amplitude; this default is generated on the variable RA as shown in figure 6. The next step is the location of default by the method of calculating contributions.

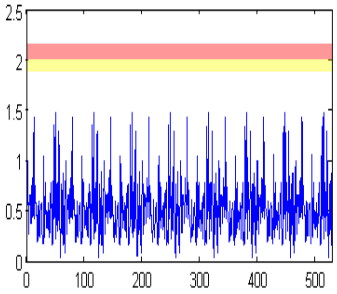

Fig. 5. SPE fault detection

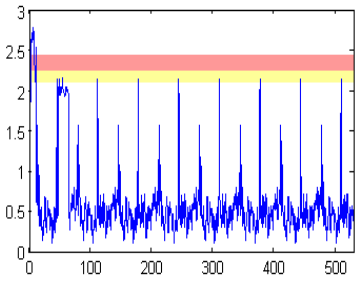

Fig.6.SPE stimulated fault detection

In the localization part, we use the method of calculating contributions. In fact, the variable which has the greatest contributions is the defected one. The results at this step are presented in figures 7 that show that the variable RA is defected because it has the greatest contributions. We note that these results are consistent with the default generation hypothesis. In fact, we locate the default at the same variable that it was generated. While, figure 7 shows that the contributions of these variables are close. That can restrict the proposed approach of ECG diagnostic.

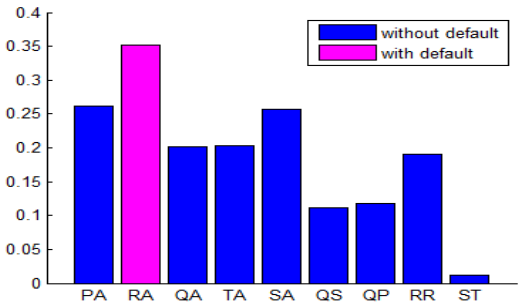

Fig. 7. Default location

6 Conclusion

In this paper, an ECG signal diagnostic method is proposed. This method is based on the multi-scale principal components analysis which combine the discrete wavelet transform (DWT) and the linear PCA. First, the multi-varied signal is decomposed using the DWT on wavelet coefficient at five scales. Then, the linear PCA is applied on each coefficient and the number of principal components is calculated.

After that, we reconstruct signal using only the retained principal components. The simplified signal is then introduced in the linear PCA steps to detect defaults. While, we know that the studied ECG is a normal one that is why we should create some default to proceed our study. The proposed method is efficient in detection and location of default. In fact, we detect and locate the default in the same variable that it was created (variable RA). In other words, this method is limited due to fact that the contributions of variables are very close and that other methods are considered to better locate defects as the reconstruction principle.

References

1. A.Algra and H.L.B.C Zeelenberg. An algorithm for computer measurement of QT intervals in 24 hour ECG. In Computer in Cardiology. Los Alamitos, CA, IEE computer Society Press, pp 117-119, 1987.

2. M.Bahoura, M.Hassani, and M.Hubin. DSP implementation of wavelets transform for real time ECG waveforms detection and heart rate analysis. Comput.Meth.Programs Biomed, n°52, pp 35-44, 1997.

3. L.Clavier and J.M Boucher. Segmentation of electrocardiograms using a Hidden Markov Model. In 18th annual international conference of the IEEE Engineering in Medicine and Biology Society October 31-November 3, 1996.

4. Z.Dokur, T.Olmez, E.Yazgan, and O.Ersoy. Detection of ECG waveswaveforms by neural networks.Med.Eng.Phys, vol 19,n°8, pages 738-741, 1997.

5.Bakshi B.R. Multiscale PCA with application to multivariate statistical process monitoring. AICHE Journal, 44(7), pp 1596-1610, 1998.

6. P.Nomikos et J.F.MacGregor. «Monitoring batch processes using multiway principal component analysis", AICHE Journal, vol.40, N°8, pp.1361-1375, 1994.

7.H.F. kaiser. « the application of electronic computers to factor analysis », Educational and Psychological Measurement, vol.20.pp 145-151, 1960.

8.D.Giancarlo et T.Chiara. « cross-validation methos in principal component analysis : a comparision », Statistical Method and Applications, vol.11, pp71-82, 2002.

9. D.Zumoffen et M.Basualdo. « From large chemical plant data to fualt diagnosis integrated to decentralized fault tolerant control: pulp mill process application », Industrial and Engineering Chemistry Research, vol. 15, pp.1201-1220, 2007.

10. J.E.Jackson et G.S. Mudeholkar. « Control procedure for residuals associated with principal component analysis », Technometrics, vol.40, N°20, pp. 457-469,1998.

11. S. J. Qin, S. Valle, et M. Piovoso. "On unifying multi-block analysis with applications to decentralized process monitoring", Journal of chemometrics, vol. 15, N°9,pp.715-742, 2001.

12. Qin.S. « Joint diagnosis of process and sensor faults using principal components analysis », Control Engineering Practice, Vol .6,N04,pp.475-469, 1998

Identification of "wing rock" phenomenon, implementing Patchy Neural Network with the use of RISE observer, on slender delta 80° wing aircrafts

Paraskevas M. Chavatzopoulos, Thomas Giotis, Manolis Christodoulou, Haris Psillakis

Department of Electronic and Computer Engineering, Technical University of Crete
Chania, Crete, Greece
Email: pchavatzopoulos@yahoo.gr
Department of Electronic and Computer Engineering, Technical University of Crete
Chania, Crete, Greece
Email: thgiotis@gmail.com
Department of Electronic and Computer Engineering, Technical University of Crete
Chania, Crete, Greece
Email: manolis@ece.tuc.gr
Department of Electrical Engineering, Technological & Educational Institute of Crete
Heraklion, Greece
Email: psilakish@hotmail.com

Abstract: In this paper, the "wing rock" phenomenon is described for slender delta 80° wing aircrafts on the roll axis. This phenomenon causes the aircraft to undergo a strong oscillatory movement with amplitude dependent on the angle of attack. The objective is to identify "wing rock" using the Patchy Neural Network (PNN), which is a new form of neural nets. For the update of the weights of the network, an observer called RISE (Robust Integral of Sign Error) and equations of algebraic form are used. This causes the PNN to be fast, efficient and of a low computational cost.
Keywords: wing rock phenomenon, RISE observer, Patchy Neural Network (PNN), slender delta 80° wing aircrafts

1. Introduction

Neural networks are the future of modern computing. They are volatile, applicable to all problems solved with hardware, software or firmware, fast and most importantly they are evolving constantly. Modern aircrafts need this fast and error tolerance computing method, making neural networks essential for aerospace.

In this paper, we present the "wing rock" phenomenon for slender delta 80° wing aircrafts. The motion of the aircraft, during this phenomenon, in the roll axis is described by the equation given in [2]. The concern of this paper is to identify this phenomenon using the Patchy Neural Network (PNN). This is a new form of neural networks proposed in [8]. For the renewal of the network's weights, the use of an observer called RISE (Robust Integral of Sign Error) is needed and equations of algebraic form. This causes the PNN to be quicker, more efficient and to have less computational cost than neural nets used now.

2. "Wing Rock" Phenomenon

Wing rock is the phenomenon during which the airplane is undergoing a strong oscillatory movement. For the purpose of this paper, the phenomenon is only approached in the roll axis.

"Wing rock" is an oscillation that occurs when the airplane increases its angle of attack(α). In this paper, we focus on this phenomenon occurring on slender tailless delta 80° wing aircraft; the model of the aircraft used to observe the phenomenon has wings swept back forming the Greek letter "Δ"(delta) and it does not have any tail wings. The aspect ratio between the wingspan and the mean value of the wing's chord is high; therefore makes the wings slender, making the aircraft aerodynamically efficient and perfect for maneuvering in low speeds (subsonic jet speeds). The angle of the sweep Λ is the angle between the leading edge of the wing and the body of the aircraft; for this paper the aircraft has Λ=80°.

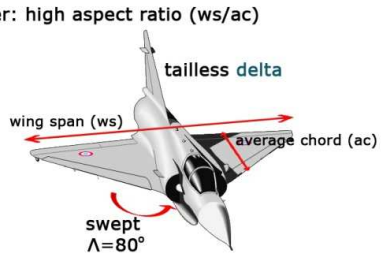

Figure 1 Slender tailless delta 80° wing aircraft

The case of the phenomenon of the "wing rock" on swept delta wings is called slender wing rock. It takes place at high angles of attack due to vortex asymmetry at the leading edge of the wing; this asymmetry can be the result of flying conditions. Furthermore, flying at high angles of attack in asymmetric flow conditions (landing in a cross-wind) or induced lateral oscillations due to unsteady flow over the wing could lead to the shedding of an asymmetric vortex.

As a result, the leading edge leeward vortex shifts outboard and the leading edge windward vortex shifts inboard causing the wing to initially roll in the positive roll direction. The sudden roll movement causes the leeward vortex on the up-going wing to compress and the windward vortex on the down-going wing to stretch, which increase the initiated rolling moment. As the roll angle increases, the kinematic-coupling between the angle of attack and the sideslip causes the effective angle of attack on the wing to decrease and the effective sideslip to increase. The increased sideslip on the wing during roll causes the windward vortex on the down-going wing to move inboard and toward the surface and the leeward vortex on the up-going wing to

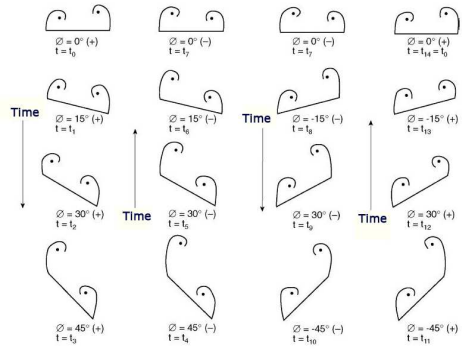

Figure 2 Graphic representation of vortices one cycle of wing rock

move outboard and lifted off. The convective time lag associated with the motion of the lifted off vortex causes the right wing to continue dipping until the lifted vortex takes its final position. Then the lift on the down-going wing together with the reduction of vortex strength due to the decrease of the effective angle of attack causes the wing to stop at a finite roll angle (the limit cycle amplitude) and then reverses its motion. As the wing reverses its motion, the effective angle of sideslip decreases and the lifted vortex starts to reattach. The convective time lag of the vortex motion helps the rolling moment to build up in the reversed direction until the vortex is completely reattached to the leeward side of the left wing. This is graphically represented in *figure 2*.
The mathematical expression describing the movement of a slender delta 80° wing aircraft during "wing rock" phenomenon in the roll axis is presented in [2]

$$\ddot{\varphi} + \omega^2\varphi = \mu_1\dot{\varphi} + b_1\dot{\varphi}^3 + \mu_2\varphi^2\dot{\varphi} + b_2\varphi\dot{\varphi}^2 \quad (1),$$

where φ is the roll angle of the plane, $\dot{\varphi}$ its first derivative and $\ddot{\varphi}$ its second derivative. The terms ω^2, μ_1, μ_2, b_1 and b_2 are given using the expressions
$\omega^2 = -c_1a_1$ (2), $\mu_1 = c_1a_2 - c_2$ (3), $b_1 = c_1a_3$ (4), $\mu_2 = c_1a_4$ (5),$b_2 = c_1a_5$ (6) where

$$c_1 = \frac{\rho S c L_c^2}{2I_{xx}} \quad (7)$$

$$c_2 = \frac{\mu_x L_c}{I_{xx}U_c} \quad (8)$$

and the coefficients a_i depend on the angle of attack(α) and provided in the paper. The values of a_i are given for angle of attack 15° and 25°, as well as the table with the variables used to calculate coefficients c_1 and c_2 are given below.

α	$\boldsymbol{\alpha_1}$	$\boldsymbol{\alpha_2}$	$\boldsymbol{\alpha_3}$	$\boldsymbol{\alpha_4}$	$\boldsymbol{\alpha_5}$
15	*-0.01026*	*-0.02117*	*-0.14181*	*0.99735*	*-0.83478*
25	*-0.05686*	*0.03254*	*0.07334*	*-0.3597*	*1.4681*

Table 1 Values of coefficients a_i for α=15° and 25°

Variable	**Quantity**	**Value**
ρ	air density	*1.1955 kg/m^3*
S	wing area	*0.0324 m^2*
c	chord of the wing	*0.429 m*
$\boldsymbol{L_c}$	characteristic length (L_c=c/4)	*0.10725 m*
$\boldsymbol{I_{xx}^c}$	mass moment inertia	*0.27·10^{-3} kg·m^2*
$\boldsymbol{\mu_x}$	damping coefficient for the bearing of the sting	*0.378·10^{-4} kg·m^2/s*
$\boldsymbol{U_c}$	characteristic speed	*15 m/s*

Table 2 Values of variables used

The use of MATLAB is necessary for the simulation of the movement the airplane is undergoing during “wing rock”. The simulation of the movement is shown below.

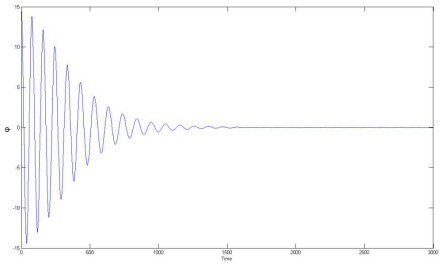

Figure 3 Roll angle as a function of time for α=15°

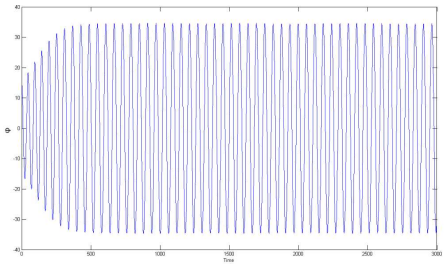

Figure 4 Roll angle as a function of time for α=25°

Comparing the two figures above, it can be deduced that a way to prevent wing rock from happening is to have an angle of attack under 20°; wing rock can also be prevented with the use of flaps.
The simulation also outputs the phase plane of the movement in the roll axis φ to its first derivative$\dot{\varphi}$, which is required for the weight update of the neural network discussed later.

3. RISE Observer

When only some measurements or outputs are available for identification and control, it is usually necessary to estimate the rest of the system’s states. This leads to the development of linear and non linear techniques with the use of observers or estimators. Observers give an estimation of non finite states, therefore the estimated states must be accurate in detecting possible errors and failures.
One approach of designing non linear observers is the high gain category. The design of these estimators aims in the disassociation of the linear and non linear part. Then, the gain of the estimator is selected so as the linear part to dominate over the non linear one. Choosing a very high gain can result in having a relatively small observation error, but it will cause large amplitude oscillation to the system’s noise.
The noise levels and the dynamic of the system change with the passing of time and the accuracy of the methods is diminished. Thus, the use of robust observers or methods of estimation with noise tolerance is essential. One method that could be used is the RISE (Robust Integral of Sign Error) observer. This method increases the robustness of the observer and at the same time the effectiveness of error tracing in comparison to typical estimators. The observer suggested offers, beyond robust estimation in case of noise, an area of asymptotic stability for state estimation. Simulations have shown that RISE is capable to estimate states with 25% accuracy with rising noise levels.
For this paper, an observer is developed, so that it can be used by a neural network for learning and unknown state identification and RISE feedback for robustness.

The full state approach of the asymptotic estimator based on the robust integral of the sign error (RISE) $\xi(t)$ is given by the equation

$$\dot{\hat{x}}(t) = \xi(t) = k\big(x(t) - \hat{x}(t)\big) + \lambda\kappa \int_0^t (x(s) - \hat{x}(s))ds + \beta \int_0^t \operatorname{sgn}\big(x(s) - \hat{x}(s)\big)ds$$

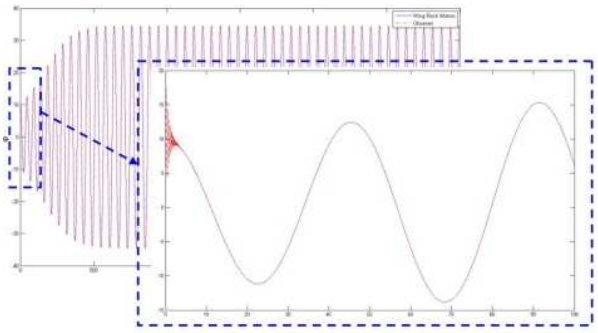

Figure 5 Comparison between the simulation of the motion of the aircraft during wing rock and the estimation of the motion from RISE observer for α=25°

where $k, \lambda, \beta > 0$, $\dot{x}$ is $\ddot{\varphi}$ and x is $\dot{\varphi}$. To use this observer to develop the Patchy Neural Network to identify wing rock phenomenon, the variables have the following values $k = 2, \lambda = 1, \beta = 20$. The observer was created with the use of MATLAB which resulted in the figures shown below. For the development of this observer, the use of the values of φ found in the simulation of the phenomenon is essential.

4. Patchy Neural Network(PNN)

For the construction of the neural network, a new category of local networks is used; it is called patchy neural network (PNN) with basis functions that are patches of the state space. This specific network with a sufficient number of nodes can approximate a general smooth non linear function over a given compact region with the desired accuracy. PNN network is used to extract and store information obtained by the estimation of an observer, using a simple algebraic weight update law. The way PNN works is presented.

Let n-dimensioned rectangles

$$I := I_1 \times I_2 \times \cdots \times I_n$$

and δ partitions of each interval I_i mathematically expressed as

$$I_i = \bigcup_{j=1}^{N_i} A_{i,j} = \bigcup_{j=1}^{N_i} [a_{i,j-1}, a_{i,j}]$$

with $\alpha_{i,j} = a_{i,0} + j\delta$, $1 \le i \le n$.

Patch functions are defined on the sets $A_{1,i_1} \times \cdots \times A_{n,i_n}$, where $1 \le i_j \le N_i$ and $1 \le i \le n$

$$p_{i_1,i_2,\cdots,i_n}(x) = \begin{cases} 1, \alpha v\ x \in A_{1,i_1} \times \cdots \times A_{n,i_n} \\ 0, else \end{cases}$$

A patchy neural network is a neural network with one hidden layer and basis vector that consists of patch functions with output

$y = \sum_{i_1=1}^{N_1} \cdots \sum_{i_n=1}^{N_n} w_{i_1,\cdots,i_n} p_{i_1,\cdots,i_n}(x) = W^T P(x),$

where

$W = [w_{1,\cdots,1}, \cdots, w_{N_1,\cdots,N_n}]^T \in \mathbb{R}^{N_1 \times \cdots \times N_n}$

and

$$P(x) = [p_{1,\cdots,1}, \cdots, p_{N_1,\cdots,N_n}]^T$$

The network's weights are updated algebraically with the use of the equation

$\widehat{w}^j_{i_1,\cdots,i_n}(t) =$

$\left(1 - p_{i_1,\cdots,i_n}(x(t))\right) \widehat{w}^j_{i_1,\cdots,i_n}(t^-) +$

$p_{i_1,\cdots,i_n}(x(t))\xi(t)$

or equivalently

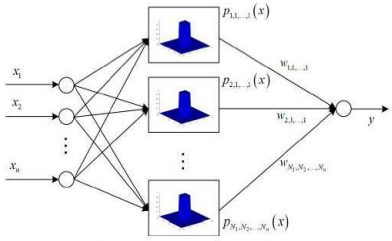

Figure 6 Structure of Patchy Neural Network (PNN)

$$\widehat{w}^j_{i_1,\cdots,i_n}(t) = \begin{cases} \widehat{w}^j_{i_1,\cdots,i_n}(t^-), & if\ p_{i_1,\cdots,i_n}(x(t)) = 0 \\ \xi_j(t), & if\ p_{i_1,\cdots,i_n}(x(t)) = 1 \end{cases}$$

where $j = 1,2,\ldots,n$ with initial values $\widehat{w}^j_{i_1,\cdots,i_n}(0) = 0$ for $1 \le i_1 \le N_1, \ldots, 1 \le i_n \le N_n$ and $1 \le j \le n$. The vector $\widehat{W}^T P(x)$ with $\widehat{W} := [\widehat{W_1} \cdots \widehat{W_n}]$, with $\widehat{W}_i = [\widehat{w}^i_{1,\cdots,1}, \cdots, \widehat{w}^i_{N_1,\cdots N_n}]^T$ can be used to estimate $f(x)$.

Specifically, the figure of the equation to be estimated is given. I_i corresponds to the i axis, which consists of N_i portions $A_{i,j}$. Each portion is an area $[a_{i,j-1}, a_{i,j}]$ with δ length. Each patch has such a portion and the union of these portions $\bigcup_{j=1}^{N_i} A_{i,j} = \bigcup_{j=1}^{N_i} [a_{i,j-1}, a_{i,j}]$ is I_i. If there is a point of x in that portion on the figure, then p equals 1, else is zero.

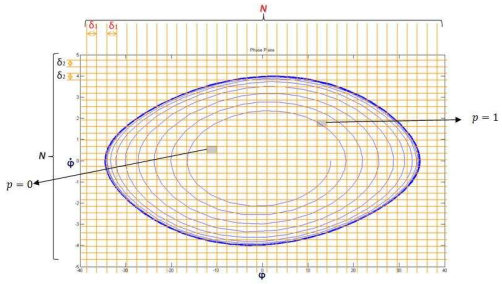

Figure 7 Patches over the phase plane for α=25°

For the weight update, the value of p is being used. If $p = 0$, then the weight remains the same as it was for the previous moment for that patch, else it takes the value of the observer in that moment.

For this paper, it is assumed that each axis will be from lowest value to the highest value that exists in the axis. Each axis will be split into the same number of patches, $N_i = N_j$, but they will have different value for δ, which depends on the length of the axis. As such, δ for each axis is calculated

$$\delta_{axis} = \frac{\max(\text{axis}) - \min(axis)}{N_{axis}}$$

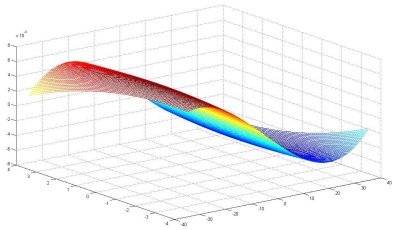

Figure 9 Function $f(\varphi,\dot{\varphi})$ for α=25°

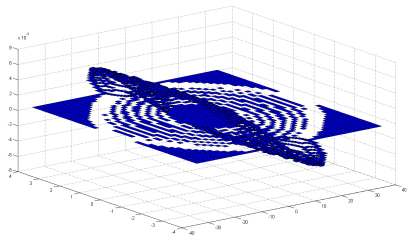

Figure 8 PNN approximation for α=25°

For the construction of the neural network, $\dot{\varphi}$ is the input in the observer. The figure used is the phase plane given from the simulation of the movement during wing rock.

5. Conclusions

The strength of the vortices depends on the angle of attack and the angle of sweep of the wing. For a given angle of attack, the strength of the vortex reduces by increasing the angle of sweep of the wing. The "wing rock" phenomenon can be eliminated with the use of the flaps of the aircraft or by reducing the angle of attack.

For angle of attack smaller than 20°, the oscillation occurring during wing rock fades out with time. But, in higher angles the oscillation starts with relatively small amplitude until it reaches maximum amplitude and continues "rocking" at that. The amplitude and the frequency of the oscillation in the final state do not depend on initial values, but on the angle of attack.

Creating the observer needs the use of the values of φ and $\dot{\varphi}$ obtained in the phenomenon's simulation. RISE observer is very fast in estimating the targeted function and is superior to other observers as it can estimate states with 25% accuracy with rising noise levels, increases the robustness of the observer and at the same time the effectiveness of error tracing. It also offers an area of asymptotic stability for state estimation.

Patchy Neural Network is easy and simple to its learning. PNN is capable of approximating generalized non linear function. It gives some advantages over other networks; the network is capable of learning the unknown nonlinearity in some region of the state space from a single visit of the state trajectories to the patches of the region. PNN has weight update laws of algebraic form, not given in the form of differential equations; this results in the significant reduction of the computational cost for learning since only n ODEs are solved form the observer, in contrast to $N_1 \times \cdots \times N_n$ ODEs needed to train the weights of a neural network of $N_1 \times \cdots \times N_n$nodes.

The MATLAB code developed in [12] makes possible the simulation of the "wing rock" phenomenon, leading to the creation of the RISE observer and the construction of the Patchy Neural Network for the identification of the

phenomenon. So, this paper concludes that the identification of wing rock, with the use of PNN and the aid from RISE observer is feasible, easily implemented with the use of MATLAB code.

References

1. **G. Guglieri, F. B. Quagliotti.** Analytical and experimental analysis of wing rock. *Nonlinear Dynamics.* 2001, 24, pp. 129-146.

2. **A. H. Nayfeh, J. M. Elzebda, D. T. Mook.** Analytical study of the subsonic wing-rock phenomenon for slender delta wings. *Journal of Aircraft.* September 1989, Vol. 26, 9, pp. 805-809.

3. **G. Guglieri, F. Quagliotti.** Experimental observation of the wing rock phenomenon. *Aerospace science and tecnology.* 1997, 2, pp. 111-123.

4. **Gurney, K.** *Introduction to neural network.* s.I.:ULC Press. 1997, p. 234

5. **Abbasi, Nasser.** *Small note on using Matlab ode45 to solve differential equations.* August 2006.

6. Slender Wing Theory. [Online] http://soliton.ae.gatech.edu.

7. **MATLAB, The Language of Technical Computing.** *Getting Started with MATLAB.* Version 5. The MathWorks. 1996.

8. **H. E. Psillakis, M. A. Christodoulou, T. Giotis, Y. Boutalis.** An observer approach for deterministic learning with patchy neural network. International Journal of Artificial Life Research, vol 2, no 1, 2011, pp. 1-16.

9. **C. Wang, D. J. Hill.** *Deterministic learning theory for identification, recognition and control.* 1st Edition. s.I:CRC Press. 2009, p. 207.

10. **J.W. Fonda, S. Jagannathan, S. E. Watkins.** Robust neural network RISE observer based fault diagnostics and prediction. Proc. of IEEE International Conference on Neural Networks. 2010.

11. **R. C. Nelson, A. Pelletier.** The unsteady aerodynamics of slender wings and aircraft undergoing large amplitude maneuvers. *Progress in aerospace sciences.* 2003, 39, pp. 185-248.

12. **Paraskevas-Marios, Chavatzopoulos.** *Use of observer, based on neural networks, for identification of the "wing rock" phenomenon on delta 80 degrees wing aircrafts.* Chania : Technical University of Crete, Dept of Electronic and Computer Engineers, 2011. p. 130. Original Title:"Χρήση παρατηρητή, βασισμένου σε νευρωνικά δίκτυα, για αναγνώριση φαινομένου "wing rock" σε δελταπτέρυγα αεροσκάφη 80 μοιρών"
[Online]https://sites.google.com/site/wingrockpnn/

Path Integrals for Drift-Diffusion Processes on Riemannian Manifolds with Applications to the Stochastic Volatility Options Pricing

Chepilko S. S.[1] and Dmitrieva L. A.[12]

[1] Department of Physics, Saint-Petersburg State University
198504, Ulyanovskaya, 3, St. Petersburg, Russia (e-mail:ar.noion@gmail.com)
[2] Department of Liberal Arts and Sciences, Saint-Petersburg State University
190000, Galernaya, 58-60, St. Petersburg, Russia
(e-mail:madam.mila-dmitrieva@yandex.ru)

Abstract. In the present paper we consider the problem of path integrals application to options pricing with stochastic volatility. In a huge literature devoted to this problem the known results on path integrals cannot be considered as complete, self-consistent and correct. Moreover, despite the fact that path integrals for stochastic volatility options are special case of that for general drift-diffusion processes on Riemannian manifolds, there are practically no links between known results in these two fields. At the same time in studies of general drift-diffusion processes themselves also there exists a deep gap between different approaches, namely, that of theoretical physicists, who use the so-called path integrals as a formal tool, and mathematicians, who obtain different exact results on functional and path integrals which do not match with results of physicists. Finally, methods of differential geometry widely used in path integrals studies for general drift-diffusion processes as well as in studies of some aspects of stochastic volatility models practically are not involved in known approaches to path integral constructions for latters. In the present work we try to build some bridges connecting the most known approaches together to get a unified construction of path integral representation for drift-diffusion processes on Riemannian manifolds with applications to options pricing with stochastic volatility. We also consider in details the so-called Heston model in stochastic volatility options pricing and give the revised path integral representation for this model. Since path integral in this model can be analytically calculated up to one-dimensional Fourier transform, we consider this model as benchmark model for the proposed approach.
Keywords: Stochastic differential equation , Backward and Forward Kolmogorov equations, Path integrals, Functional integrals, Drift-diffusion processes on Riemannian manifold, Onsager-Machlup functional, Smolyanov-Weizsacker surface measures, Heat kernel expansion, Stochastic volatility option pricing.

1 Introduction

It is well known [1] that solution of the diffusion equation with scalar potential can be written as the integral of some functional in the space of trajectories with respect the Wiener measure. This integral can be constructed in two

different ways. Firstly, it can be understood as Lebesgue integral over the Wiener measure, then it is called a functional integral. On the other hand, it can be understood as the limit of multiplicative integrals obtained by replacing the functional space by finite-dimensional space of broken-line (or step) functions with fixed abscissas of nodes. If the limit exists, is unique and does not depend on the choice of nodes, it is called a path integral. As shown by Fomin [2], for a wide class of functionals both ways lead to the same result, thus the Wiener functional and path integrals coincide.

However if one tries to generalize the above result to the case of the second-order parabolic type equation with variable coefficients

$$\partial_t \psi(t,x) = \left(\frac{1}{2} a^{ij}(x) \partial_{ij} + b^i(x) \partial_i \right) \psi(t,x). \tag{1}$$

one meets the serious difficulties. From the one hand, there exist mathematically rigorous and consistent theory of functional integration for this equation, which was mainly implemented in works by Daletskkii [3], [4]. As a result one can write down the fundamental solution of (1) in terms of the functional integral with respect to the so-called Ito measure. The latter can be considered as generalization of the Wiener measure for the case of drift-diffusion process with variable coefficients. However in this case there is no explicit representation for the Ito measure and up to now there is no unambiguous constuctive way of calculation of functional integral through the corresponding path integrals. The main direction of researches in this field is construction of the multiplicative path integral representation for the fundamental solution $p_M(\tau, x; t, y)$ of the equation (1) in the form

$$p_M(\tau,x;t,x') = \lim_{n\to\infty} \int_M ... \int_M d\mathrm{vol}_M(x_1)...d\mathrm{vol}_M(x_n) \prod_{i=0}^{n} p_M(t_i,x_i;t_{i+1},x_{i+1}), \tag{2}$$

$$x_0 = x,\ t_0 = \tau,\ x_{n+1} = x',\ t_{n+1} = t.$$

The further commonly used step is the substitution of the multipliers (exact kernels) in the right hand side of (2) by the local asymptotics of fundamental solution as $\Delta t \to 0, \Delta x \sim \sqrt{\Delta t}$ or by equivalent in some sense kernels, which are called approximating ones. A great number of works [5]-[13] both by physicists and mathematicians are devoted to this approach. Among them we emphasize the papers devoted to Heat kernel expansion [5],[6], the concept of Onsager-Machlup functional [7], [8], and making use of Smolyanov-Weizsacker surface measures [9],[10],[11].

It should be noted that a rich source of diffusion processes with complex geometry has recently appeared in modeling of financial markets, where finding the fundamental solutions of the backward Kolmogorov equation is highly topical and relevant problem [12] - [16].

In the present paper we propose a method of reducing the functional integral with respect to the Ito measure for two-dimensional drift-diffusion

process to the functional integral over the Wiener measure. Such reduction allows to deal with the latter integral using a unique relationship with the Wiener path integral. The main advantages of our approach are the following three factors. First, we do not use the momentum representation for the original operator, and thus we do not face the problem of ordering of noncommuting operators, whose solution is not unique. Second, we use the discretization procedure only for Wiener functional integral for which the link with the path integral is known and thus discretization procedure is unambiguous. Third, we do not use the concept of approximating kernels, which is based on various asymptotics of fundamental solutions. The latter concept being mathematically correct, seems to be not constructive and do not allow efficiently compute the corresponding path integrals.

2 Preliminaries

The stochastic differential equation

$$dq^i(t) = b^i(q(t))dt + e^i_a(q(t))dW^a(t) \tag{3}$$

defines the Ito diffusion process $q(t) \in \mathbb{R}^m$ with drift vector b and diffusion matrix e^i_a. Here $W(t)$ is m-dimensional Wiener process. Since we consider the coefficients which do not explicitly depend on t, the generating operator L_x of the Ito process (3) is homogenous. The backward Kolmogorov equation is defined by the generator L_x as follows $\partial_\tau u = -L_x u$. The fundamental solution $p(t-\tau, x, x')$ satisfies the backward Kolmogorov equation with respect to variables (τ, x)

$$\partial_\tau p(t-\tau, x, x') = -\left(\frac{1}{2}e^i_a(x)e^j_a(x)\partial_{ij} + b^i(x)\partial_i\right)p(t-\tau, x, x') \tag{4}$$

Being the probability transition density of the Ito process (3) this fundamental solution is given by the functional integral

$$p(t-\tau, x, x') = \int\limits_{\mathcal{C}^{(\tau,t)}_{x,x'}(\mathbb{R}^m)} dm^{(b,e)}_{x,x'} \equiv \int\limits_{q(\tau)=x}^{q(t)=x'} dm^{(b,e)}_{x,x'}. \tag{5}$$

Here $dm^{(b,e)}_{x,x'}$ is the conditional Ito measure linked with the Ito measure $dm^{(b,e)}_x$ by the relation $dm^{(b,e)}_x = \int\limits_{\mathbb{R}^m} dm^{(b,e)}_{x,x'}dx'$. The Ito measure is concentrated on the Ito process (3) continuous trajectories which begins at the point $q(\tau) = x$. The set $\mathcal{C}^{(\tau,t)}_{x,x'}(\mathbb{R}^m) = \{q(t') : [\tau, t] \longmapsto \mathbb{R}^m,\ q(\tau) = x,\ q(t) = x'\}$ consists of continuous trajectories which begin at the point x and ends at the point x'.

3 Reduction Theorem for Functional Integral

In this section we briefly show the way how to prove the declared theorem. It is well-known [14] that coefficients of the homogenous diffusion Ito process $q(t)$ in $\mathbb{R}^m$ given by (3) generates the structure of the Riemannian manifold $M = (\mathbb{R}^m, g)$ in $\mathbb{R}^m$. Namely, let us supply $\mathbb{R}^m$ by the metrics $g = (ee^*)^{-1}$ or $g^{ij}(x) = e^i_a(x)e^j_a(x)$, $g^{ij}g_{jk} = \delta^i_k$ and the affine Levi-Civita connection which coefficients coincide with Gauss-Christoffel symbols defined in a standard way in terms of the metrics g as follows $\Gamma^i_{jk} = \frac{1}{2}g^{il}(-\partial_l g_{jk} + \partial_k g_{lj} + \partial_j g_{kl})$. Then generator of the Ito process (3) can be written in covariant way $L_x = \frac{1}{2}\Delta_M + f^i\partial_i$, where $\Delta_M = g^{ij}\partial_{ij} - g^{ij}\Gamma^k_{ij}\partial_k = g^{-\frac{1}{2}}\partial_i(g^{\frac{1}{2}}g^{ij}\partial_j)$ is invariant Laplace-Beltrami operator on M and $f^i = b^i + \frac{1}{2}g^{lj}\Gamma^i_{lj}$ is contravariant drift vector.

Along with diffusion process (3) consider the Brownian motion on the Riemannian manifold M. The Brownian motion is the Ito process $\tilde{q}(t)$ with generator $L = \frac{1}{2}\Delta_M$. It is defined by the stochastic equation $d\tilde{q}^i(t) = \tilde{b}^i(\tilde{x})dt + e^i_a(\tilde{x})dW^a$, where $\tilde{b}^i = -\frac{1}{2}g^{lj}\Gamma^i_{lj}$.

The crucial role in further constructions belongs to the Girsanov-Gihman-Shorohod-Daletskii measure equivalence theorem [4] which links the measures of two diffusion processes with the same diffusion matrix and different drift vectors. In the considered cases such processes are $q(t)$ and $\tilde{q}(t)$ and this theorem leads to the following transformation of (5)

$$p(t-\tau, x, x') = \int\limits_{\tilde{q}(\tau)=x}^{\tilde{q}(t)=x'} \exp\left(\int\limits_\tau^t \alpha^a(\tilde{q})dW^a - \frac{1}{2}\int\limits_\tau^t \alpha^a(\tilde{q})\alpha^a(\tilde{q})dt\right) dm^{(\tilde{b},e)}_{x,x'}, \quad (6)$$

where integration is fulfilled over the space of continuous functions $\mathcal{C}^{(\tau,t)}_{x,y}(\mathbb{R}^m)$. The vector α^a is given as $\alpha^a = e^a_i(b^i - \tilde{b}^i) \equiv e^a_i f^i$. Here the matrix e^a_i is inverse to the diffusion matrix e^i_a: $e^i_a e^a_j = \delta^i_j$, and f^i is contravariant drift vector of the process $q(t)$.

The functional integral in the right hand side of equation (6) admits further transformation in the case when 1-form $d\mathcal{A} = f_i dx^i$, generated by the covariant drift vector $f_i = g_{ij}f^j$ is exact. Namely, let there exists such scalar function $\phi(x)$, that $f_i = \partial_i\phi$. Then

$$p(t-\tau, x, x') = e^{\phi(x')-\phi(x)} \int\limits_{\tilde{q}(\tau)=x}^{\tilde{q}(t)=x'} e^{\int\limits_\tau^t Q(\tilde{x}(t))dt} dm^{(\tilde{b},e)}_{x,x'}. \quad (7)$$

Here the scalar potential Q is given by $Q = -\frac{1}{2}(\Delta_M\phi + g^{ij}\partial_i\phi\partial_j\phi)$.

Due to the lack of place we do not give the derivation of equation (7). Besides the Measure Equivalence Theorem, the Feynman-Kac theorem has been used. Let us note that the structure of the above equation corresponds to the gauge transformation rules. The obtained reduction formula plays an important role in our further constructions.

4 Factorization Coordinates for Two-Dimensional Ito diffusion process

All known stochastic volatility models can be written as two-dimensional Ito process (3) with process coordinates $q(t) = (f(t), a(t))$ and drift and diffusion coefficients of the form

$$b^i(q) = \begin{pmatrix} d(f) \\ b(a) \end{pmatrix}, \quad e^i_c(q) = \begin{pmatrix} C(f)\Omega(a) & 0 \\ \xi\rho\sigma(a) & \xi\sqrt{1-\rho^2}\sigma(a) \end{pmatrix}, \tag{8}$$

where ξ, ρ are constants. Such process describes the dynamics of the price $f(t)$ of some asset in financial applications (see [12], [14]). The second component $a(t)$ corresponds to the volatility of this asset. The backward Kolmogorov equation (4) in the considered case is called the Merton-Garman equation and describes the dynamics of the price of the option with underlying asset $f(t)$. In what follows we use the general notations given in (8). The concrete examples of coefficients will be given in Conclusions in comparison of our results with the known ones for the concrete stochastic volatility models.

The important point in further consideration is introduction of the coordinates $q = (f, a) \mapsto q' = (y, z)$, where $y = \int_{\cdot}^{f} \frac{df'}{C(f')} - \rho \int_{\cdot}^{a} \frac{\Omega(a')da'}{\xi\sigma(a')}$, and $z = \frac{1}{\xi}\int_{\cdot}^{a} \frac{da'}{\sigma(a')}$. We shall call these coordinates as factorization ones. They slightly differ from the conformal coordinates [14]. The metric in these coordinates takes the form $ds^2 = g_{i'j'}dq^{i'}dq^{j'} = \frac{dy^2}{(1-\rho^2)\Omega^2(a(z))} + dz^2$. Let us further move from (W^1, W^2) to another uncorrelated basis of one-dimensional Winer processes $(\tilde{W}^1, \tilde{W}^2)$ of the form $d\tilde{W}^1 = \sqrt{1-\rho^2}dW^1 - \rho dW^2$ and $d\tilde{W}^2 = \rho dW^1 + \sqrt{1-\rho^2}dW^2$. In the uncorrelated basis $(\tilde{W}^1, \tilde{W}^2)$ and the factorization coordinates (y, z) the considered Ito process (3), (8) takes the form

$$\begin{array}{l} dy(t) = b^y(y,z)dt + e(z)d\tilde{W}^1 \\ dz(t) = b^z(z)dt + d\tilde{W}^2 \end{array}. \tag{9}$$

Here $b^y(y,z) = \frac{d(f)}{C(f)} - \frac{\rho}{\xi}\frac{\Omega(a)b(a)}{\sigma(a)} - \frac{1}{2}\Omega^2(a)\partial_f C(f) - \frac{\xi\rho}{2}\sigma^2(a)\partial_a\left(\frac{\Omega(a)}{\sigma(a)}\right)$ and $b^z(z) = \frac{\sqrt{1-\rho^2}}{\xi e(z)}\left(\frac{\Omega(a)b(a)}{\sigma(a)} + \frac{\xi\sigma(a)}{2}\partial_z\left(\frac{\Omega(a)}{\sigma(a)}\right)\right) - \frac{\partial_z e(z)}{e(z)}$ are drift coefficients. The diffusion coefficients reads $e(z) = \sqrt{1-\rho^2}\Omega(a(z))$.

The structure of the obtained Ito process leads to the possibility of factorization of functional integral

$$p(t-\tau, y, z; y', z') = \int\limits_{y(\tau)=y,\ z(\tau)=z}^{y(t)=y',\ z(t)=z'} dm^{(b',e')} = \int\limits_{z(\tau)=z}^{z(t)=z'} dm^{(b^z,1)} \int\limits_{y(\tau)=y}^{y(t)=y'} dm^{(b^y,e)}. \tag{10}$$

Here we omitted the down indexes in notation of conditional Ito measure $dm^{(b',e')}$ associated with the Ito process (9). The same is done for conditional measures $dm^{(b^y,e)}$ and $dm^{(b^z,1)}$ associated with one-dimensional processes $y(t)$ and $z(t)$ in (9) respectively.

5 Calculation of Functional Integral for Fundamental Solution

In the present paper the functional integral with respect to y-component in (10) is calculated under the simplifying condition $b^y(y,z) \equiv b^y(z)$. Note, that this condition holds for all models for stochastic volatility options, in which $d(f) = rf$, $C(f) = f$. In order to calculate functional integral with respect to y-component one has apply measure equivalence theorem to one-dimensional process $y(t)$ in (9) and the process with the same diffusion coefficient and zero drift coefficient. Then one has to use the corresponding path integral representation for the obtained Wiener functional integral which coefficients parametrically depends on the process $z(t)$ and finally use the Ito discretization rule for the stochastic integral which appears in calculations. The final result reads

$$\int\limits_{y(\tau)=y}^{y(t)=y'} dm^{(b^y,e)} = \frac{1}{\sqrt{2\pi\bar{e^2}[z]}} \exp\left(-\frac{(y'-y-\bar{b^y}[z])^2}{2\bar{e^2}[z]}\right). \tag{11}$$

where $\bar{e^2}[z] = \int\limits_\tau^t e^2(z(t))dt$ and $\bar{b^y}[z] = \int\limits_\tau^t b^y(z(t))dt$.

For our further purposes we expand right hand side of (11) into the Fourier integral and insert this expansion into (10). This yields

$$p(t-\tau,y,z;y',z') = \int\limits_{\mathbb{R}} \frac{dk}{2\pi} e^{ik(y'-y)} \int\limits_{z(\tau)=z}^{z(t)=z'} dm^{(b^z,1)} e^{\int\limits_\tau^t V_i(z(t))dt}, \tag{12}$$

where we introduced the "interaction potential" $V_i(z(t)) = -\frac{1}{2}k^2e^2(z(t)) + ikb^y(z(t))$.

The functional integral (12) with respect to the Ito measure $dm^{(b^z,1)}$ by means of one-dimensional version of reduction theorem (7) transforms into the functional integral with respect to the conditional Wiener measure $dm_W^{(0,1)}$

$$p(t-\tau,y,z;y',z') = \int\limits_{\mathbb{R}} \frac{dk}{2\pi} e^{\,ik(y'-y)+\int\limits_z^{z'} b^z(\tilde{z})d\tilde{z}} \int\limits_{z(\tau)=z}^{z(t)=z'} dm_W^{(0,1)} e^{\int\limits_\tau^t V_{eff}(z(t))dt}, \tag{13}$$

where "effective potential" is given by equation $V_{eff}(z(t)) = k^2e^2(z(t)) + 2ikb^y(z(t)) + \partial_z b^z(z(t)) + (b^z(z(t)))^2$.

Thus up to the Fourier transform, we express the fundamental solution of the backward Kolmogorov equation in factorization coordinates as Wiener functional integral with effective potential. As it has been mentioned above such Wiener functional integral is equal to the Wiener path integral I_W^{path} which is understood as the limit

$$I_W^{path} = \lim_{n\to\infty} \frac{1}{\sqrt{2\pi\varepsilon}} \prod_{i=1}^{n} \int_{\mathbb{R}} \frac{dz_i}{\sqrt{2\pi\varepsilon}} \exp\left(-\sum_{i=0}^{n} \left(\frac{(z_{i+1}-z_i)^2}{2\varepsilon} - V_{eff}(z_i)\varepsilon \right) \right), \tag{14}$$

where $z_0 = z,\ z_{n+1} = z',\ \varepsilon = \frac{t-\tau}{n+1}$.

The commonly used symbol expression for the Wiener path integral (14) is written with formal "effective Lagrangian" $\mathcal{L}_{eff} = -\frac{1}{2}\dot{z}^2(t) + V_{eff}(z(t))$. So the functional integral representation of fundamental solution (13) is equivalent to the path integral representation of the form

$$p(t-\tau, y, z; y', z') = \int_{\mathbb{R}} \frac{dk}{2\pi} e^{ik(y'-y) + \int_z^{z'} b^z(\tilde{z})d\tilde{z}} \int_{z(\tau)=z}^{z(t)=z'} Dz e^{-\frac{1}{2}\int_0^t (\dot{z}^2(t) + V_{eff}(z(t)))dt}, \tag{15}$$

Using this form one can try to calculate the corresponding path integral. If the "effective potential" V_{eff} belongs to the class of exactly solvable, than the initial two-dimensional model is exactly solvable in terms of factorization coordinates y, z up to inverse Fourier transformation.

6 Conclusion

Let us compare the obtained result given by equations (13) and (15) with results known in literature for the widely used stochastic volatility models.

The Heston model correspond to the following choice of coefficients in the general model (8): $d(f) = \mu f,\ C(f) = f,\ \Omega(a) = \sqrt{a},\ \ b(a) = k(\theta - a),\ \sigma(a) = \sqrt{a}$, where μ, k, θ are constants. For such coefficients the Wiener path integral in (15) can be calculated exactly. The obtained result completely coincide with result of the paper [15], which uses the technique of path integrals. However the technique used in [15] works only in the case of the Heston model and can not be extended for more general models.

The most general case of stochastic volatility models uses the coefficients of the form $d(f) = rf,\ C(f) = f,\ \Omega(a) = \sqrt{a},\ b(a) = \lambda + \mu a,\ \sigma(a) = a^\alpha$, where r, λ, μ, α are constant and $\alpha > 0$ is arbitrary. Our results (13) and (15) for this case being transformed to the initial variables essentially differs from the well-known result of the work [12]. For the first time the errors in [12] for the case $\alpha = 1$ has been pointed out in the paper [16]. We completely agree with remarks in [16] concerning the case $\alpha = 1$. However the results for

$\alpha \neq 1$ in [16] differers from our. Remind that our approach for Heston model at $\alpha = \frac{1}{2}$ completely coincides with [15] and initial paper [17], in which calculations were made directly without functional integration. Thus, we assume that our approach is more consistent and versatile and can correlate the results obtained by different methods in different special cases.

References

1. M. Kac,"On distributions of certain Wiener functionals", *Trans. Amer. Math. Soc.*, 65 (1), 1-13, (1949).
2. S. V. Fomin,"About inclusion of integral over Wiener measure into general theory of Lebesgue integral" (in Russian),*Nauchnyie Doklady Vischei Shkoly*, 2 (1958).
3. Yu. L. Daletskii, "Functional integrals connected with operator evalution equations", *Russian Mathematical Surveys*, 17 (5), 1-107, (1962).
4. Ya. I. Belopol'skaya, Yu. L Daletskii, "Ito equations and differential geometry", *Russian Mathematical Surveys*, 37 (3), 109-163, (1982).
5. A. L. Alimov, V. S. Buslaev, "About continual integral for second order parabolic equation" (in Russian), *Vestnik LGU*, 1, (1972).
6. I. G. Avramidi, *Analytic and geometric methods for heat kernel applications in finance*, (2007).
7. Y. Takahashi, S. Watanabe, "The probability functionals (Onsager-Machlup fucntions) of diffusion processes", *Stochastic integrals, Lecture notes in Math.* (D. Williams, ed.), 851, pp. 433-463, Springer, Berlin-New-York, (1981).
8. M. Capitaine, "On the Onsager-Machlup fucntional for elliptic diffusion processes", *In Seminaire de Probabilities*, XXXIV, vol. 1729 of Lecture Notes in Math., pp. 313-328, Springer, Berlin, (2000).
9. L. Andersson, B. Driver, "Finite dimensional approximations to Wiener measure and path integrals formulas on manifolds", *J. of funct. anal*, 165,430-498 (1999).
10. O. G. Smolyanov, H. Weizsacker, O. Wittich, "Chernoff's theorem and discrete time approximations of brownian motion on manifolds", arXiv:math/0409155v3 [math.PR], 15 Sep 2005, (rev. 2008).
11. C. Bar, F. Pfaffle, "Path integrals on manifolds by finite dimensional approximation", arXiv:math/0703272v1 [math.AP] 9 Mar 2007.
12. B. Baaquie, *Quantum finance*, Cambridge University Press, (2004).
13. M. Rosa-Clot, S. Taddei, "A path integral approach to derivative security pricing: I. Formalism and analytical results", arXiv: cond-mat/9901277v1.
14. P. Henry-Labordere, *Analysis, geometry and modelling in finance: advanced methods in option pricing*, Chapman and Hall/CRC, London, (2009).
15. D. Lemmens, M. Wouters, J. Tempere, S. Foulon, "Path integral approach to closed-form option pricing formulas with applications to stochastic volatility and interest rate models", *Physycal Review E*, 78, 016101 (2008).
16. L.F. Blazhyevskyi, V.S. Yanishevsky, "The path integral representation kernel of evolution operator in Merton-Garman model", *Condensed Matter Physics*, vol. 14, No 2, 23001: 116 (2011).
17. S. L. Heston, "A closed-form solution for options with stochastic volatility with applications to bond and currency options", *The Review of Financial Studies*, vol. 6, No 2, pp. 327-343, (1993).

Application of Artificial Neural Networks to Study the Properties of Reconstructed Attractors for Time Series

Stepan S. Chepilko[1], Ludmila A. Dmitrieva[1,2] and Yuri A. Kuperin[1,2]

[1]Department of Physics, St. Petersburg State University
Email: ar.noion@gmail.com
[2]Department of Liberal Arts and Sciences, St. Petersburg State Unuversity
St. Petersburg, Russia
Email: madam.mila-dmitrieva@yandex.ru
Email: yuri.kuperin@gmail.com

Abstract: A method for calculating local rates of divergence (LDR) for the family of trajectories on the reconstructed attractor of short time series is elaborated with the help of neural network committees. This method is based on neural network forecasting of the original time series and its perturbations. It is shown that the character of "distribution" of LDR and information about the quality of neural networks training allow us to identify in which mode a dynamical system associated with a time series in question is situated. After a series of the LDR averages a quantitative characteristics similar to the Lyapunov exponent has been obtained. It is shown that in the case of one-dimensional dynamical systems, the average of LDR gives the Lyapunov exponent for the studied time series. It also has been shown that in the case of the model three-dimensional flows (the Lorenz system, the Rössler system) the distribution of LDR identifies in which mode the system is situated - in a chaotic regime or in regular periodic one. When we deal with random time series, the distribution of LDR also has its own specifics and identifies the random nature of the series. Thus, we developed a method, which is based on a qualitative prediction made by the neural networks committee, and which allows on the base of time series to identify in which mode dynamic system associated with this time series is situated.
Keywords: Quantitative measure of chaos, Local rates of divergence, the Lyapunov exponents, Reconstructed attractor, Neural networks committees.

I. Introduction

The purpose of this paper is to construct the algorithm for calculating local characteristics of divergence of neighboring trajectories on the reconstructed attractor of arbitrary time-series by method of neural networks forecasting of this series and its perturbations. The idea of this study occurred after the study of cycle of papers [1-3] devoted to solving the problems which is much more ambitious, namely to computing largest Lyapunov exponent and the entire spectrum of Lyapunov exponents for a short time-series by methods of neural network forecasting. In [4] we have shown that neural network method for calculating the largest Lyapunov exponent, proposed by the authors of [1-3], after its substantial modification works well only in the case of one-dimensional maps, where this exponent is single. In [4] it also was shown that this method gives a positive Lyapunov exponent for stochastic time series and is faced serious problems in

calculation of a zero Lyapunov exponent in the periodic case. The attempt to overcome these problems showed that the idea put forward in [1-3] after extensive modifications may serve as a rational basis for constructing the algorithm for calculating the characteristics which we called as the local rates of the divergence (LDR) of neighboring trajectories on the reconstructed attractor of the time series. We emphasize that the purpose of the method and algorithm presented in this paper is not the calculation of the largest Lyapunov exponent of the time series, but the possibility of a reliable classification of short time series in terms of their dynamic origin on the basis of LDR. In the case of one-dimensional dynamical systems, the mean value of LDR gives the largest Lyapunov exponent. In the case of three-dimensional flow model (Lorenz system, Rössler system) distribution of LDR shows in which mode the system is - in a chaotic or regular periodic. When we are dealing with random series, the character of the distribution of LDR also has its own specifics and points out the random nature of the series. After a series of LDR averages some characteristics is obtained, which is analogous to the Lyapunov exponent, but which (except for the one-dimensional maps) is not coincide with it. Of course, this paper does not claim the final status of completion. Many aspects of the problem require significant elaboration. Some quantitative observations require formalization in the form of statistical tests. All of this is beyond the scope of this paper. Also here we do not consider the application of this method and algorithm for analysis of the real world time series.

II. Preliminary Discussions

The time series in general are complex one-dimensional projection of the multidimensional behavior of dynamic systems. Since most of the observed dynamical systems exhibit more or less stable behavior, it is appropriate to speak about corresponding attractors and, therefore, to take into account the concept of attractors when working with time series. We assume that the reader is familiar with the idea of consideration of reconstructed attractor in lag space of time series [see, e.g, 5].

We will not stop on details of the method for estimating the largest Lyapunov exponent of the time series by means of neural networks proposed in [1-3]. It can be shown that this method will work properly only for one-dimensional systems, where time series reflects the behavior of a single dynamical variable. For example, in the case of the logistic map (with control parameter equal to 4), for which the value of the largest exponent is known analytically and equal to $\ln 2$, the method can give this value with an accuracy to three decimal places. The error is estimated as described in the modified version of the method proposed by the authors of this paper in [4].

In the case of short time series, which are linked with multi-dimensional systems, it makes sense to talk about local rates of divergence (LDR), which characterize precisely the part of the global attractor reconstructed by this short time series. The

LDR will not characterize the system as a whole, but will describe the divergence of the trajectories on that "section" of the global attractor, which can be reconstructed by the considered time series.
In calculating the largest Lyapunov exponent by the standard Benettin algorithm [5] a large number of quantities characterizing the rate of divergence of neighboring trajectories in different parts of the attractor are averaged. The obtained values clearly lie in the interval whose boundaries are determined by the largest and smallest Lyapunov exponents. As it follows from the Oseledets theorem [5], the average process allows us to "single out" the value of the highest exponent. In the case of short time series, the analogue of the above method does not work. Therefore, in this paper, we study a "distribution" of local rates of divergence and calculate some of their characteristics. Only in the case of one-dimensional maps the mean of all local rates of divergence gives the highest Lyapunov exponent.

III. The Method of Obtaining a "Distribution" of the Local Rates of Divergence

An important aspect of the proposed method is the use of neural networks committees. Advantages of committees over the single networks in forecasting problems are known and described. For the proposed algorithm, the use of networks committees, as shown below, is crucial. In the first step of the algorithm the committee of neural networks, each of which is, for example, the 4-layer perceptron is trained. The Levenberg-Marquardt learning algorithm is used, which is known to work well for short time series. The committee includes only those networks for which the multiple regression coefficient R^2 is greater than a certain threshold and the network training error is less than the fixed value of MSE. Each network contains m inputs and m outputs, where m is the dimension of the embedding phase space of time series. The networks are learned to approximate the map $X_{t+1}^{(m)} = F(X_t^{(m)})$. Here $X_t^{(m)} = (x_t, x_{t-\tau}, ..., x_{t-(m-1)\tau})$ is a point on the reconstructed attractor in the m-dimensional lag space with a lag τ.
Each trained network is used further in the following way. For each point x_t of the series, the corresponding point on the reconstructed attractor $X_t^{(m)} = (x_t, x_{t-\tau}, ..., x_{t-(m-1)\tau})$ is predicted by multi-step prediction procedure for a certain horizon h ahead. So the number of steps in multi-step prediction procedure is equal to h (as a rule we took $h = 7$). Thus obtained h points are considered to form a piece of the reference trajectory on the reconstructed attractor. Further, one takes N random perturbations of the point x_t, forms the corresponding perturbed points on reconstructed attractor $\tilde{X}_t^{(m)}$ and realizes

multi-step forecasts of these perturbations for the same horizon ahead. Thus, along with reference trajectory one obtains N "perturbed" trajectories, each consisting of h points.

Next, for each number of step of multi-step prediction procedure, the Euclidean m - dimensional distances between points on the reference and perturbed trajectory are calculated. These distances then are averaged over all neural networks in committee. Further, the linear regression is constructed between logarithms of averaged distances and the corresponding step numbers. Such linear regressions are obtained for each pair of reference and perturbed trajectories. Perturbations of points x_t are obtained by using a random number generator and did not exceed 10^{-7} in absolute value.

Among all regressions only "good" regression lines are selected. The regression line is considered to be good if the standard deviation of regression error does not exceed the fixed threshold. We call the values of slopes of "good" regression lines as local rates of divergence (LDR) and denote them as λ. Finally, all values of LDR are united into the single sample and the resulting distribution histogram is constructed.

In the section describing the results of application of this algorithm to the specific example of time series we discuss interpretation of these histograms and the way of extraction of numerical characteristics to classify time series.

IV. Description of Results

The method and algorithm proposed in the previous section was tested on model time series. The length of each time series is equal to 1500 observations.

In the upper left panel of Fig. 1. the time series generated by the logistic map with the value $r = 4$ of the control parameter (chaotic regime) is given. Lyapunov exponent in this case is known analytically and is equal to $\Lambda = \ln 2 \approx 0.69$. The distribution histogram of LDR is given under the graph of time series. In this case, the histogram gives the mean value $\overline{\lambda} = 0.70 \pm 0.03$ and we receive the value of Lyapunov exponent $\Lambda = \ln 2 \approx 0.69$ with good accuracy. In the case of one-dimensional maps the histogram mean value always coincides with the Lyapunov exponent with good accuracy.

The upper right panel of Fig. 1. shows the time series of x-component of the Rössler system in the chaotic regime. More than 96% of the LDR values form the well defined peak in the positive area. This clearly indicates the chaotic nature of the studied series. The mean value of the positive LDR is $\bar{\lambda} = 0.13 \pm 0.11$. We emphasize that the proposed approach for time series related to multi-dimensional

chaotic dynamical systems results in overwhelming concentration of LDR in the positive area of histogram.

Histogram in Fig. 2. for a series generated by the x-component of Lorenz system

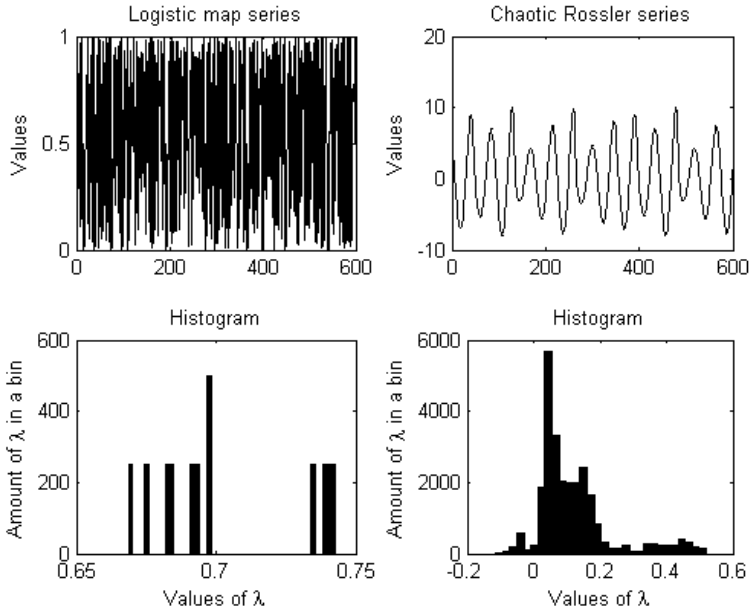

Fig. 1. Histograms for the logistic map and the chaotic Rössler system.

gives result similar to those for the Rössler system. Here 100% of LDR are positive, and the mean value is $\overline{\lambda} = 0.53 \pm 0.06$.

The right panels of Fig.2. shows the time series and corresponding histogram generated by Lorenz system with additive adding of noise (noise level = 0.5). The influence of noise leads to the shift of the histogram into the region of negative LDR. In recognition of noisy chaos two circumstances are important. First, the quality on neural networks learning is sharply worsen. Namely, the MSE threshold rises from $4 \cdot 10^{-5}$ to $3.4 \cdot 10^{-2}$, and the R^2 threshold drops from 0.99 to 0.70 for the noisy Lorenz series. Second, the structure with a large histogram peak in the positive area is preserved.

Below we show that a random series histogram is quite different compared to the noisy chaos. In particular, Figure 3 shows a histogram for the surrogate Lorenz series (obtained by random mixing of the initial series). The histogram is strongly shifted to the left, forming a negative peak. In general, the histogram for the random series is symmetric about zero with a possible predominance of either positive or negative peaks. However, the mean value across the histogram, within the error of calculations is always zero. For the surrogate Lorenz series mean value of LDR is $\overline{\lambda} = -0.02 \pm 0.03$. Zero mean histogram, together with relatively low

quality of networks learning clearly indicates the random nature of the studied series. In the case of surrogate Lorentz the MSE threshold was equal to $2.3 \cdot 10^{-2}$ and the R^2 threshold as equal to 0.85).

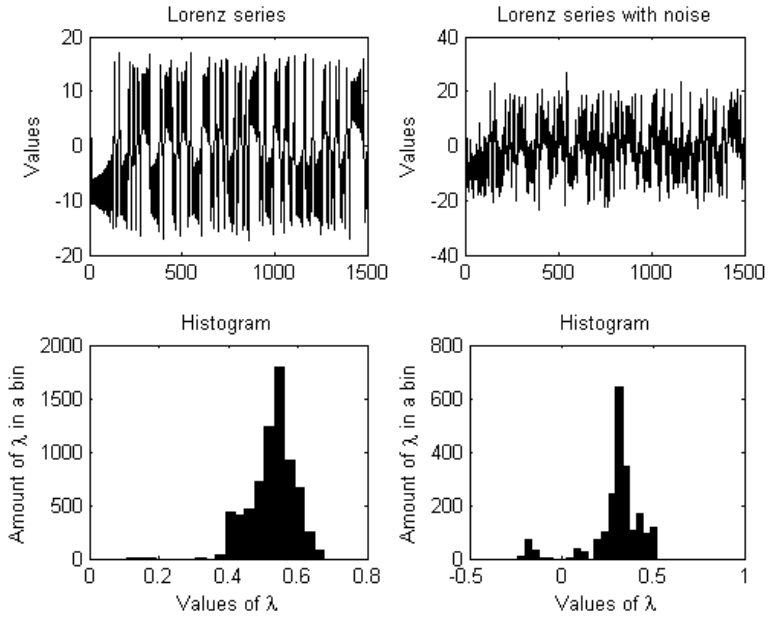

Fig. 2. Histograms for the Lorenz series and for the noisy Lorenz series.

Finally, the histogram for the 4-periodic series of x-component of Rössler system in periodic regime, presented in Fig. 3, looks the same as for a random series. On the whole it is symmetric and has the zero mean ($\overline{\lambda} = -0.02 \pm 0.04$) within the limits of error. However, the quality of networks learning (MSE = $3 \cdot 10^{-5}$ and $R^2 = 0.99$) leaves no doubt that we are dealing with a deterministic time series.

V. Conclusions

We emphasize once again that the purpose of the method and algorithm presented in this paper is not the calculation of the Lyapunov exponent of the time series, but the possibility of a reliable classification of short time series in terms of their origin on the basis of the "distribution" of local rates of divergence of neighboring trajectories on the reconstructed attractor. The proposed method allowed to distinguish the chaotic time series, time series of noisy chaos type, periodic and random time series.

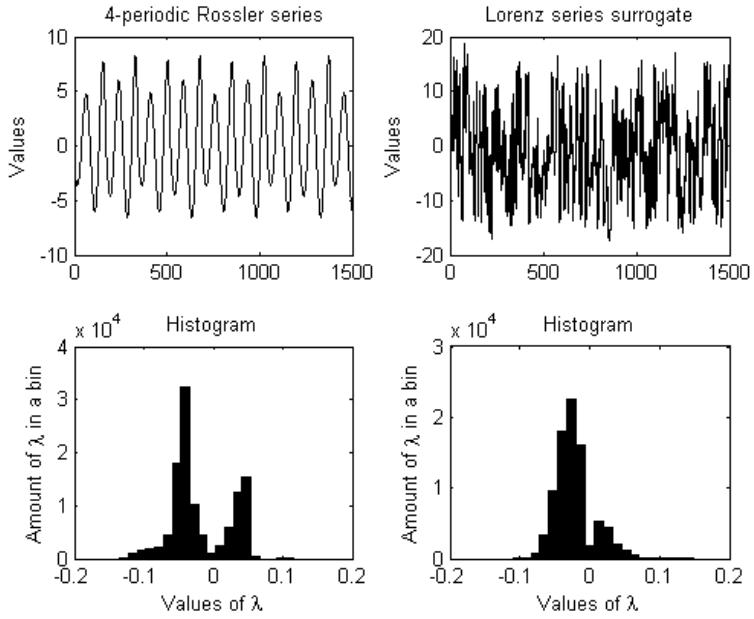

Fig. 3. Histograms for the 4-periodic Rossler series and Lorenz surrogate series.

References

1. Golovko V.A., Neural networks methods of chaotic processes processing, in *Neu-roinformatics-2005, Lectures in neuroinformatics,* Moscow, MEPI, 43-91 (2005) (in Russian)
2. Golovko V.A., Savitsky Yu.V., Neural network methods for determining the Lyapunov spectrum from the observed realization, *International Journal "Computing",* **1,** 80-86 (2002)
3. Golovko V.A., Chumerin N.Y., Savitsky Yu.V., Neural network method for estimating the Lyapunov spectrum *Bulletin of the Brest State Technical University*, **4,** 66-70 (2002)
4. Dmitrieva L.A., Chepilko S.S., Kuperin Yu.A. Method of Neural Networks Committees in Calculation of Time Series Maximal Lyapunov Exponents, *Proceedings of the International Conference "DAYS on DIFFRACTION 2008". June 3-6 2008. Saint-Petersburg, Russia,* 34-41 (2008)
5. Kantz H., Schreiber T., *Nonlinear time series analysis,* Cambridge University Press, Cambridge (1997)

Testing goodness-of-fit of parametric AFT model for censored samples

Ekaterina V. Chimitova and Natalia S. Galanova

Department of Applied Mathematics, Novosibirsk State Technical University
Novosibirsk, Russia
Email: natalia.galanova@gmail.com

Abstract: This paper is devoted to the problems of testing goodness-of-fit of the parametric AFT model for censored samples. We consider the approach to testing goodness-of-fit based on residuals. The statistical distributions of Kolmogorov, Cramer-von Mises-Smirnov, Anderson-Darling and chi-squared statistics are all investigated by means of Monte Carlo simulations. A power study by the Monte Carlo method has also been carried out for these tests to distinguish between various baseline models.

Keywords: AFT model, censored data, samples of residuals, Kolmogorov test, Cramer-von Mises-Smirnov test, Anderson-Darling test, chi-squared test, Monte-Carlo simulations.

1 Introduction

There are many problems of longevity and aging data in different areas such as medicine, survival analysis, reliability studies, econometrics, etc. These are the so-called time-to-event data. In medicine this event may be time of death, time of changes in some bio-chemical indices or time of remission after some treatment. In engineering this event may be the time of failure for some interesting device or technical system.

Let the nonnegative random variable T denote the time-to-event or failure time of an individual. The surviving probability of an item up to the time τ is given by the following survival function:

$$S(\tau) = \Pr(T > \tau) = 1 - F(\tau), \qquad (1)$$

where $F(\tau)$ is the cumulative distribution function.

In the survival analysis an individual's survival usually depends on some characteristics or conditions of the experiment. Usually these characteristics are coded as the so-called covariates, which can be time-dependent.

In this work we consider one of the most popular models in the reliability studies – the parametric Accelerated Failure Time model (AFT model).

2 Accelerated Failure Time model

Let us consider the following plan of the experiment [1]: the experimenter divides items into k groups and they are tested under some accelerated stress conditions $\bar{x}_1, ..., \bar{x}_k$ which are constant over time. Therefore n_i items are tested under $\bar{x}_i$ stress condition, where $i = 1, ..., k$.

According to the parametric AFT model survival function $S_{x(\cdot)}(t)$ is determined by the baseline survival function $S_0(t,\theta)$ and the positive stress function $r[\cdot]$:

$$S_{x(\cdot)}(t) = S_0\left(\int_0^t \frac{ds}{r[x(s)]}, \theta\right). \quad (2)$$

The stress function $r[\cdot]$ is usually parameterized in one of the following ways: log-linear model: $r(x) = e^{\beta_0+\beta_1 x}$, power rule model: $r(x) = e^{\beta_0+\beta_1 \ln(x)}$, Arrhenius model: $r(x) = e^{\beta_0+\beta_1/x}$ and model for vector stress: $r(x) = e^{\beta_0+\beta_1 x_1+\ldots+\beta_m x_m}$.

For parametric AFT models it is supposed that the baseline survival function $S_0(t,\theta)$ belongs to some parametric family of distributions. For example, the exponential model, the Weibull model, the Gamma model, the log-normal model, the power generalized Weibull model, the inverse Gaussian model and so forth.

In the survival analysis and reliability studies, time-to-event data are usually right censored. This means that a time-to-event T is observed only if $T \le T_C$, where T_C is a censoring time.

There are three types of right censoring schemes [2]:

1. Type I censoring: all items are tested until the pre-specified censoring time T_C;

2. Type II censoring: only $k < n$ first failure times are observed, and for remained subjects censoring time is $T_C = T_k$, where T_k is the failure time of k-th item;

3. Type III censoring (random censoring): the failure times $T_1,\ldots,T_n$ and the censoring times $C_1,\ldots,C_n$ are independent positive random variables.

Let denote T_i and C_i as the failure and censoring times of i-th item respectively. Let set i-th observation as

$$X_i = \min\left(T_i, C_i\right). \quad (3)$$

Usually right censored time-to-event data are presented as:

$$\mathbf{X}_n = \left\{(X_1, \delta_1, \bar{x}^1), \ldots, (X_n, \delta_n, \bar{x}^n)\right\}, \quad (4)$$

where $\delta_i = 1_{\{T_i \le C_i\}}$, $i = 1,\ldots,n$ is an indicator of the event and $\bar{x}^i$ the covariate vector under which the observation X_i was obtained.

Estimates of the parameters of the parametric AFT model can be found with the maximum likelihood method, where the likelihood function has the following form:

$$L(\mathrm{T}_n) = \prod_{i=1}^{n} f^{\delta_i}(X_i) \cdot S^{1-\delta_i}(X_i),\ i = 1,\ldots,n. \quad (5)$$

3 Testing goodness-of-fit of the parametric AFT model

It is often difficult to choose the distribution law for the baseline survival function $S_0(t,\theta)$ because usually there is no prior information about lifetime distribution.

After the estimation of the model parameters one should test goodness-of-fit of the constructed model to the sample of observations. One approach to testing goodness-of-fit of the parametric AFT model is based on using residuals which can be calculated as follows:

$$Z_i = \frac{t_i}{r[x^i(\cdot), \hat{\beta}]}. \quad (6)$$

If the model (2) is appropriate the sample of residuals $Z_1,...,Z_n$ belongs to the baseline distribution $F_0(t,\hat{\theta})$, which is standardized by the scale parameter (the scale parameter is equal to 1).

The hypothesis about goodness-of-fit of the sample of residuals to $F_0(t,\hat{\theta})$ can be tested with the classical nonparametric goodness-of-fit tests such as Kolmogorov, Cramer-von Mises-Smirnov and Anderson-Darling tests.

It should be noted that we have a composite hypothesis, for which test statistic distributions $G(S|H_0)$ are affected by a number of factors: the form of assuming lifetime distribution $F_0(t,\theta)$, the type and the number of estimated parameters, the method of parameter estimation and other factors. In papers by Lemeshko [3-4] the approximations of statistic distribution models and the tables of percentage points were obtained for testing composite hypotheses by the Kolmogorov, Cramer-von Mises-Smirnov and Anderson-Darling tests using the maximum likelihood estimates of unknown parameters. These approximations were obtained for uncensored data without covariates.

But the main problem of analysis of time-to-event data is censorship. When the data are censored we face the problems with estimation, with properties of ML estimates and with testing goodness-of-fit of the constructed model, because the above tests cannot be applied to censored data. That is why in this paper we discuss modified goodness-of-fit tests, where the Kaplan-Meier estimator is used instead of the empirical distribution function [5].

Let denote as $s_1 < s_2 < ... < s_k = \tau$, $k \le n$ complete observations $(Z_i, \delta_i = 1)$ in the sample of residuals $(Z_1,\delta_1),(Z_2,\delta_2),...,(Z_n,\delta_n)$. Then the Kaplan-Meier estimator can be calculated as follows:

$$\hat{F}_n(t) = 1 - \prod_{a_i \le t}\left(1 - \frac{d_i}{c_i}\right), \quad (7)$$

where $d_i = \sum_{Z_j = s_i} \delta_j$, c_i the number of complete observations, for which $Z_j \ge s_i$, $j = 1,...,n$.

According to this modification the tests statistics can be calculated as follows:
the modified Kolmogorov test statistic with the Bolshev correction has the following form:

$$S_K^C = \frac{6nD_n + 1}{6\sqrt{n}}, \quad (8)$$

where $D_n = \max\{D_n^+, D_n^-\}$, $D_n^+ = \max_i \left\{\hat{F}_n(s_i) - F_0(s_i;\boldsymbol{\theta})\right\}$, $D_n^- = \max_i \left\{F_0(s_i;\boldsymbol{\theta}) - \hat{F}_n(s_{i-1})\right\}$;

the modified Cramer-von Mises-Smirnov test statistic:

$$S_\omega^C = \frac{n}{3}\cdot F_0(s_1;\boldsymbol{\theta}) + n\cdot\sum_{j=1}^{k-1}\Big[\hat{F}_n^2(s_j)\left(F_0(s_{j+1};\boldsymbol{\theta}) - F_0(s_j;\boldsymbol{\theta})\right) - \\ - \hat{F}_n(s_j)\left(F_0^2(s_{j+1};\boldsymbol{\theta}) - F_0^2(s_j;\boldsymbol{\theta})\right) + \frac{1}{3}\left(F_0^3(s_{j+1};\boldsymbol{\theta}) - F_0^3(s_j;\boldsymbol{\theta})\right)\Big]; \quad (9)$$

the modified Anderson-Darling test statistic:

$$S_\Omega^C = n\cdot\Big\{-F_0(s_1;\boldsymbol{\theta}) + \sum_{j=1}^{k-1}\Big[F_0(s_j;\boldsymbol{\theta}) - F_0(s_{j+1};\boldsymbol{\theta}) + \\ + \hat{F}_n^2(s_j)\left(\ln F_0(s_{j+1};\boldsymbol{\theta}) - \ln F_0(s_j;\boldsymbol{\theta})\right) - \left(1-\hat{F}_n(s_j)\right)^2\cdot \quad (10) \\ \cdot\left(\ln\left(1-F_0(s_{j+1};\boldsymbol{\theta})\right) - \ln\left(1-F_0(s_j;\boldsymbol{\theta})\right)\right)\Big] - \ln\left(1-F_0(s_1;\boldsymbol{\theta})\right)\Big\}.$$

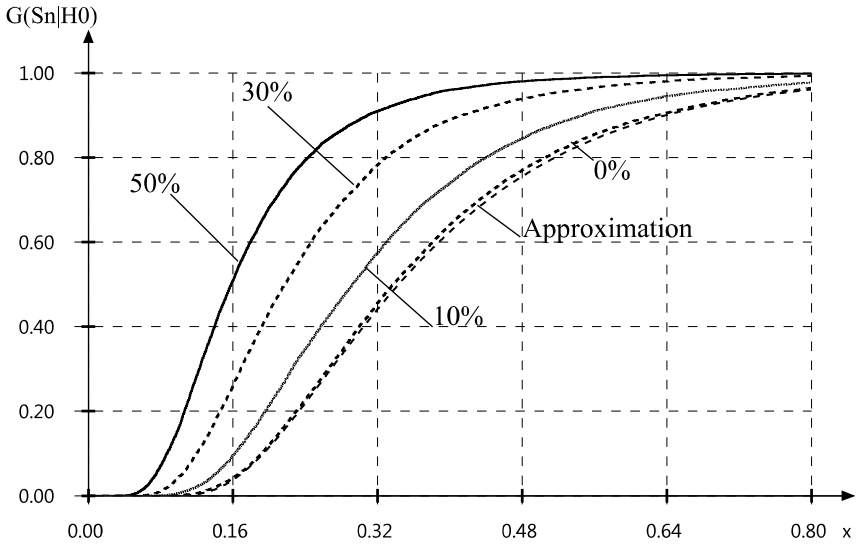

Figure 1. The modified Anderson-Darling test for censored data

Figure 1 shows the modified Anderson-Darling test statistic distributions obtained by simulation for various censoring degrees: 0% (complete data), 10%, 30% and 50%. The simulations were made for testing goodness-of-fit by samples of residuals of the Weibull AFT model, the number of observations was $n = 100$ and the type II censoring scheme was used. Also this figure presents the approximation of the classical Anderson-Darling test statistic distribution $G(S|H_0)$ for testing

composite hypothesis with the Weibull distribution (both shape and scale parameters are supposed to be estimated). This approximation was obtained in [3-4] for complete and identically distributed data and has the form of the Sb-Johnson distribution function:

$F\left(x,\theta_0,\theta_1,\theta_2,\theta_3\right)=\frac{1}{2}+\frac{1}{2\sqrt{\pi}}\Gamma\left(\frac{1}{2}\left(\theta_3\cdot\ln\left(\frac{x-\theta_0}{\theta_1-x+\theta_0}\right)+\theta_2\right)^2,\frac{1}{2}\right)$ with parameter values $\theta_0=0.07,\ \theta_1=3.00,\ \theta_2=3.4830,\ \theta_4=1.5138$.

One can see from fig. 1, that for complete data in testing goodness-of-fit of the parametric AFT model by samples of residuals one can use approximations of test statistic distributions $G(S|H_0)$ from papers [3-4] for obtaining *p*-values. But if we have censored data modified test statistic distribution are affected by the censoring degree and are unknown. In this case we can obtain *p*-values only by simulation. In such a case we face the problem of simulating the censored data. It is not the problem for type I or type II censored data, because these censoring schemes are quite simple and reproducible. But if we have a random censoring process which often occurs in the survival analysis there is a problem of ambiguity in simulating censored observations because the distribution of censoring times is usually unknown.

Another test for testing goodness-of-fit of the sample of residuals to the baseline distribution $F_0(t,\hat{\theta})$ is a modified χ^2 test. This test was suggested in [6] and this is a modification of the Rao-Robson-Nikulin test for censored data. Modified χ^2 test statistic has the following form:

$$Y^2=\sum_{j=1}^{k}\frac{\left(U_j-e_j\right)}{U_j}+Q\ , \tag{11}$$

where $U_j=\sum_{i=1}^{n}1_{\{Z_i\le a_j,\delta_i=1\}}-\sum_{i=1}^{n}1_{\{Z_i\le a_{j-1},\delta_i=1\}}$ is the number of observations on the *j*-th interval $[a_{j-1},a_j]$, $e_j=\sum_{i:Z_i>a_{j-1}}\left[\Lambda\left(\min\left(a_j,Z_i\right),\hat{\theta}\right)-\Lambda\left(a_{j-1},\hat{\theta}\right)\right]$ is the number of expected observations on the *j*-th interval, and Q is calculated as:

$$Q=W^T\hat{G}^{-}W\ , \tag{12}$$

where $W=\hat{C}\hat{A}^{-1}V$, $\hat{C}_{ij}=\frac{1}{n}\sum_{a_{j-1}<Z_q\le a_j}\delta_q\frac{\partial\ln\lambda\left(Z_q,\hat{\theta}\right)}{\partial\theta_i}$, $\hat{A}=diag\left\{\frac{U_j}{n}\right\}$,

$V_j=\frac{1}{\sqrt{n}}\left(U_j-e_j\right)$, $\hat{G}=\hat{I}-\hat{C}A^{-1}\hat{C}^T$, $\hat{I}_{lj}=\frac{1}{n}\sum_{q=1}^{n}\delta_q\frac{\partial\ln\lambda\left(Z_q,\hat{\theta}\right)}{\partial\theta_l}\frac{\partial\ln\lambda\left(Z_q,\hat{\theta}\right)}{\partial\theta_j}$,

$j=\overline{1,k}$, $i,l=\overline{1,m}$ and k is the number of intervals and m is the number of estimated parameters. If matrix is $\hat{G}$ degenerate the limit distribution of this

statistic is the χ^2 distribution with $(k-1)$ degrees of freedom else the limit distribution of this statistic is the χ^2 distribution with k degrees of freedom.
Figure 2 shows the modified χ^2 test statistic distributions obtained by simulation for various censoring degrees. In the simulation was used the same parametric AFT model as in the previous example with the Anderson-Darling test. The number of intervals was $k = 3$ and the equifrequent grouping method was used.

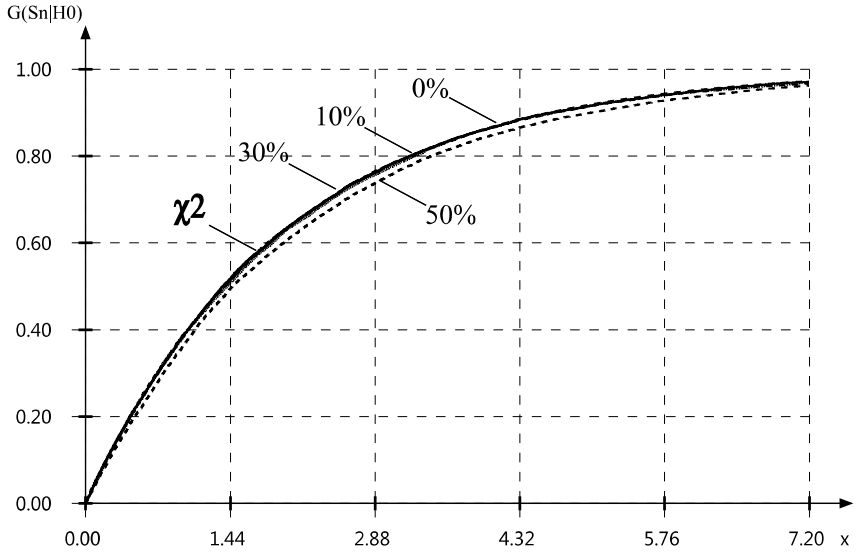

Figure 2. The modified χ^2 test for censored data

It can be seen from this figure that modified χ^2 test statistic distributions practically are not affected by the censoring degree. That means that even for heavy censored data we can use the limit distribution and we do not have to simulate statistic distributions to calculate *p*-values. So, using the modified χ^2 test simplifies significantly the procedure of testing goodness-of-fit of the parametric AFT model by sample of residuals.

4 Power study

This section presents the power study for the above modified tests depending on censoring degrees and sample sizes.
Table 1 presents test powers for the following hypotheses:

$$H_0 : Weibull\ AFT\ model - H_1 : Gamma\ AFT\ model$$

and table 2 presents test powers for the following hypotheses:

$$H_0 : Weibull\ AFT\ model - H_1 : LogNormal\ AFT\ model$$

As we can see from the tables, the modified χ^2 test is less powerful than the modified Anderson-Darling test but it is more powerful than the modified Kolmogorov test and it is comparable in power with the modified Cramer-von

Mises-Smirnov test. So, using the modified χ^2 test instead of the modified Anderson-Darling test we can lose in power, but we can sacrifice it to the simplicity of testing goodness-of-fit procedure.

Table 1 – Power study for Gamma-Weibull

Cens.	Sample size	S_K^C	S_ω^C	S_Ω^C	$\chi^2_{k=3}$	$\chi^2_{k=5}$	$\chi^2_{k=7}$	$\chi^2_{k=9}$
0%	n=100	0.23	0.29	0.36	0.21	0.38	0.29	0.32
	n=300	0.58	0.74	0.84	0.61	0.75	0.73	0.75
	n=500	0.81	0.93	0.97	0.79	0.92	0.92	0.93
10%	n=100	0.16	0.22	0.27	0.18	0.22	0.23	0.24
	n=300	0.44	0.59	0.67	0.51	0.58	0.58	0.58
	n=500	0.68	0.82	0.88	0.74	0.80	0.84	0.80
30%	n=100	0.16	0.18	0.18	0.14	0.15	0.17	0.17
	n=300	0.31	0.38	0.41	0.33	0.35	0.35	0.35
	n=500	0.43	0.56	0.60	0.53	0.52	0.52	0.52
50%	n=100	0.11	0.13	0.13	0.11	0.11	0.12	0.12
	n=300	0.16	0.22	0.23	0.19	0.19	0.20	0.20
	n=500	0.23	0.33	0.36	0.28	0.31	0.31	0.31

Table 2 – Power study for LogNormal-Weibull

Cens.	Sample size	S_K^C	S_ω^C	S_Ω^C	$\chi^2_{k=3}$	$\chi^2_{k=5}$	$\chi^2_{k=7}$	$\chi^2_{k=9}$
0%	n=100	0.67	0.82	0.88	0.58	0.86	0.83	0.85
	n=300	0.99	1.00	1.00	0.97	1.00	1.00	1.00
	n=500	1.00	1.00	1.00	1.00	1.00	1.00	1.00
10%	n=100	0.45	0.63	0.72	0.52	0.64	0.69	0.70
	n=300	0.94	0.99	1.00	0.97	0.99	0.99	0.99
	n=500	1.00	1.00	1.00	1.00	1.00	1.00	1.00
30%	n=100	0.33	0.43	0.45	0.35	0.40	0.44	0.45
	n=300	0.73	0.87	0.91	0.82	0.87	0.89	0.89
	n=500	0.92	0.99	0.99	0.97	0.98	0.98	0.98
50%	n=100	0.19	0.24	0.25	0.21	0.24	0.26	0.25
	n=300	0.36	0.58	0.64	0.56	0.61	0.63	0.64
	n=500	0.61	0.82	0.88	0.78	0.84	0.86	0.85

5 Conclusions

In this paper we have briefly discussed the problem of testing goodness-of-fit of the parametric AFT model for censored data. The approach based on using residuals has been considered using modified nonparametric goodness-of-fit tests such as the Kolmogorov. Cramer-von Mises-Smirnov and Anderson-Darling tests for which the Kaplan-Meier estimator is used instead of the empirical distribution function. Also, the modified χ^2 test based on residuals has been discussed. By

means of computer simulation we have investigated the modified test statistics distributions for testing goodness-of-fit of the AFT model. It has been shown, that the modified goodness-of-fit test statistic distributions are affected by the censoring degree and in case of complete samples it is possible to use the approximations of classical nonparametric goodness-of-fit test statistic distributions given in [5]. [6] or to obtain *p*-values by simulation for data without covariates. In the case of censored data we have to simulate the modified test statistic distributions to calculate *p*-values. Also, it has been shown that the modified χ^2 test statistic distributions practically are not affected by the censoring degree and we can use the limit distribution even for heavy censored data.
The comparative analysis of the modified tests by power has been carried out. It has been shown that the modified χ^2 test is less powerful than the modified Anderson-Darling test but it is more powerful than the modified Kolmogorov test and it is comparable in power with the modified Cramer-von Mises-Smirnov test. Further investigations of the modified χ^2 test depending on the number of intervals and grouping method would be useful.

6 Acknowledgements

This research has been partially supported by the Russian Foundation for Basic Research (Grant No. 12-01-09206).

References

1. Bagdonavicius V.. Nikulin M. (2002). Accelerated Life Models. Modeling and Statistical Analysis. Chapman&Hall/CRC. London.
2. Klein J.P.. Moeschberger M.L. (2003). Survival analysis: techniques for censored and truncated data. Springer. New York.
3. Lemeshko B.Yu.. Lemeshko S.B. (2009). Distribution models for nonparametric tests for fit in verifying complicated hypotheses and maximum-likelihood estimators. Part 1. Measurement Techniques. Vol. 52. No. 6. pp. 555-565.
4. Lemeshko B.Yu.. Lemeshko S.B. (2009). Models for statistical distributions in nonparametric fitting tests on composite hypotheses based on maximum-likelihood estimators. Part II. Measurement Techniques. Vol. 52. No. 8. pp. 799-812.
5. Koziol J.A. (1980). Goodness-of-Fit Tests for Randomly Censored Data. Biometrika. Vol. 67 No. 3.. pp. 693-696
6. Bagdonavicius V.. Kruopis J.. Nikulin M. (2010). Nonparametric Tests for Censored Data. Wiley-ISTE.

System Identity Method used for the Analysis of Human Resources Management Process

Application for Aircrew

Jitka Civinova

Department of Transportation Engineering, Czech University of Technology
Prague, Czech Republic
Email: jitka.civinova@seznam.cz

Abstract: Process system analysis is the tool enabling the identification of operation critical subjects and parameters. The aim of this study is to use the system identity to identify potential weaknesses in the process of flight crew human resources management and to provide the best solution to stabilize them. The term stable system defines a system that can be for its reliability and objectivity applied repeatedly without scattering resulting values. By monitoring individual elements of the process, the optimization of complex process is achieved. The main emphasis is placed primarily on the items with the highest probability of destabilization of the resulting system. Identification of this weak points is performed by system analysis based on the System identity theory formulated by Prof. Ing. Jaroslav Vlček. The solution to the problem of "Performance critical points" is their elimination, the bypass (backup and strengthen weak joints), or the mitigation of consequences.
Keywords: System analysis, system identity, human resources management, process stability

1 Introduction

Aviation related disciplines are very sensitive due to taking direct responsibility for the lives of people. For this reason the selection process of human resources is subject to strict rules – it must always be the same quality and stable. Any mistake which could indirectly threaten the safety can be admitted.
Moreover this field has always been prestigious and sought after for the uniqueness and attractiveness of the aviation environment. But the high number of interested people applying for any position in the aviation contains only a fraction of enough qualified people.
There are two main aspects influencing the output from resources selection, improvement and evaluation process. The first one is the set up of selection and examination screen. If the parameters are poorly defined, unsuitable adepts can get through. On the other hand the very strict setting of conditions can cause that there are only few successful. The same attention must be devoted to the selection of higher level of management who represent a back-up element to identify any failure.
The second aspect is the stability of the process itself. All elements of the system have to be optimally adjusted due to a number of actors who go through this process and a number of recurrences. The sources of instability can be captured by analytic definition of critical elements. Their elimination allows versatile use of the process with consistent quality.

2 Theoretical background

Human resources management is a discipline by which we can quite safely say that is most affected by human factor and the so-called soft skills. In the last 20 years, it has gained a position of a significant component of business management. It has been proven, that properly applied human resources management best practices can significantly enhance business performance. J. Pfeffer (Pfeffer, 1994) defines seven main functions including: providing employment security, selective hiring, extensive training, sharing information, self-managed teams, high pay based on company performance and the reduction of status differentials. Today a lot of companies use the model articulated by (Ulrich, 2005) and use the support of shared services, centers of expertise, and business partners to manage their human resources. Due to the specifics of the aviation industry most of the aviation operators keep the practice of internally managed resourcing and development of workforce. Anyway, it is now generally accepted fact that personnel management control is not only a task of HR department. This discipline blends through the whole company and managers at all levels are involved.
For purposes of this system analysis will be used only strong processes supporting the genetic code, in order to minimize the effect of random uncontrolled factors. Always when speak about a human-oriented fields we must take into account the influence of soft parameters and processes.

3 Human Resources Management Process Model

Based on external (sub-system) sources, such as company strategy, organization charts etc. the main human resources control documents are created. They define needed number of each position and their specific content. The fulfilment of these requirements is tested on regularly basis. If not met, the sourcing sub-process is launched. The inputs come from already mentioned superior human resources control documents and define requested quantity and quality of adepts. Quality in this case means personal skills and abilities without the knowledge gained from trainings (as defined in description of work position). There are two alternatives where to search resources. For the internal search personal performance assessment is used as the main source of information. External applicants are evaluated on the basis of information presented in the CV. Selected candidates undergo basic training followed by exams and/or certification. During the service performance every employee passes periodic trainings and examination on a yearly basis and personal performance assessment several times per year.
This process can be represented by the following flowchart (Figure1). Supporting documents which are also called external inputs in the following paragraphs are the outputs from higher management level process. They are based on strategy, corporate goals, financial results atc. but should also include feedback from these processes that are created for.

Figure1: Flow chart of aircrew human resources management process

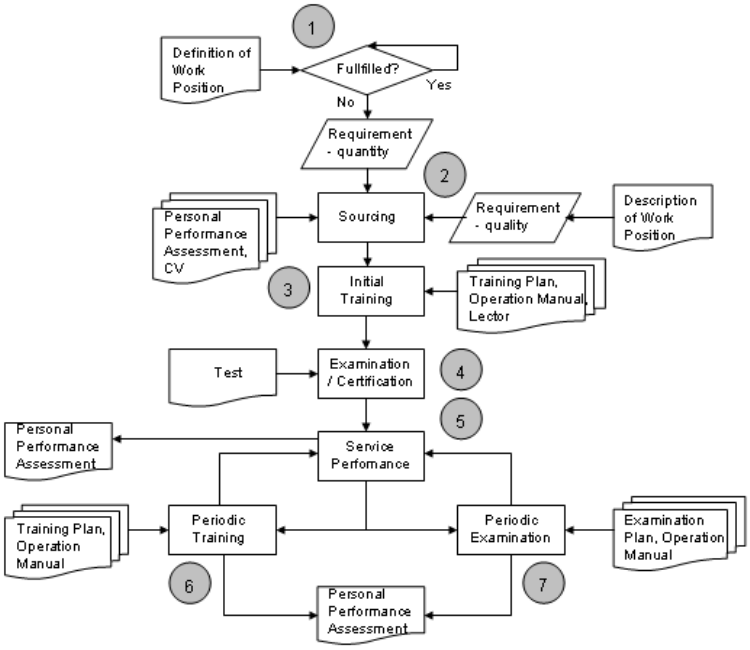

Source: author

Developing the process flowchart to the system network provides schematic basis for subsequent stability analysis. The numbers below represent the process elements from the Figure1. This schematic representation simplifies the preparation of the table of elements (Table1). It shows only the sequence of main elements (strong processes), inputs and outputs such as for example manuals, plans, documentation etc. are not graphically depicted. As well each element represents a complex sub-process and it would be possible to continue with similar analysis at lower resolving level.

Figure2: Oriented network of aircrew human resources management process

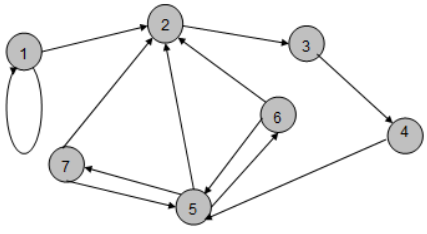

Source: author

4 Identification of the most sensitive elements

Using the System identity theory formulated by (Vlček, 1999) and (Votruba, 2004), we can try to increase the identity and subsequently the stability of the process. The relation between identity and stability has not been demonstrated but it is reasonably anticipated and can be subject of further research. Identity is defined as the coefficient on the basis of the elements defining the system. It can be increased by influencing of these components. Among them reduction of regular interfaces, strengthening behavior according to genetic code or supporting the target oriented behaviour are the easiest achievable.
Our goal is thus to identify and eliminate elements, where the assigned function is not sufficiently robust and design mitigation or better proactive tools to support requested behaviour. The main guideline to find out the weak points is the Table of elements (see. Table1). The next step is detailed breakdown of risks parameter by parameter and also those contained directly in sub-processes (elements).

Table1: Table of elements

Code	Definition	Foregoing Element	Following Element	Required Parameter	Offered Parameter
1	Requirement fulfilment test	External	1 2	Definition of Work Position	Requirement - quantity
2	Sourcing	External 1	3	Personal Performance Assessment CV Requirement - quality Requirement - quantity	Selected human resources
3	Initial Training	External 2	4	Selected human resources Lectors Training Plan Operation Manual	Trainee
4	Examination / Certification	3 External	5	Trainee Test	Workforce
5	Service Perfomance	4	6 7	Workforce	Personal Performance Assessment Workforce
6	Periodic Training	External 5	5	Workforce Training Plan Operation Manual	Personal Performance Assessment
7	Periodic Examination	External 5	5	Workforce Training Plan Operation Manual	Personal Performance Assessment

Source: author

4.1 Requirement fulfillment test

Potential risk: decision is based on Definition of work position (external document from the process perspective) therefore any inaccuracy is brought in from superior control level. The occurrence probability is low.

4.2 Sourcing

Potential risk: the most sensitive sub-process, strongly affected by soft factors such as personal antipathy during the selection activity itself. The advantage of mass process with a high amount of repetition is the possibility to eliminate these factors to a minimum by the use of unified fixed test content and evaluation scale.

Requirements on quantity can be affected by external error (see above).

Requirement on quality used in the case of external sourcing can be subject of external error, ie. caused by incorrect content of Description of work position (external document). The second possibility is wrong transcription of correct content of Description of work position in Requirements on quality. The occurrence probability is low.

Personal performance assessment represents the key document for several process elements stability. Related to sourcing, potential instability can be caused by different evaluation of results by individual decision-makers. There is a high probability that the scale of weight/relevance of evaluated parameters will be different. For example somebody considers the test results as the most objective, other person can give more weight to personal evaluation made by inspector. The mitigation actions can be: fixed common rating of individual parts, one same evaluator for each candidate (which is unrealistic in bigger companies) or more evaluators for each candidate.

CV is very subjective external document. In aircrew selection process, where the conditions can be due to high number of repetitions strictly defined, is CV mostly used as a reference information in final stages of decision-making.

4.3 Initial Training

Potential risk: this area is mainly influenced by disbalance in input parameters.

Selected human resources show different individual qualities, even there was the attempt to unite them as much as possible during the selection process. One of the training targets is to reduce the spread. This attribute can be easily verified by capturing the test results by histogram (Gauss curve)

The Lectors - character and experience of trainers bring more instability, caused by the human factor. The test results can be used as a feedback again. In this case it is worthy to stratify the results for each lector and to investigate individual deviations.

Inappropriate content curriculum document can lead to distortion of the whole process. The easiest way of control is the full analysis (tools as mentioned above) after each change.

4.4 Examination / Certification

Potential risk: even though this activity is strictly described and controlled by authorities human factor is involved. As the test content should be consistent and certain level of variance of outputs caused by different human abilities is expected, the main problem is cheating in exams. Protective methods are obvious.

Service Performance

During the service performance, all crewmembers are monitored and evaluated on irregular basis by superiors. Rating is usually given on special occasions, after

emergency situation for example, or on management request. The scale is defined, but not always followed. Also personal antipathy or friendship can significantly influence the result. In this case visual management graphically showing individual results to the whole interested group of employees can help to eliminate these potential risks. And again histogram is a very powerful tool, showing any deviation from the average and especially outlying point which should be properly double checked.

4.5 Periodic Training and Examination

Potential risk: training and examination issues were discussed in previous paragraphs. Substantial difference which must be mentioned is oral examination during flight. It is virtually impossible to set uniform conditions and results are significantly influenced. This area could be interesting topics to explore, because inputs (inspector, flight, time etc.) and output (examination results) data are available. Of course, we must assume a certain error caused by human factor, as always if there are present purely human decisions and evaluations.

5 Conclusion

By identification of process bottlenecks we can anticipate potential risks and optimize these elements so that the resulting process shows the maximal stability. Optimization in this case means process of strengthening of critical areas by adding control mechanisms or eliminating the "soft" elements.

In order to correctly identify weak points and to take mitigation measures, the first necessary step is to describe and break down the process into different stages correspondingly and to determine the relationships between them.

This study is a brief guide to proceed in this degradation to the elements in order to achieve proper efficiency of the resulting process. It also takes into account the specificity of the aviation environment (aircraft industry) and the aspects that affect this field.

Increased attention is devoted to pointing out the most important weak points and design solutions, which leads to increased stability of the resulting system. Application is not strictly limited to this area, because this method is very versatile.

References

1. BECKWITH, K. System Analysis for Riordan Manufacturing's Human Resources Department .*Human Resources Analysis*, http://kellybeckwith.com/Papers/HumanResourcesAnalysis.doc (b.r.)
2. BROWNING, T. R. The many views of a process: Toward a process architecture framework for product development processes. *Systems Engineering*. **12**, 69-90 (2009).
3. COLLISON, Ch. and PARCELL, G. (2006). *Knowledge management: Praktický management znalosti z prostředí předních světových učících se organizací.* Computer Press.
4. DANI, S., et al. A methodology for best practice knowledge management. Proceedings of the Institution of Mechanical Engineers : Part B. *Journal of Engineering Manufacture*. **220**, 1717-1728, (2006).
5. DEMAREST , M. Understanding Knowledge Management**.** Long-Range Planning. **30**, 374-384. (1997).
6. EPPLER , M.J. Conceptual management tools : A Guide to Essential Models for Knowledge Workers**.** University of St. Galen, http://www.knowledge-communication.org/pdf/conceptual-mngt-tool-mep.pdf (2000).
7. HARRISON, R. and KESSELS, J. (2004). *Human resource development in a knowledge economy: An organisational view.* Palgrave Macmillan.
8. LUNAU, S. et al. (2007). *Six Sigma + Lean Toolset : Verbesserungsprojekte erfolgreich durchführen*. Springer.
9. MOTELEB, A.A. and WOODMAN, M. Notions of Knowledge Management Systems : A Gap Analysis. *The Electronic. Journal of Knowledge Management*. **5**, 55-62 (2007). http://www.ejkm.com
10. SAGSAN, M. (2006). *A New Life Cycle Model For Processing Of Knowledge Management.* 2nd International Conference on Business, Management and Economics http://www.knowledgeboard.com/download/3562/A-NEW-LIFE-CYCLE-MODEL-FOR-PROCESSING-OF-KNOWLEDGE-MANAGEMENT.pdf
11. PFEFFER, J. (1994). *Competitive advantage through people : unleashing the power of the work force*. Harvard Business School Press.
12. VLČEK, J. (1999). *Systémové inženýrství*. 1. Vydavatelství ČVUT.
13. VOTRUBA, Z. and KALIKA, M. and KLEČÁKOVÁ, J. (2004). *Systémová analýza*. Vydavatelství ČVUT.